Supporting Information

Molecular Recombination Phenomena in Palladium(II) based Self-Assembled Complexes

*Sudhakar Ganta and Dillip K. Chand**

Department of Chemistry, Indian Institute of Technology Madras, Chennai 600036, India

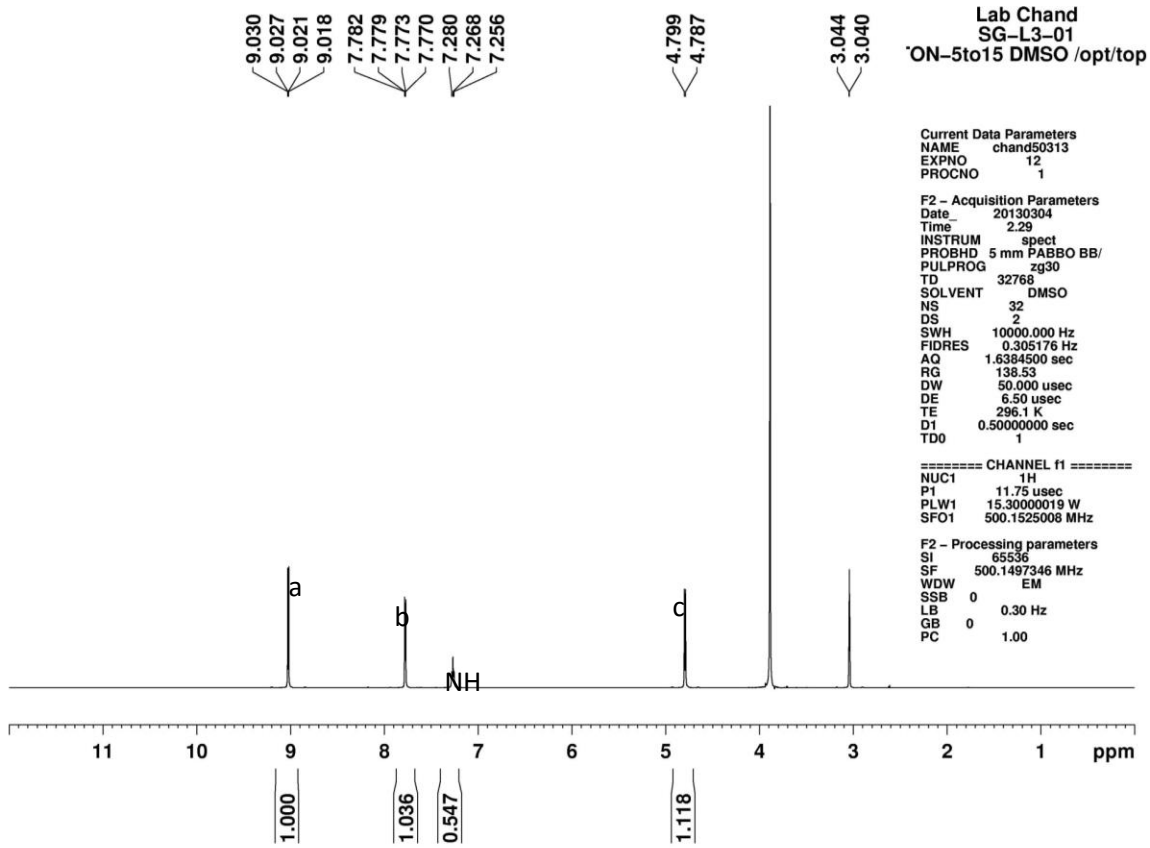

Figure S1 ^{1}H NMR spectrum of ligand **L** in DMSO-d_6 .

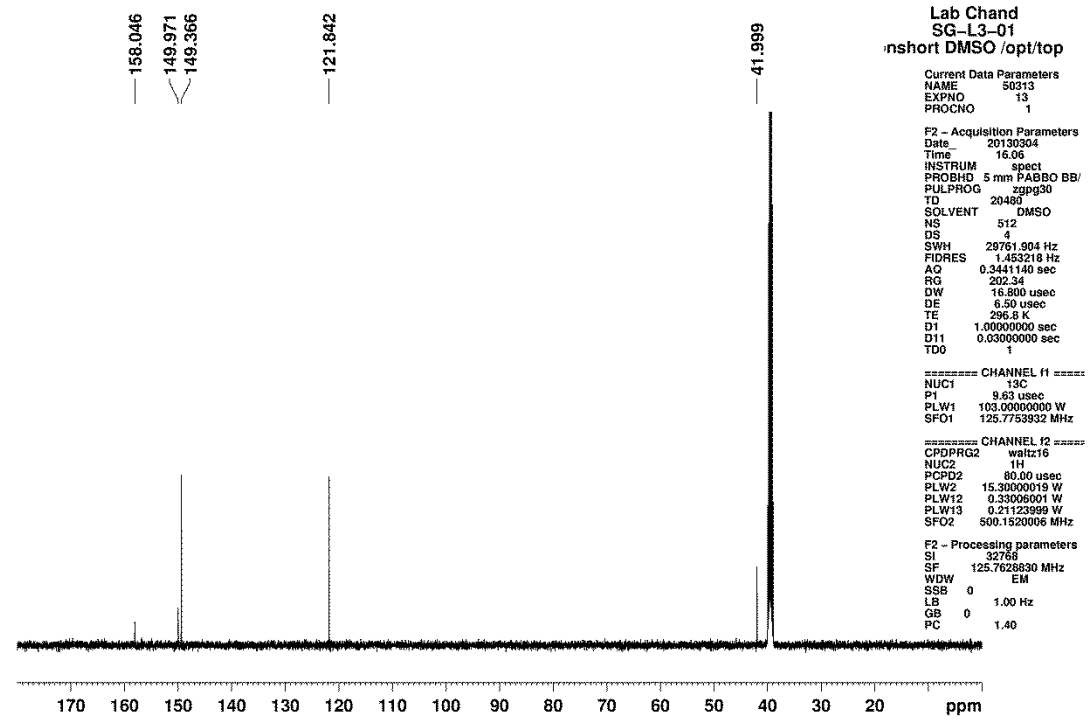

Figure S2 ^{13}C NMR spectrum of ligand **L** in DMSO-d_6 .

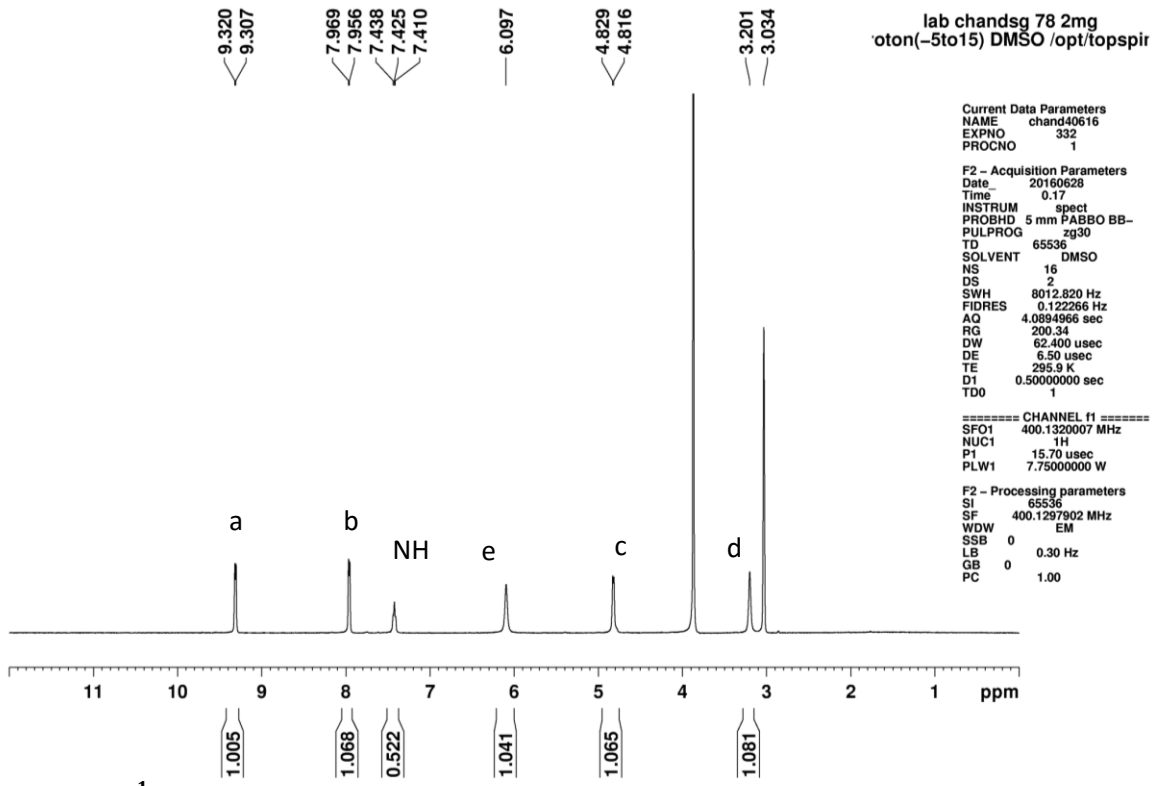

Figure S3. ^{1}H NMR spectrum of **1** in DMSO-d_6 .

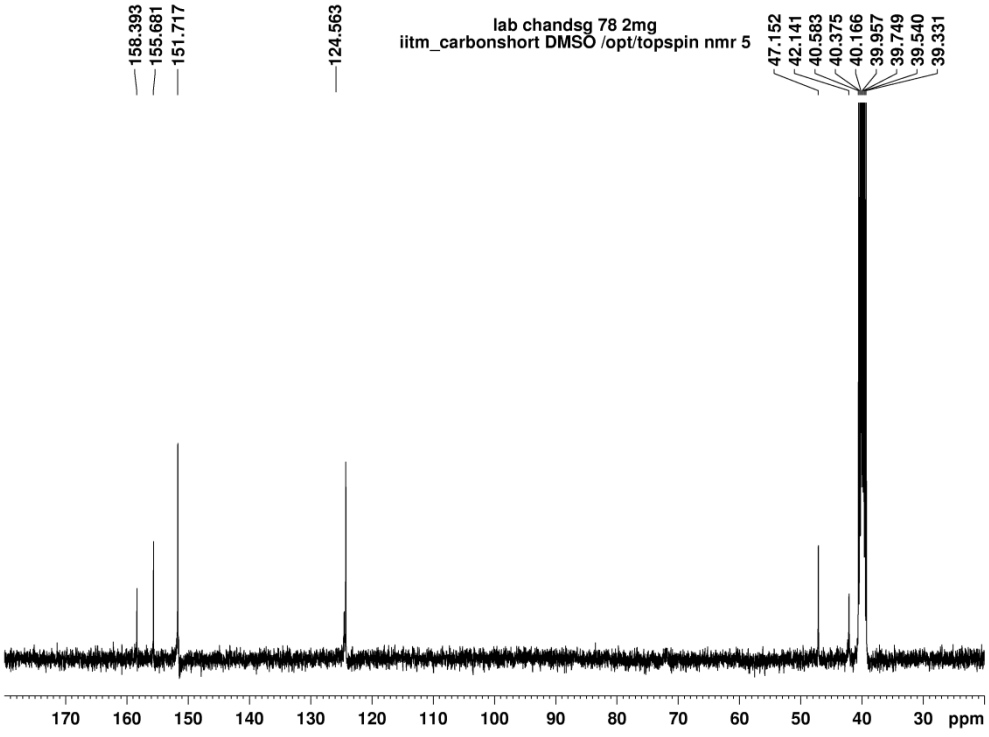

Figure S4. ^{13}C NMR spectrum of **1** in DMSO-d_6 .

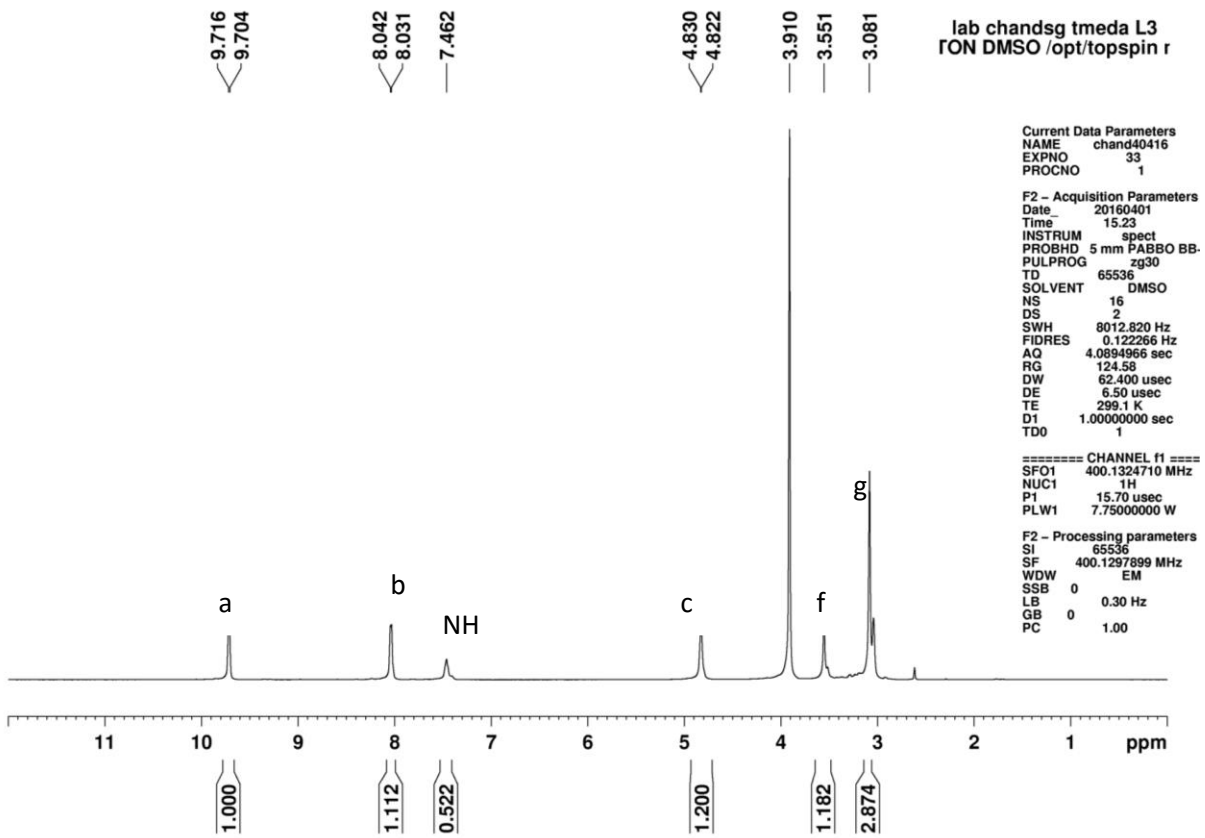

Figure S5. ^{1}H NMR spectrum of **2** in DMSO-d_6 .

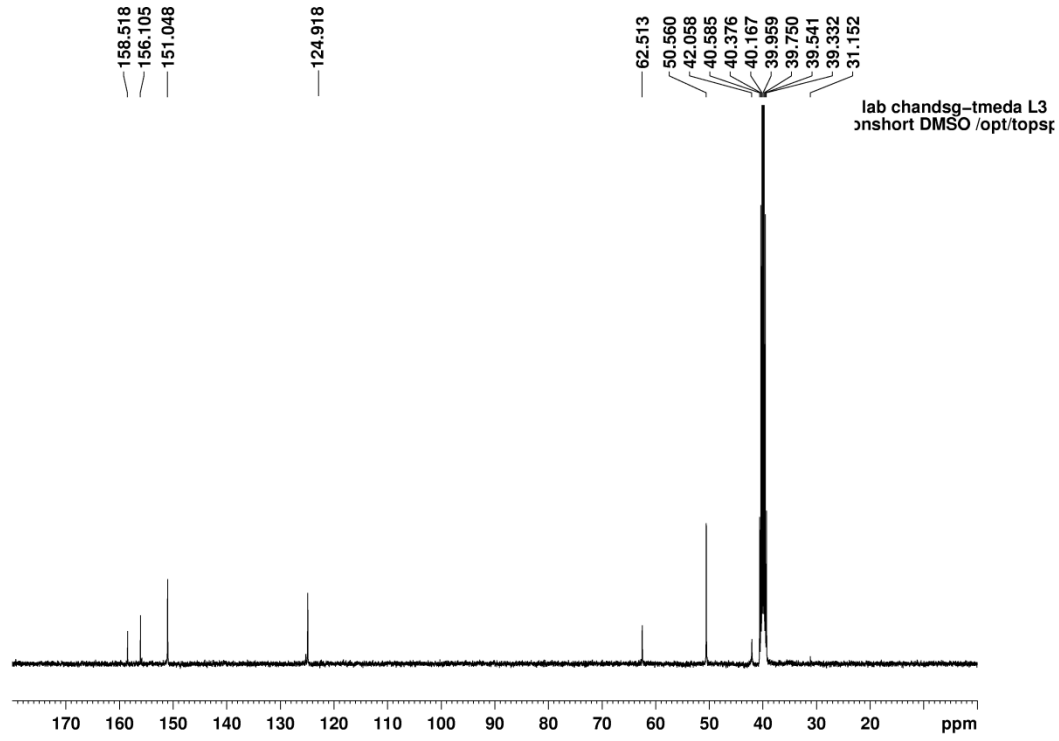

Figure S6. ^{13}C NMR spectrum of **2** in DMSO-d_6 .

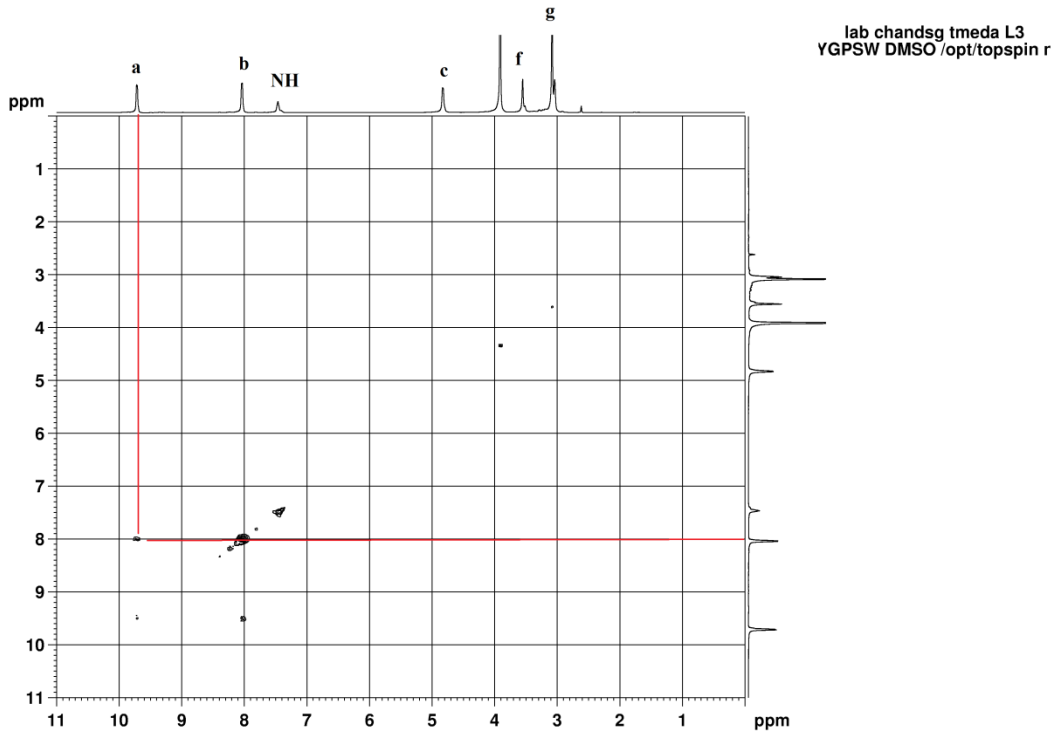

Figure S7. H-H COSY of **2** in DMSO-d_6 .

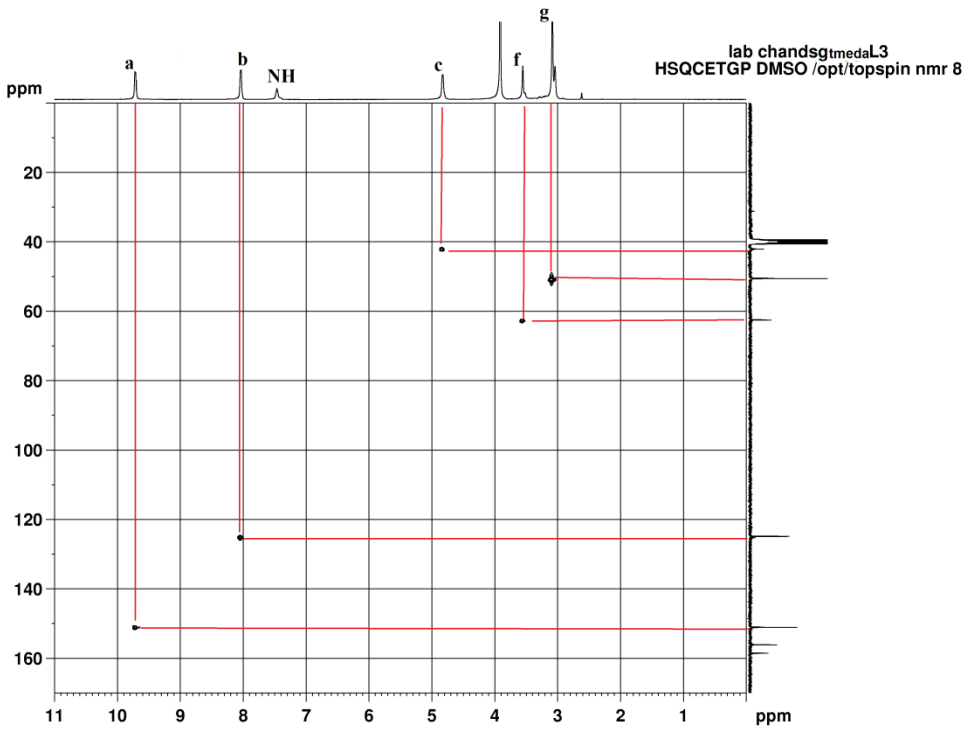

Figure S8. HSQC of **2** in DMSO-d_6 .

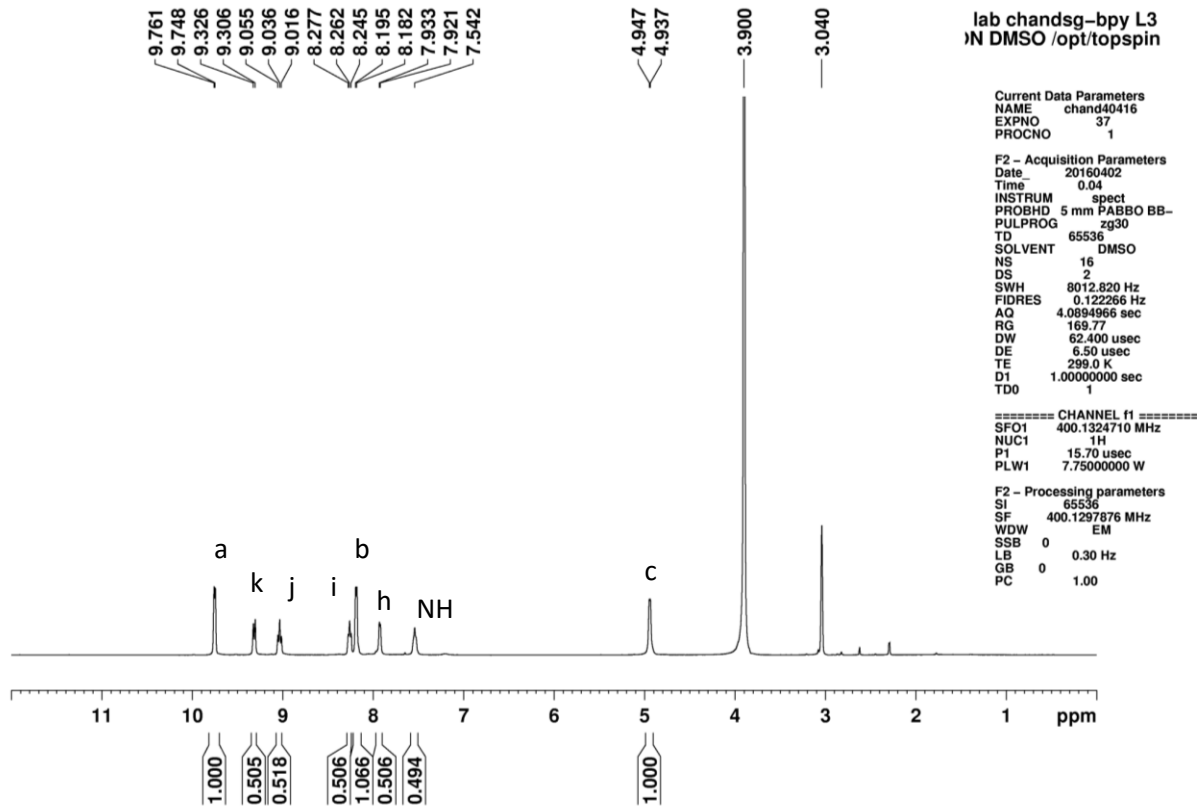

Figure S9. ^{1}H NMR spectrum of **3** in DMSO-d_6.

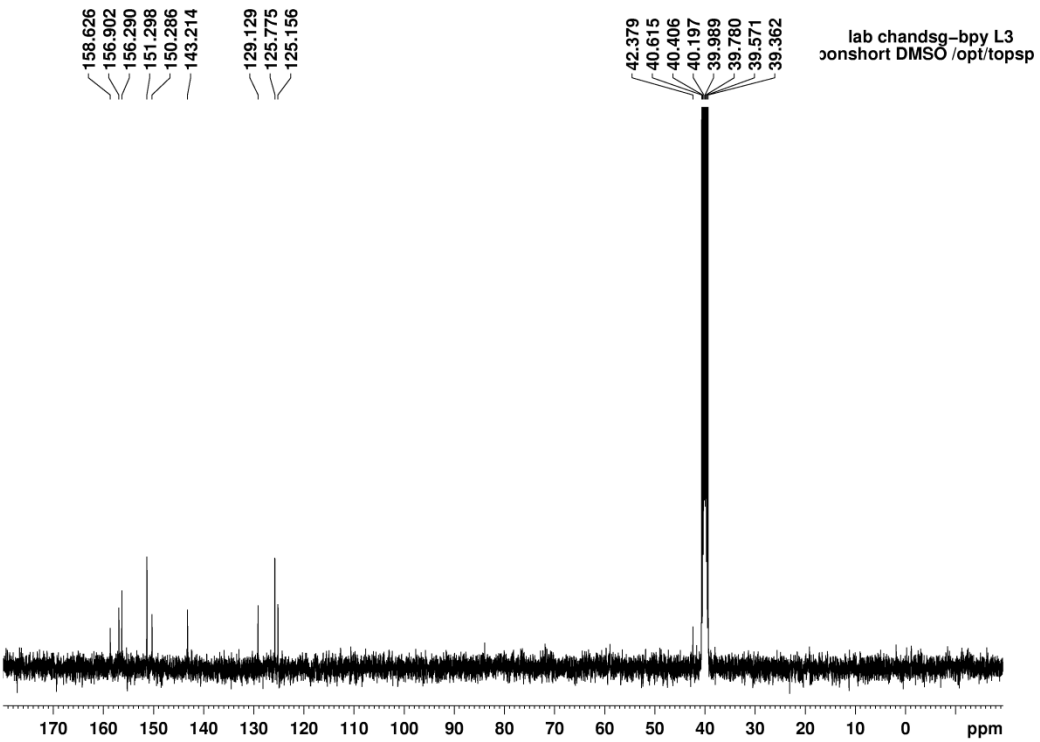

Figure S10. ^{13}C NMR spectrum of **3** in DMSO-d_6 .

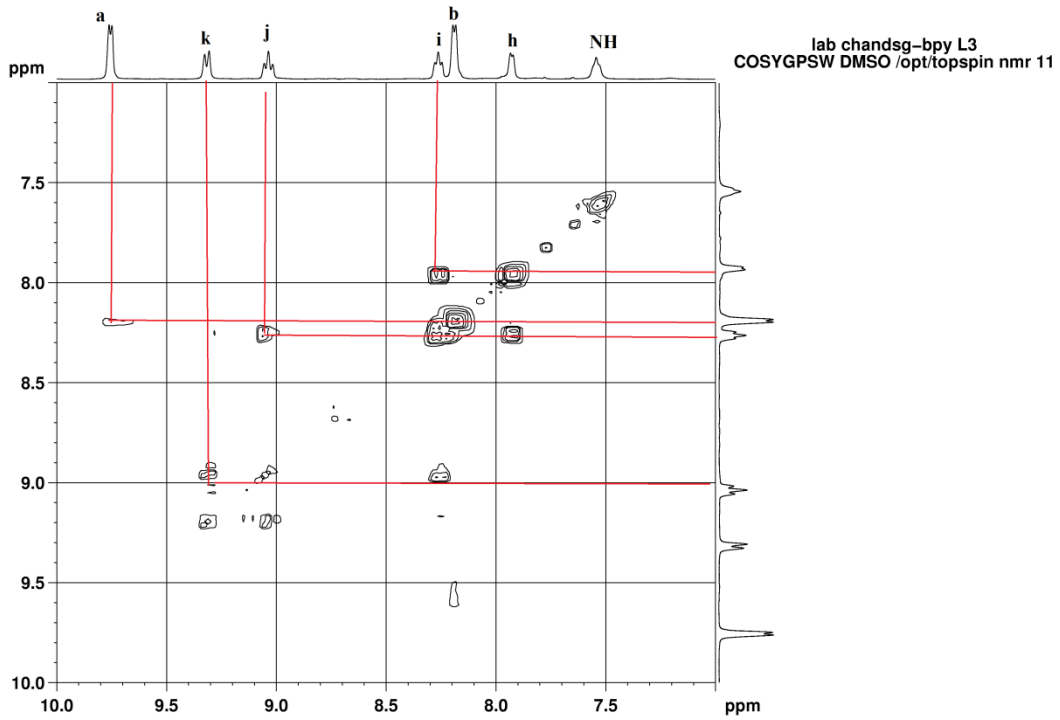

Figure S11. H-H COSY of **3** in DMSO-d_6 .

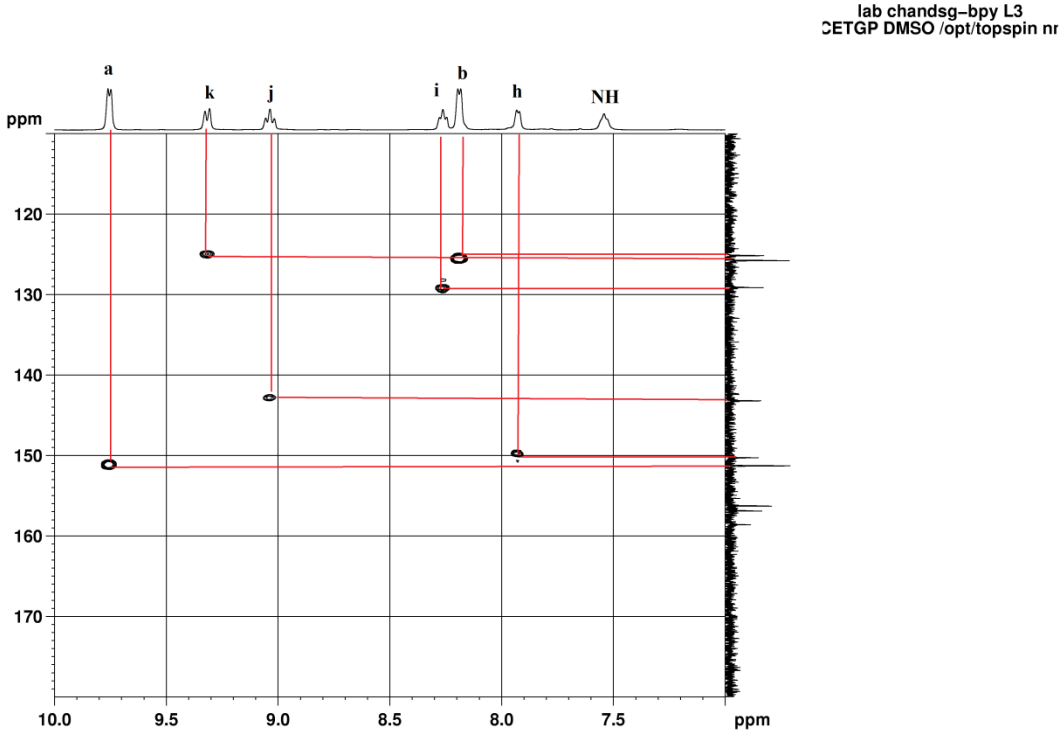

Figure S12. HSQC of **3** in DMSO-d_6.

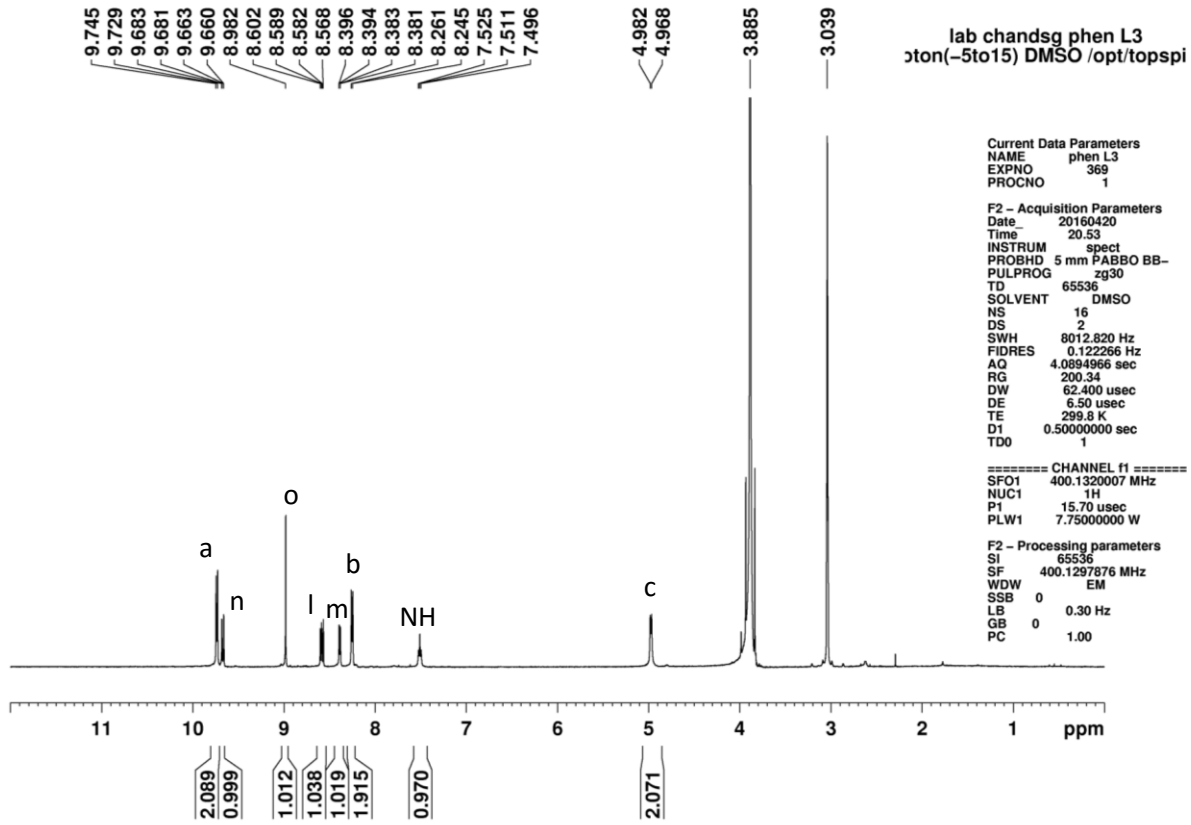

Figure S13. ^{1}H NMR spectrum of **4** in DMSO-d_6 .

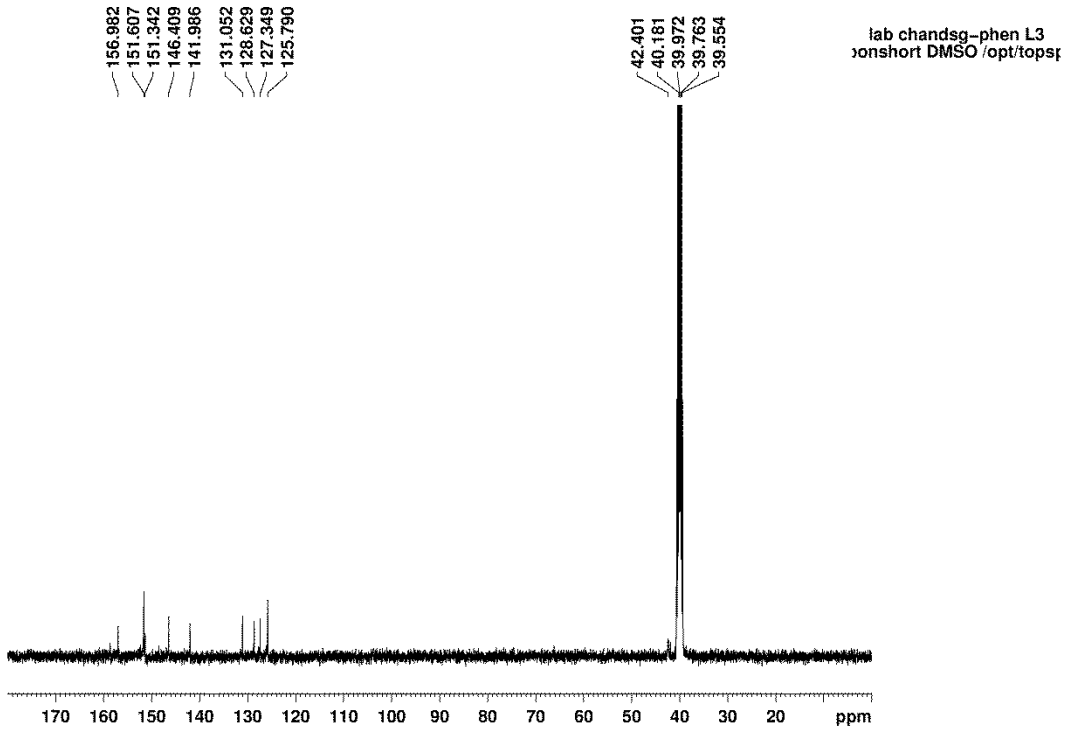

Figure S14. ^{13}C NMR spectrum of **4** in DMSO-d_6.

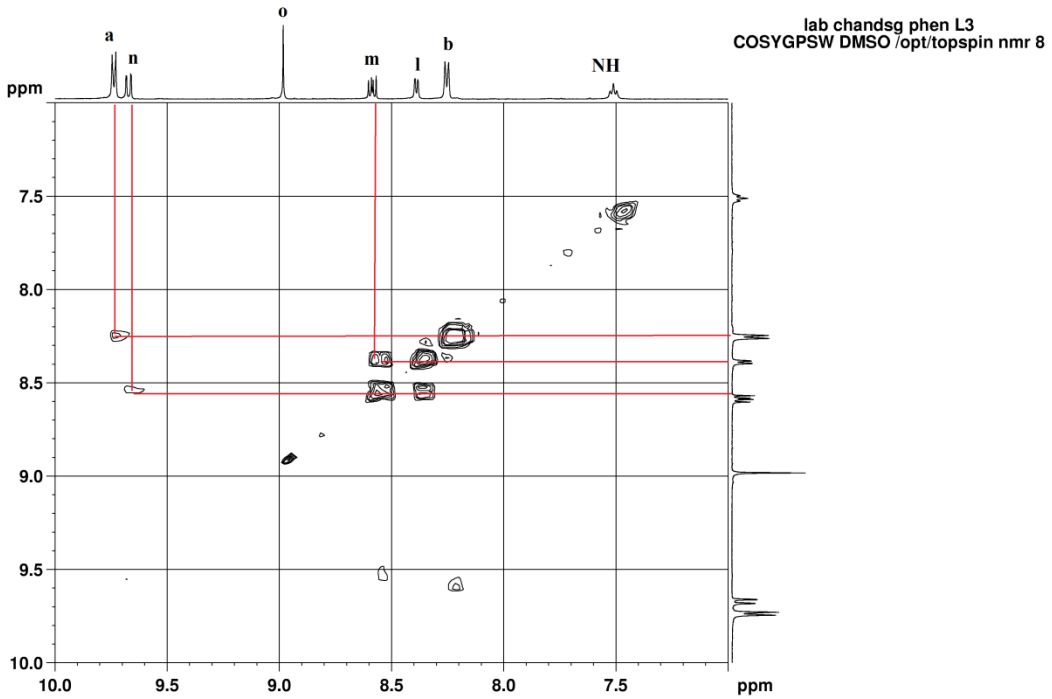

Figure S15. H-H COSY of **4** in DMSO-d_6.

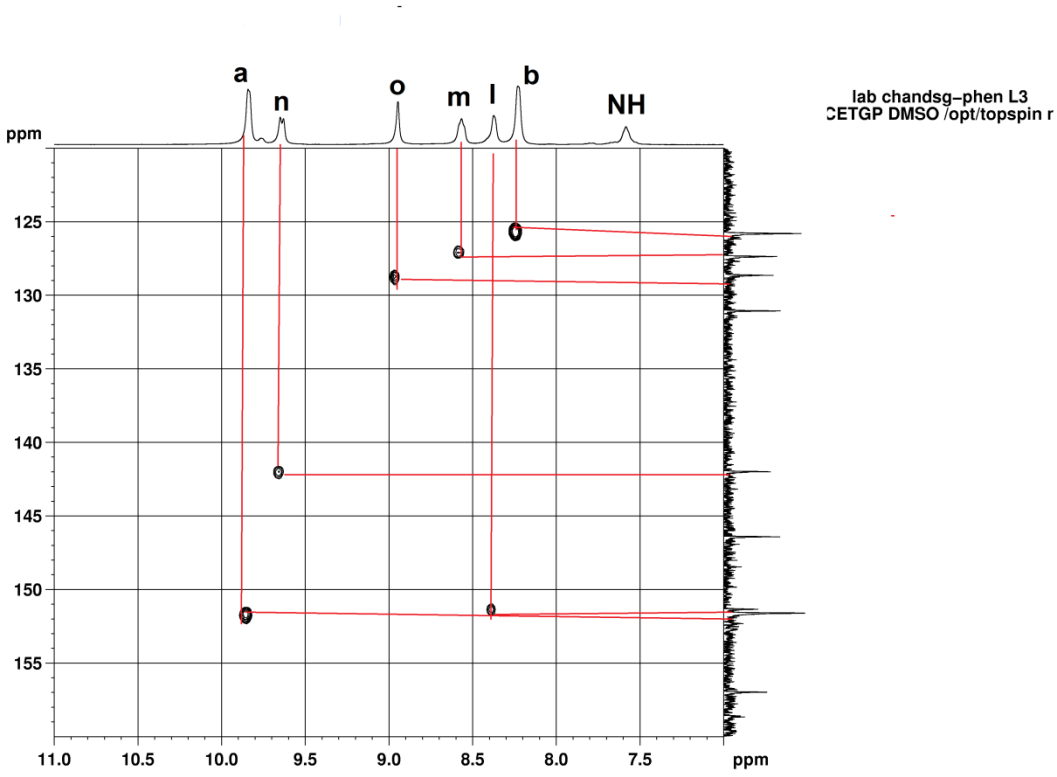

Figure S16. HSQC of **4** in DMSO-d_6.

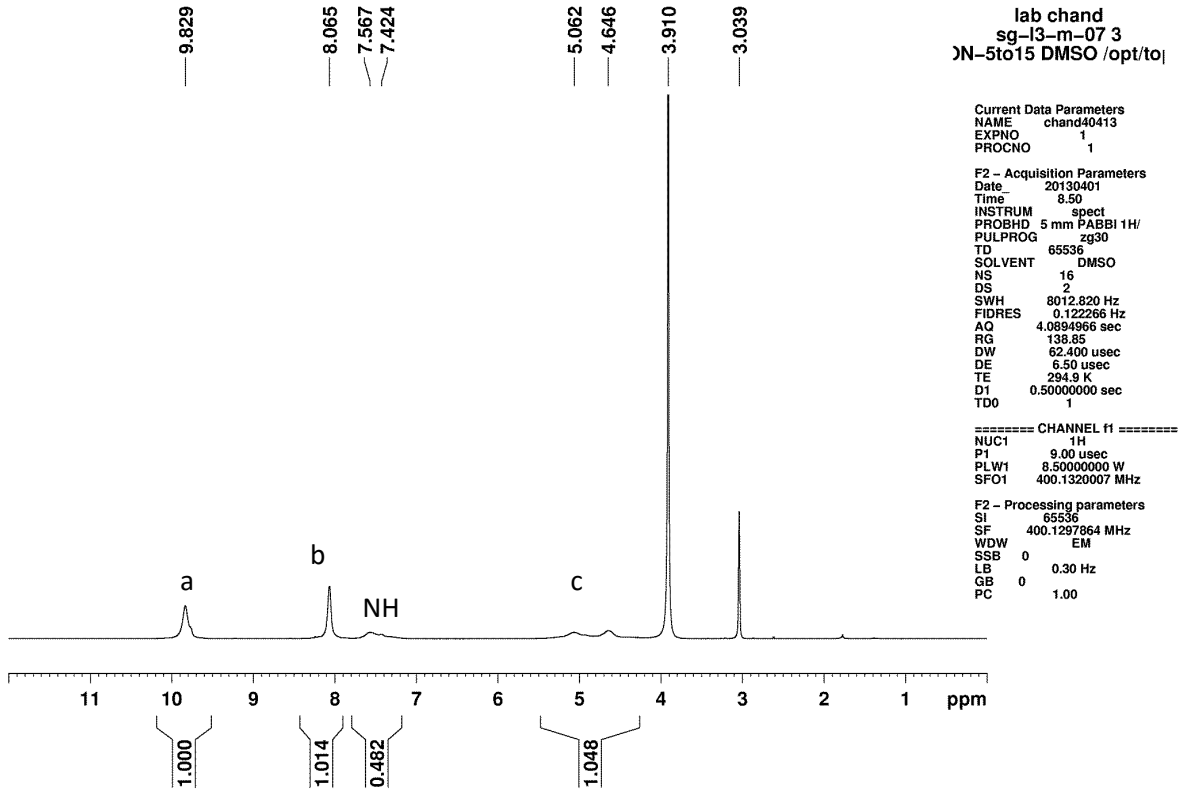

Figure S17 ^{1}H NMR spectrum of **5** in DMSO-d_6.

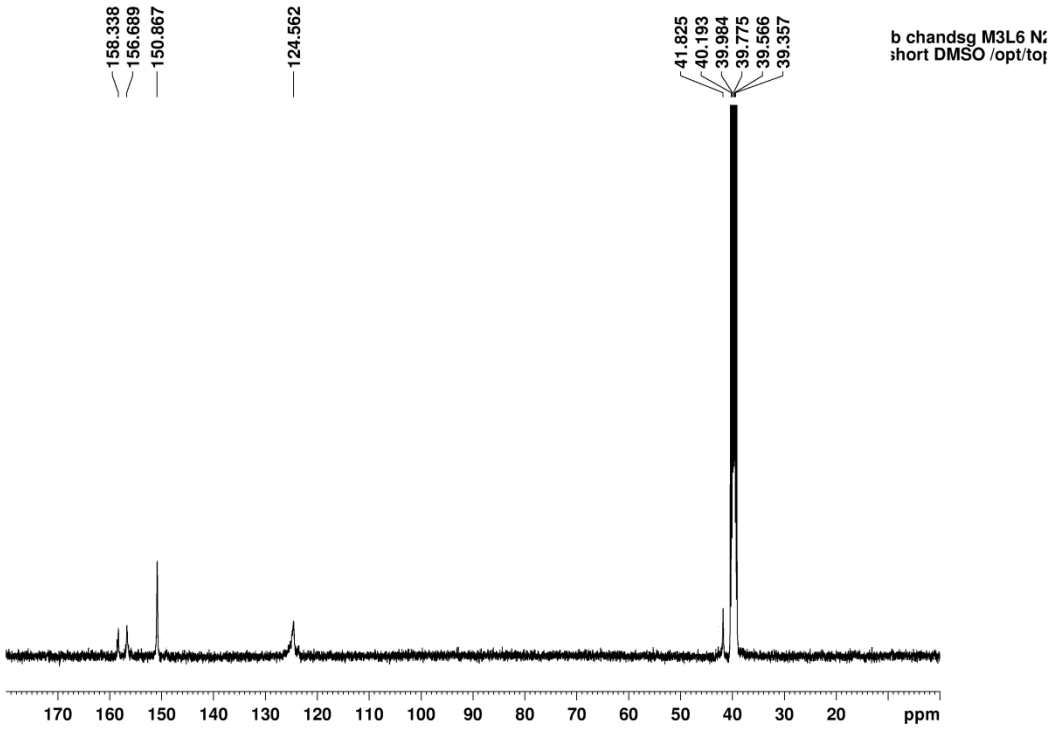

Figure S18 ^{13}C NMR spectrum of **5** in DMSO-d_6.

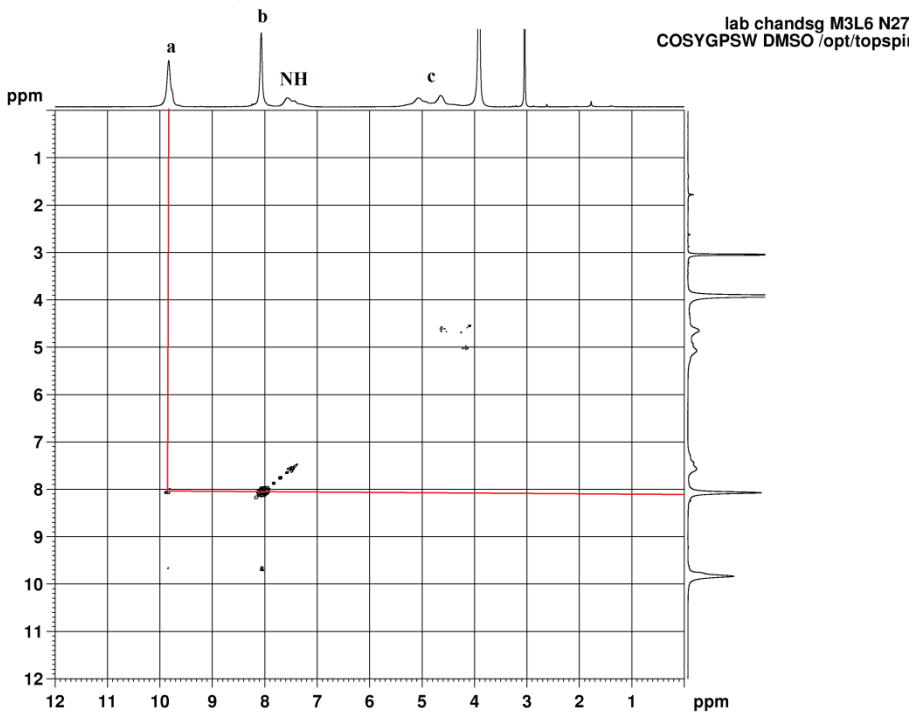

Figure S19. H-H COSY of **5** in DMSO-d_6.

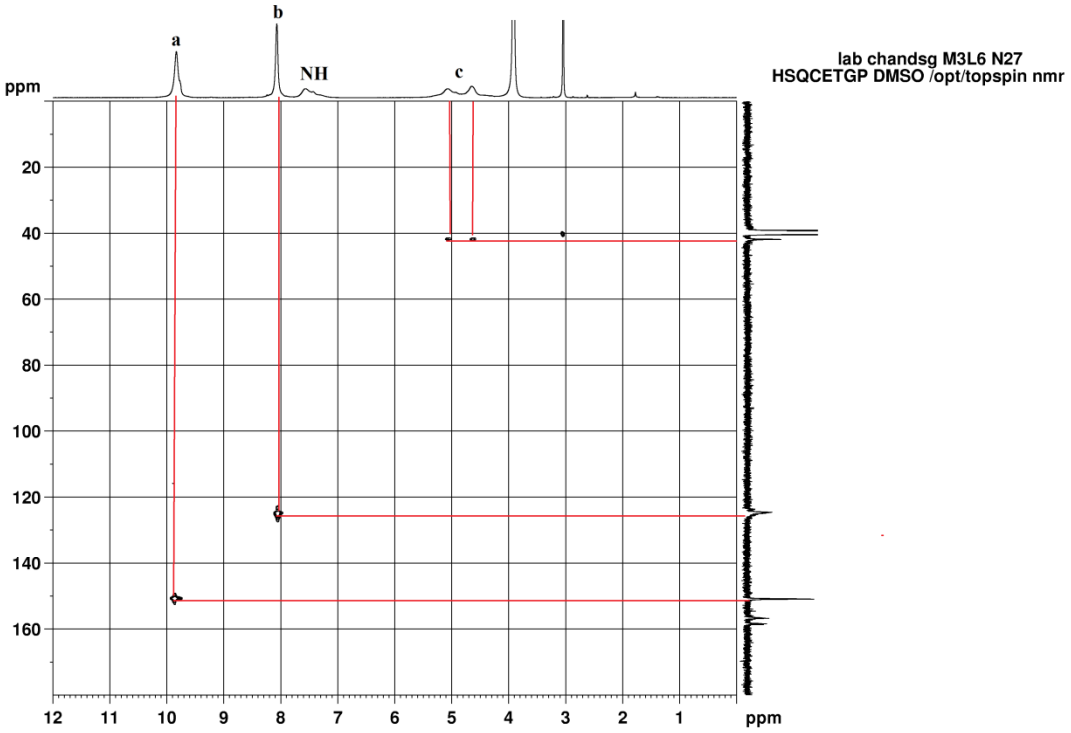

Figure S20. HSQC of **5** in DMSO-d_6.

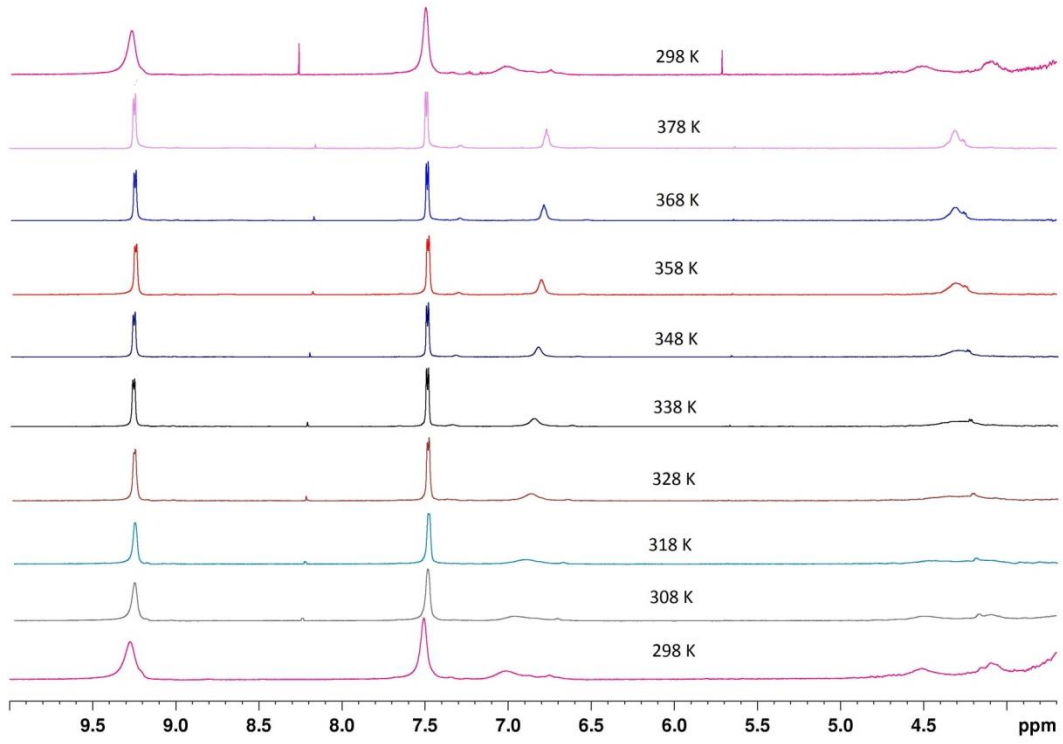

Figure S21: Variable temperature ^{1}H NMR spectra of **5** (298 to 378 K, then cooled down to 298 K) in DMSO-$d_{6.}$

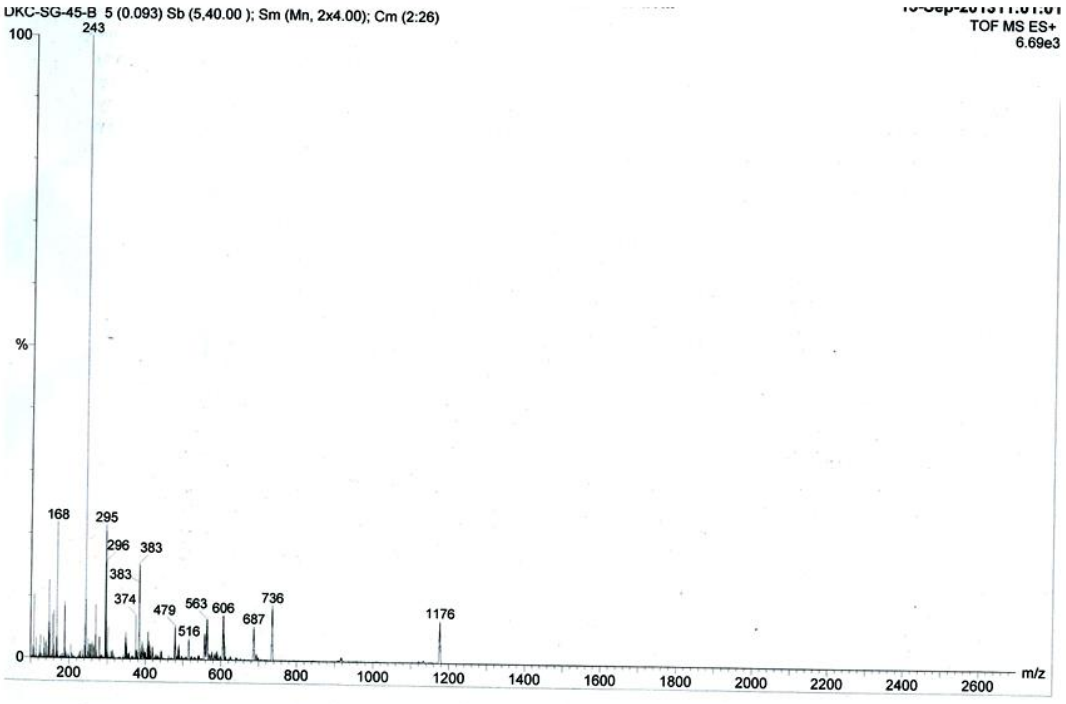

Figure S22. ESI-MS spectrum of **1**.

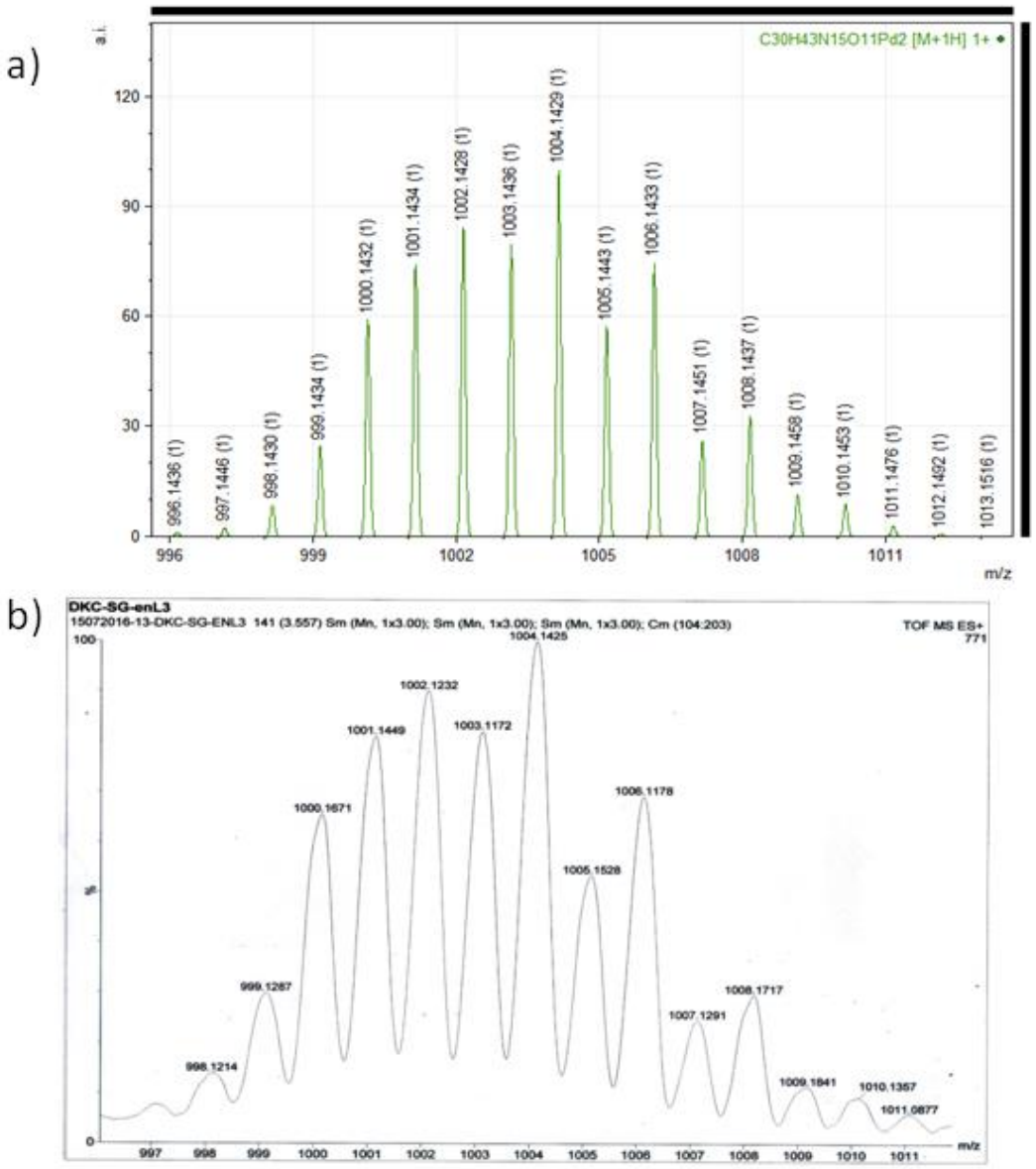

Figure S23. ESI-MS of complex **1** showing the isotopic distribution of the cation $[\mathbf{1}\text{-}NO_3]^{1+}$, a) theoretical and b) experimental.

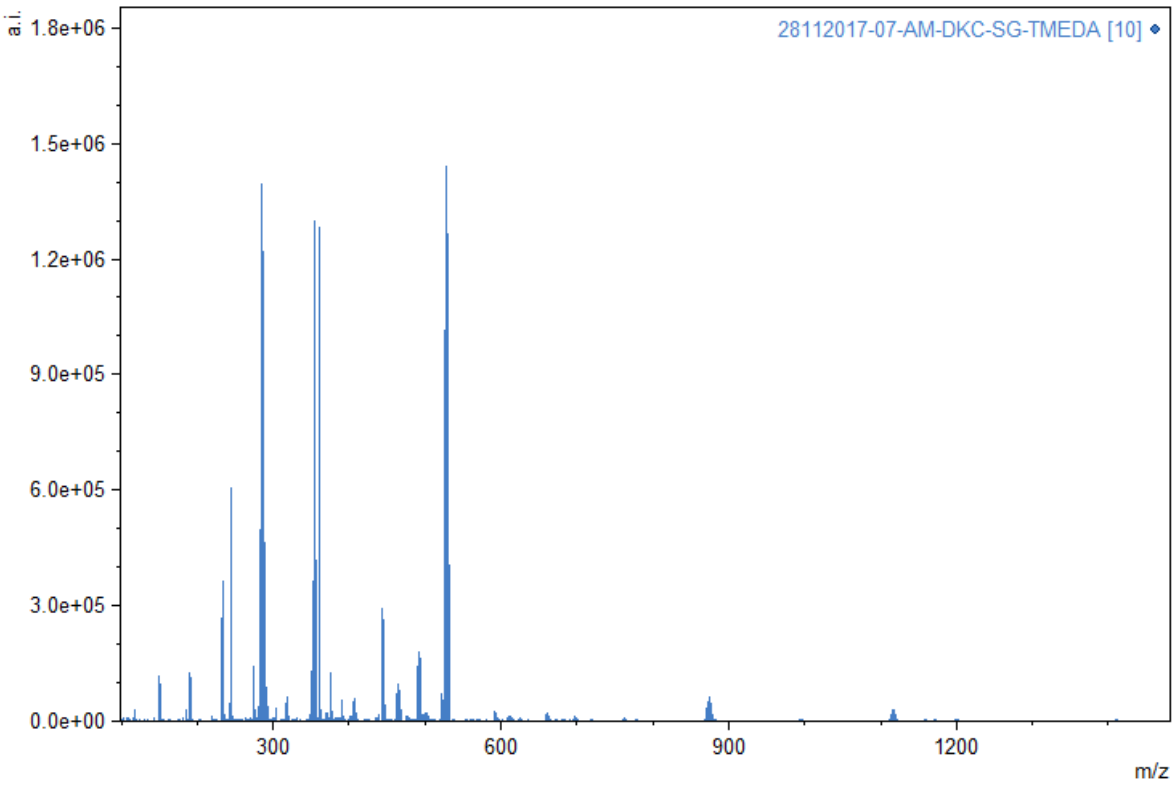

Figure S24. ESI-MS spectrum of **2**.

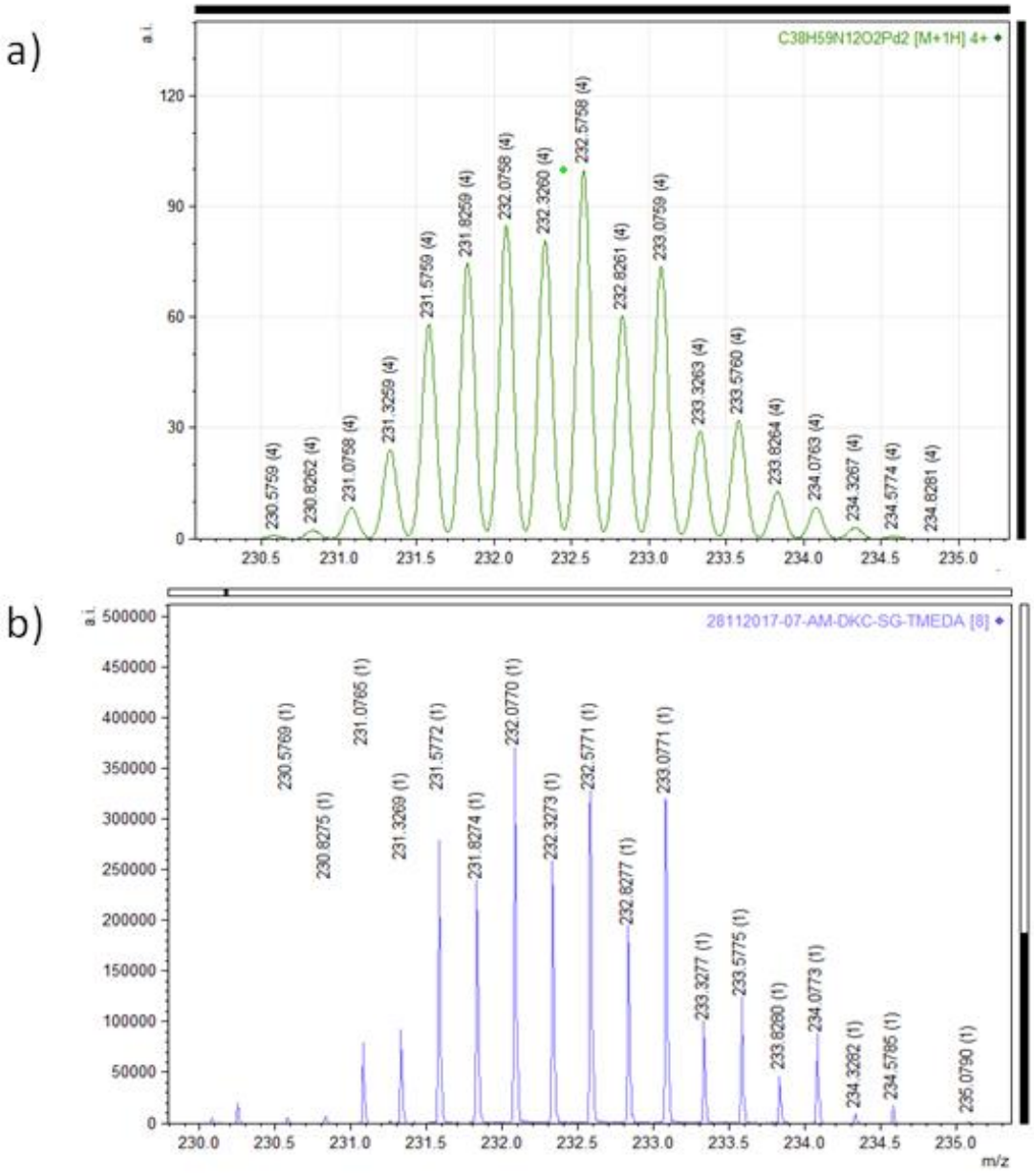

Figure S25. ESI-MS of complex **2** showing the isotopic distribution of the polycation [**2**-$4NO_3$]$^{4+}$, a) theoretical and b) experimental.

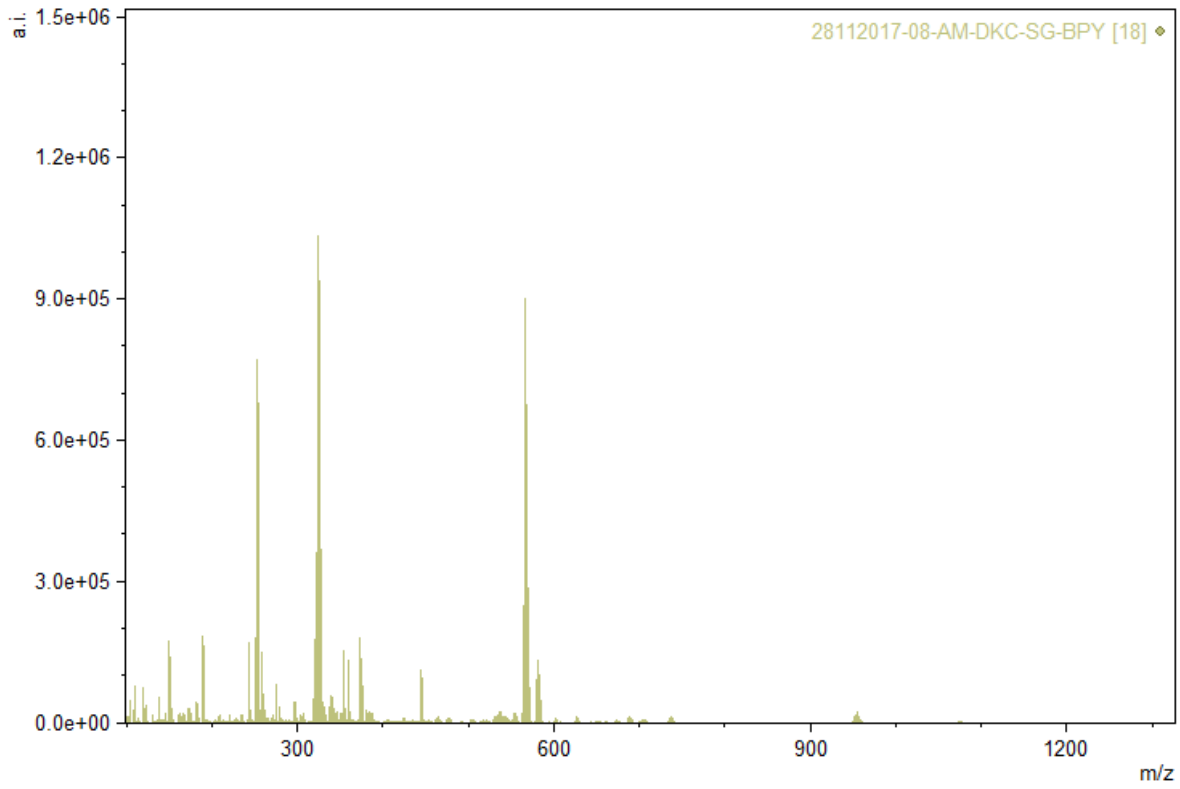

Figure S26.ESI-MS spectrum of **3**.

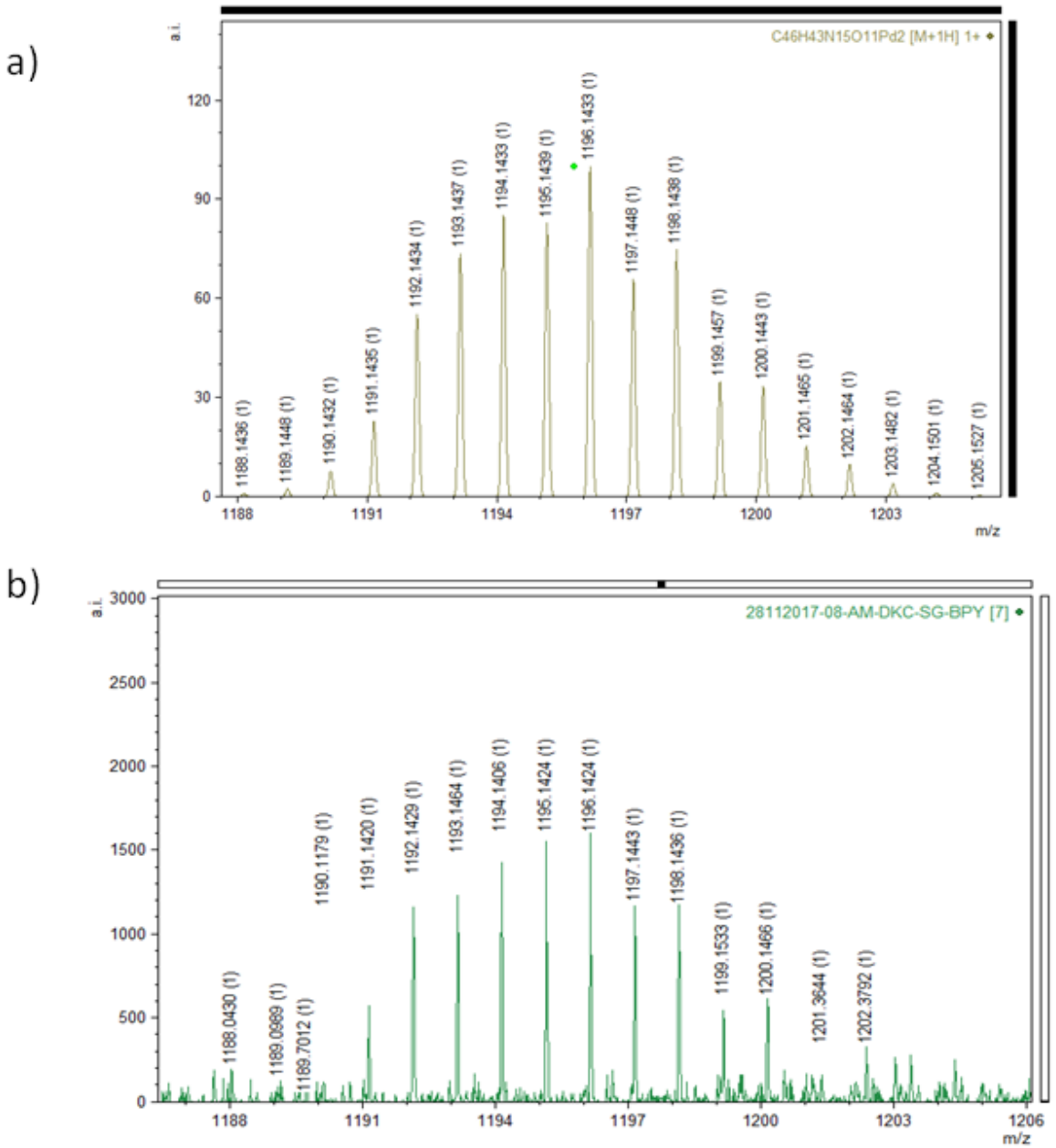

Figure S27. ESI-MS of complex **3** showing the isotopic distribution of the cation [**3**-NO_3]$^{1+}$, a) theoretical and b) experimental.

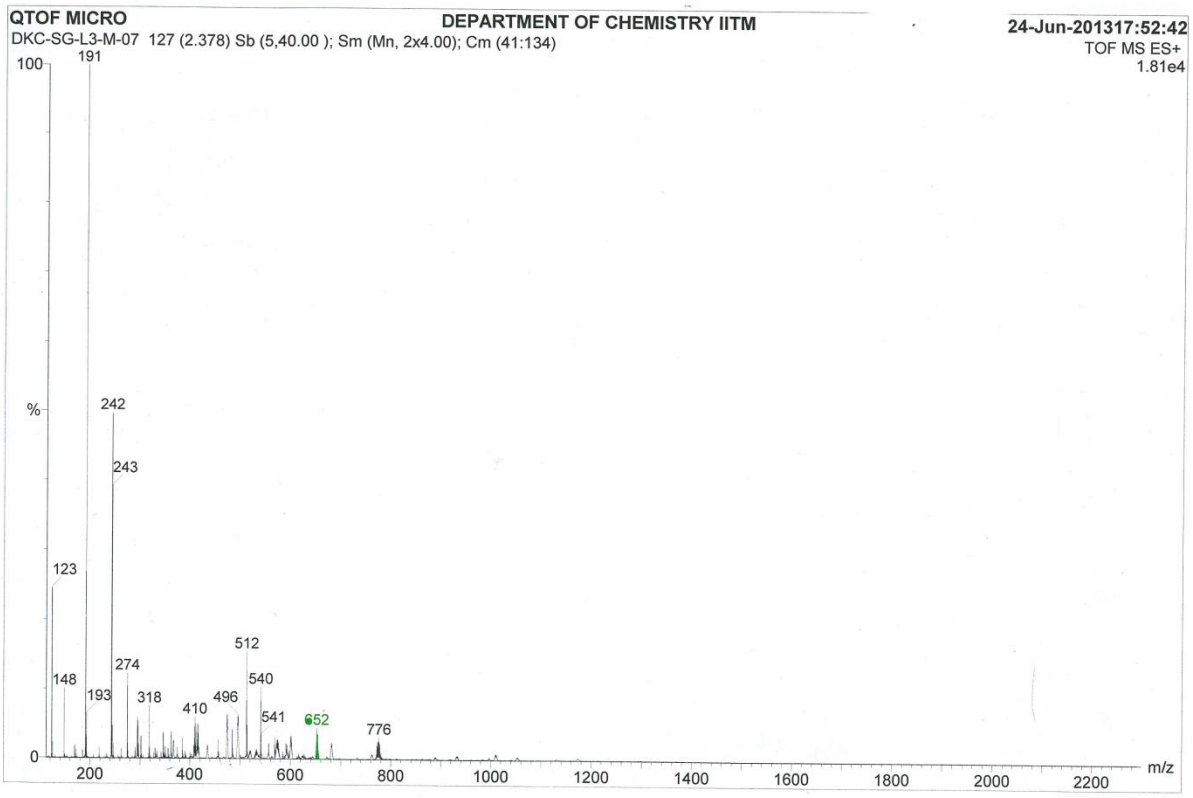

Figure S28. ESI-MS spectrum of **5**.

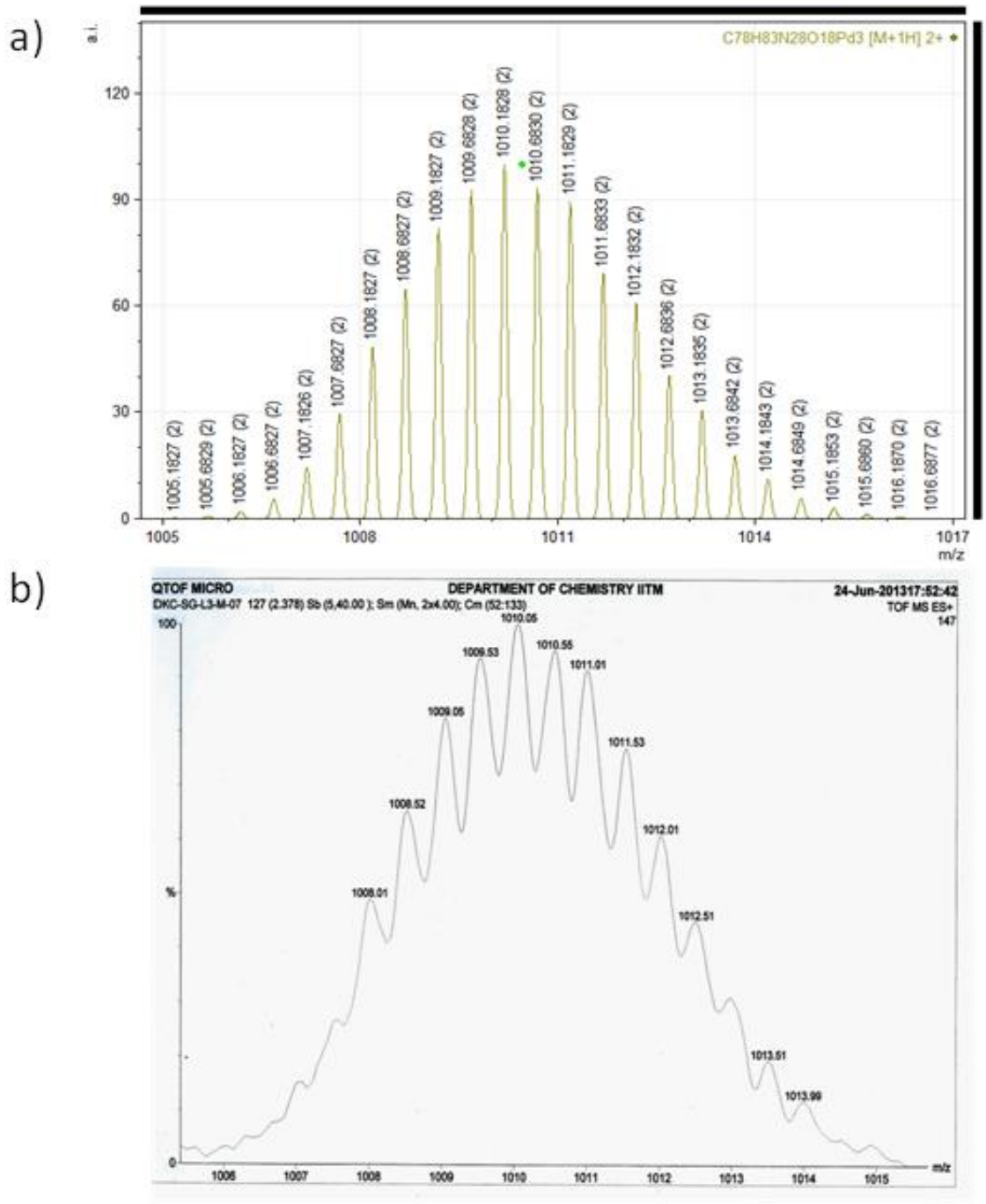

Figure S29. ESI-MS of complex **5** showing the isotopic distribution of the polycation [**5**-2NO_3]$^{2+}$, a) theoretical and b) experimental.

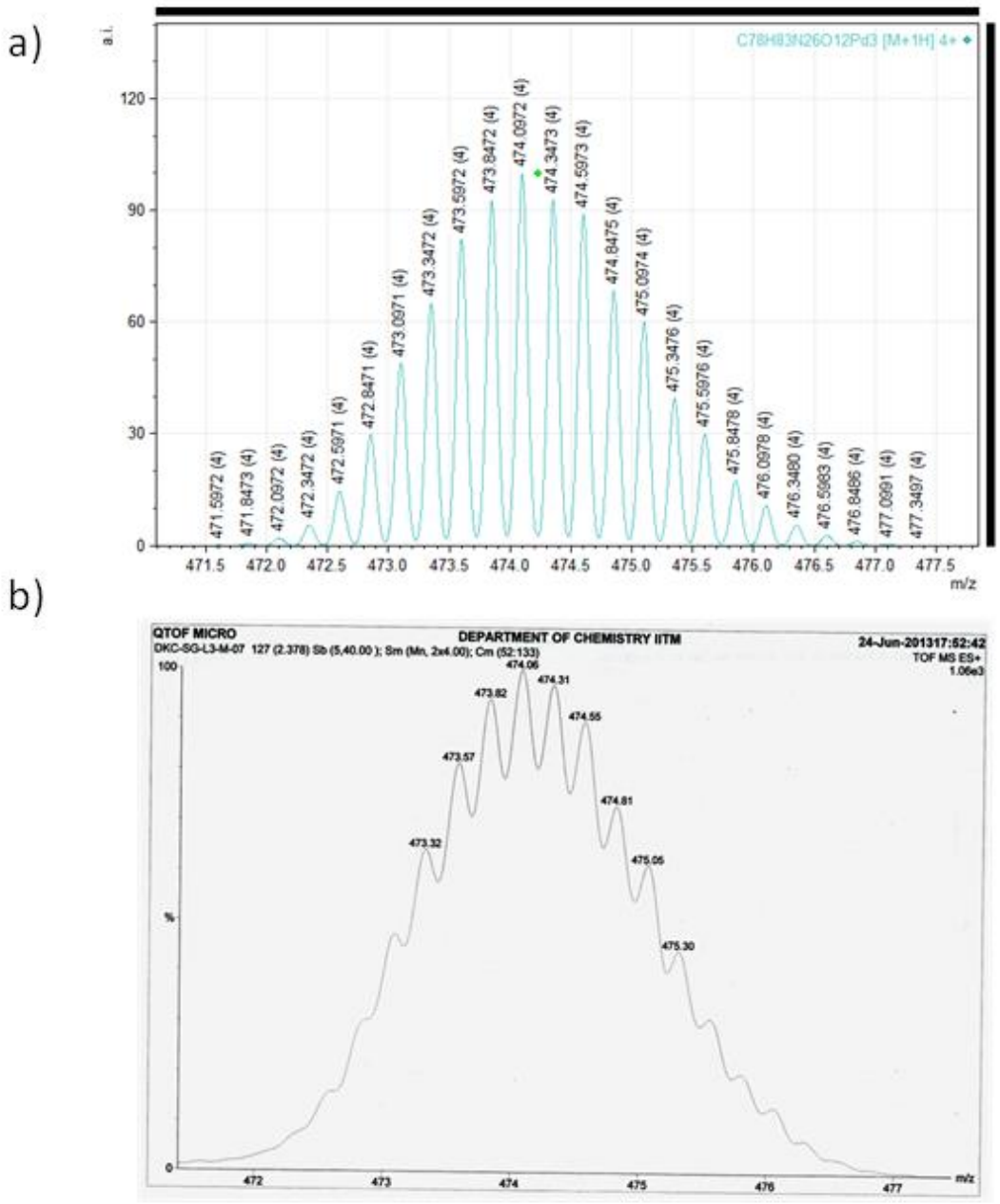

Figure S30. ESI-MS of complex **5** showing the isotopic distribution of the polycation [**5**-$4NO_3$]$^{4+}$, a) theoretical and b) experimental.

Geometry optimizations were performed by using density functional theory (DFT). DFT study was performed with the Gaussian 09 software package. The B3LYP (Becke's three parameter hybrid functional using the LYP correlation) functional was used for geometry optimizations and frequencies with LANL2DZ for Pd atom, and the 6-31G* basis set for carbon, nitrogen, oxygen and hydrogen. Frequency calculations were performed for the optimized structures to confirm the absence of any imaginary frequencies.[1]

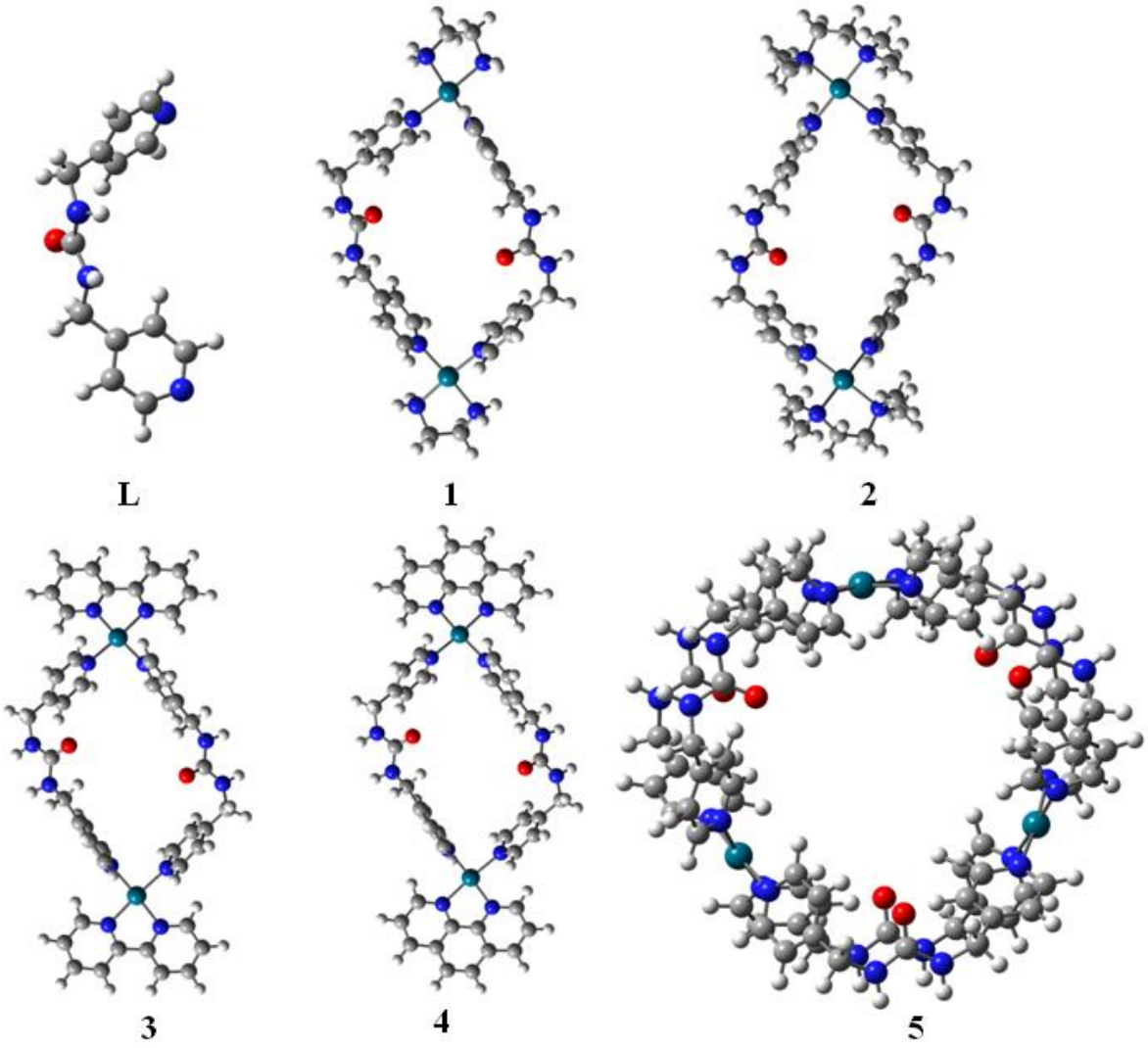

Figure S31. Energy-minimized structures of the ligand **L** and complexes **1-5**.

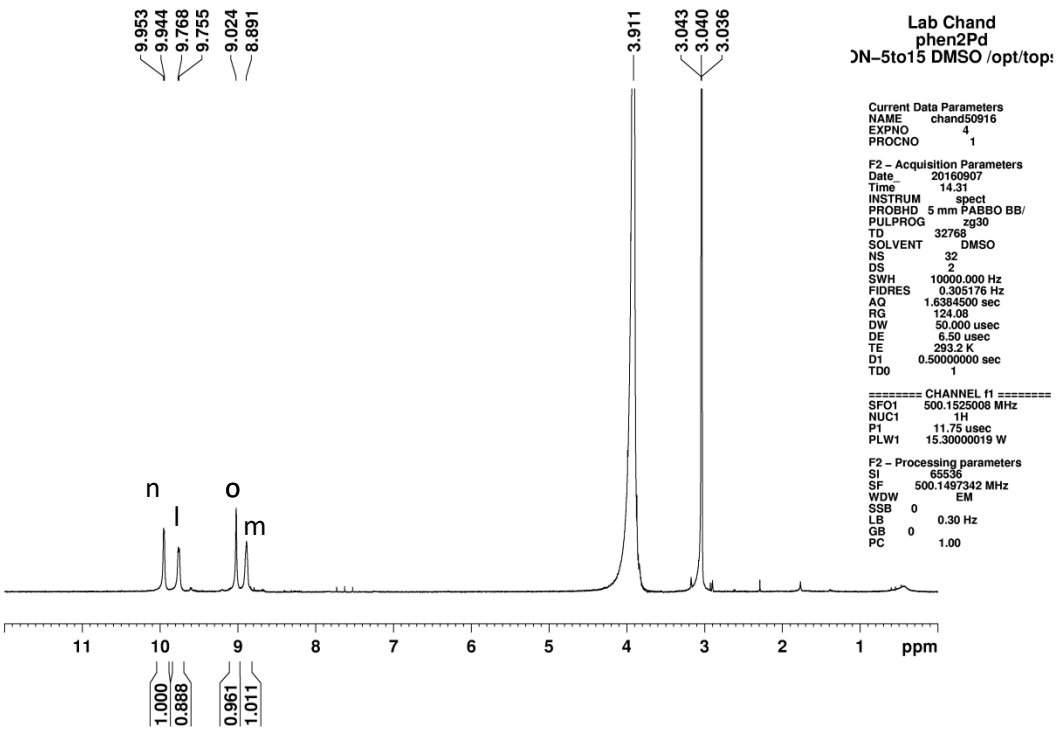

Figure S32. [1]H NMR spectrum of complex **9** in DMSO-d_6.

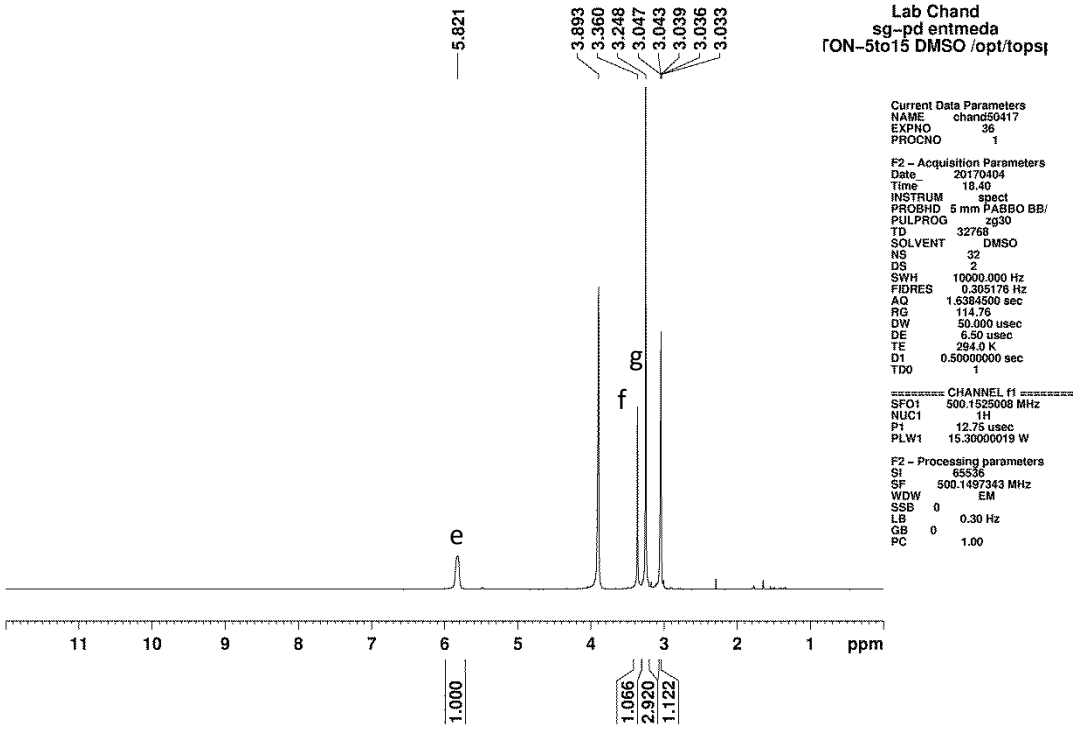

Figure S33. [1]H NMR spectrum of complex **10** in DMSO-d_6.

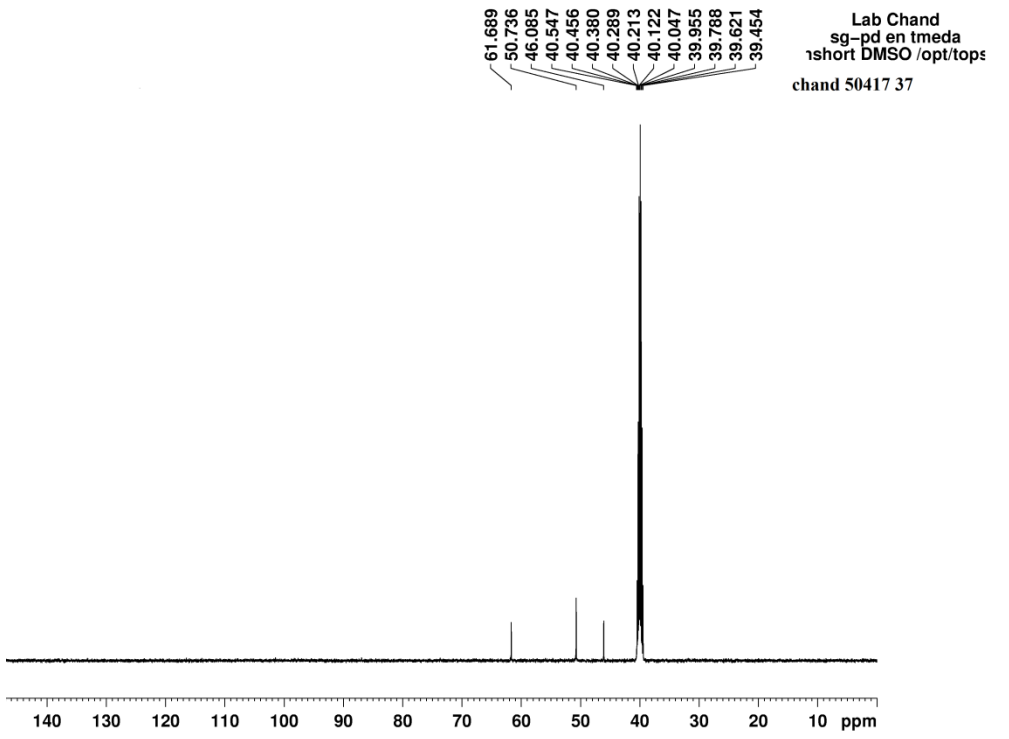

Figure S34. [13]C NMR spectrum of complex **10** in DMSO-d_6.

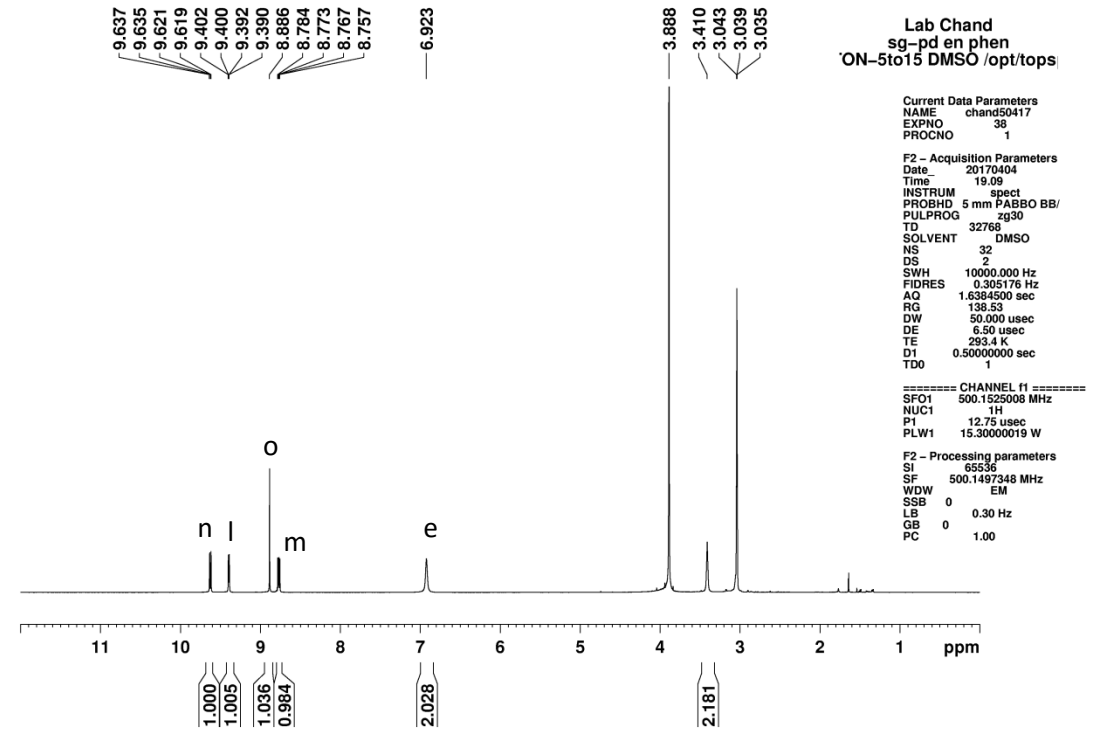

Figure S35. [1]H NMR spectrum of complex **12** in DMSO-d_6.

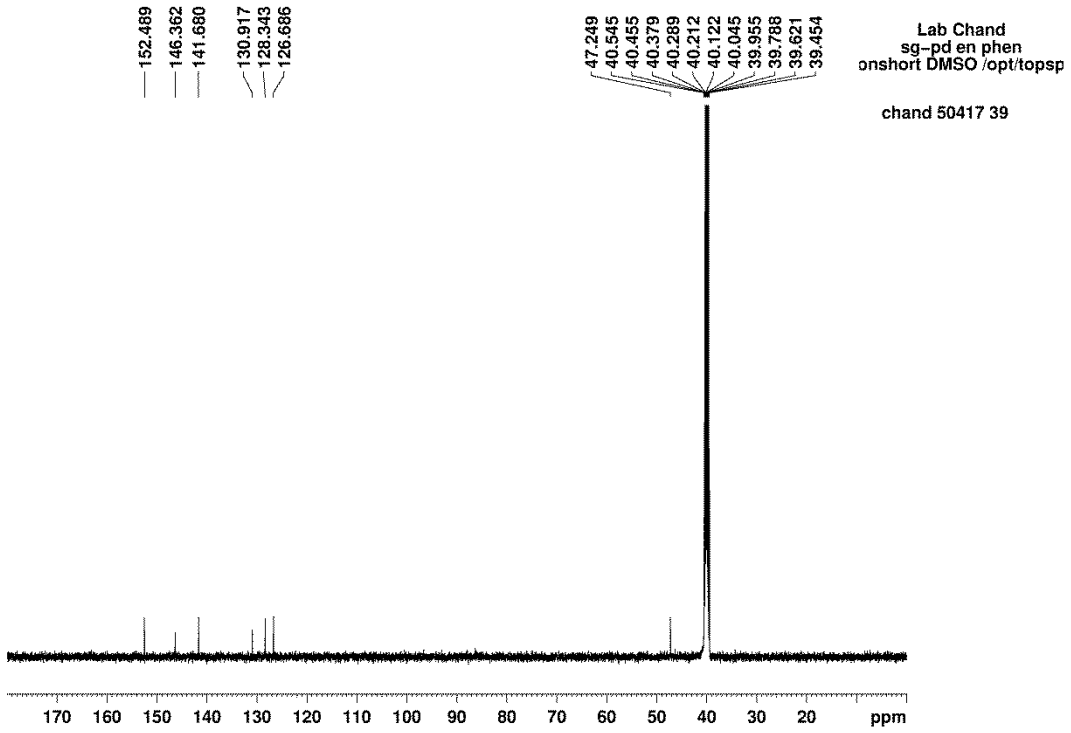

Figure S36. ^{13}C NMR spectrum of complex **12** in DMSO-d_6.

Interaction of 6 with 7 (fusion type) forming 10:

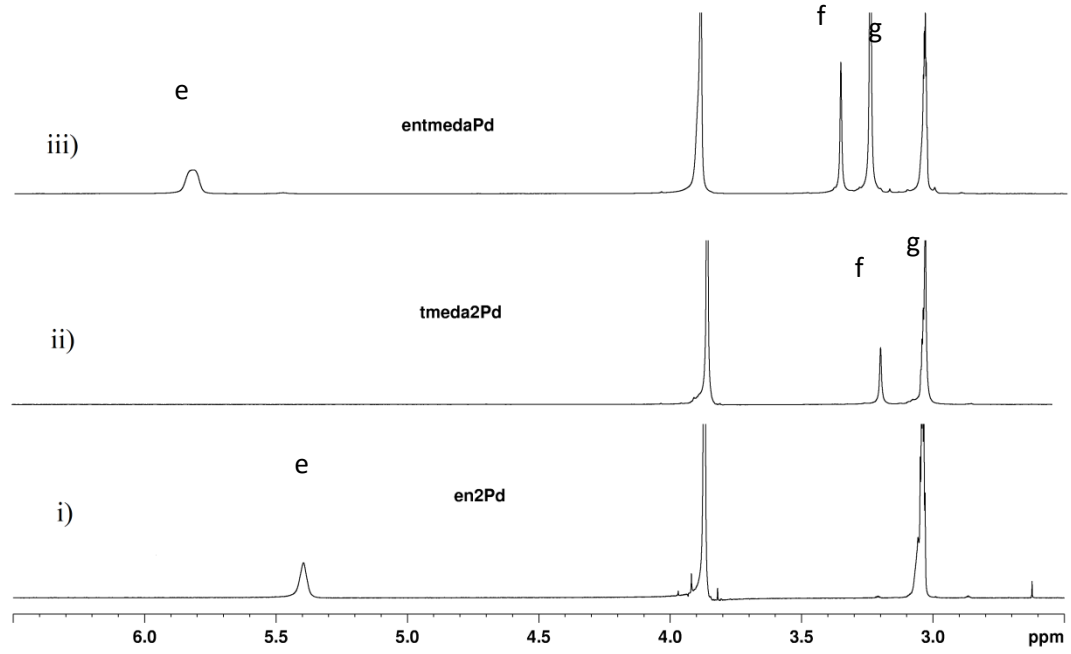

Figure S37. ^{1}H NMR spectra in DMSO-d_6 at room temperature for the complex (i) **6**, (ii) **7**, and (iii) **10** (obtained by combining **6** and **7** at 90 °C over a period of for 12 h).

Interaction of 6 with 8 (fusion type) forming 11:[2]

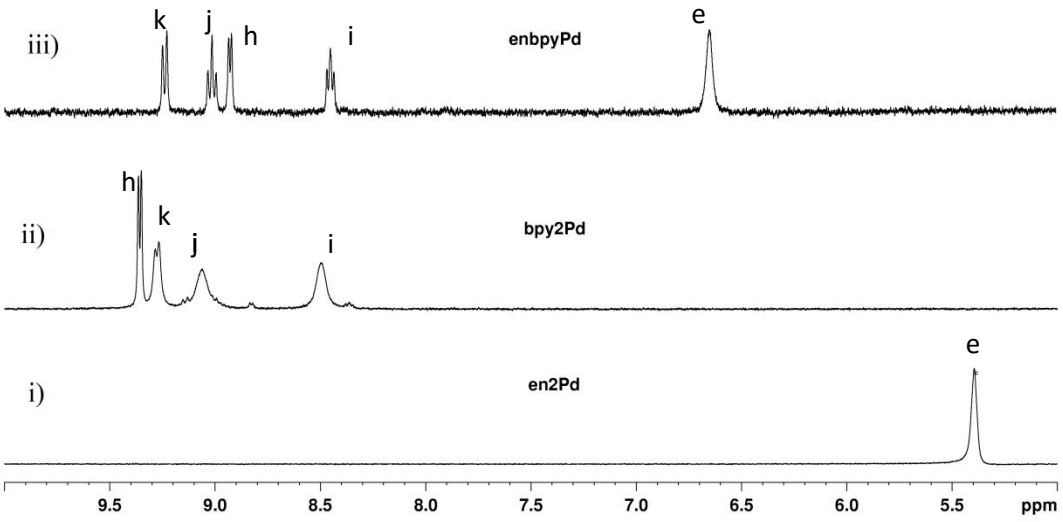

Figure S38. ^{1}H NMR spectra in DMSO-d_6 at room temperature for the complex (i) **6**, (ii) **7**, and (iii) **11**, (obtained by combining **6** and **8** at 90 °C over a period of for 12 h).

Interaction of 6 with 9 (fusion type) forming 12:

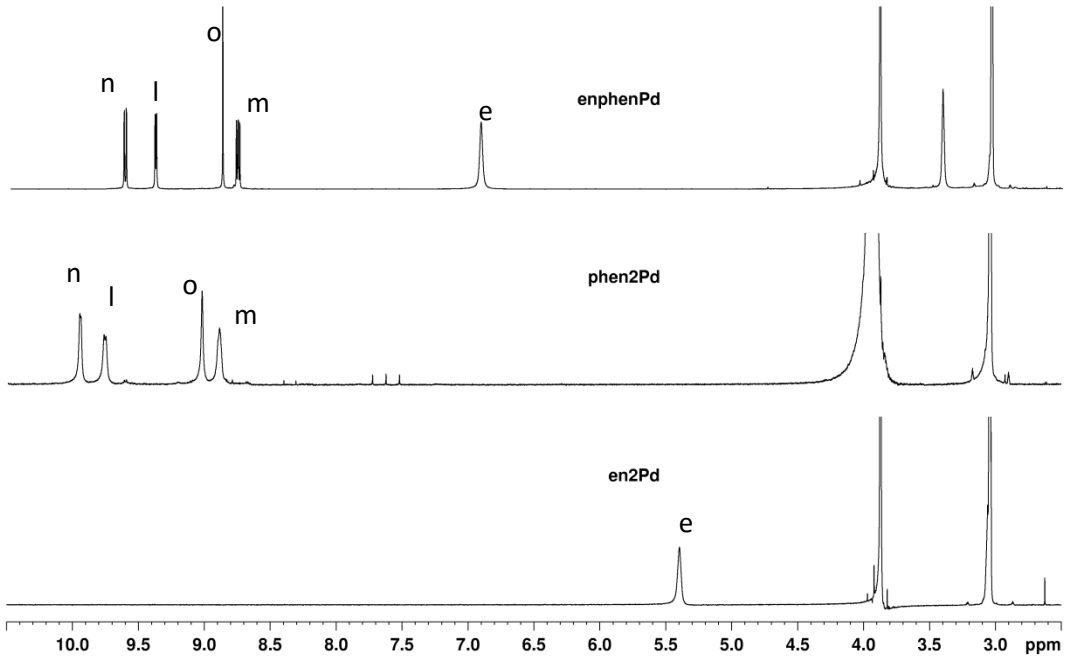

Figure S39. ^{1}H NMR spectra in DMSO-d_6 at room temperature for the complex (i) **6**, (ii) **9**, and (iii) **12**, (obtained by combining **6** and **9** at 90 °C over a period of for 12 h).

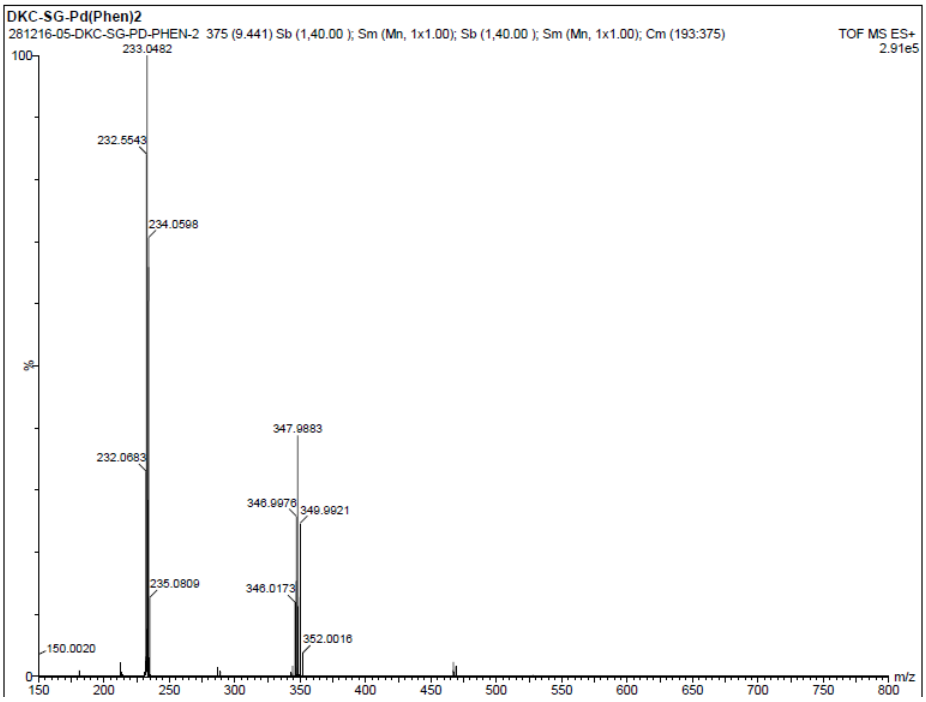

Figure S40. ESI-MS spectrum of **9**.

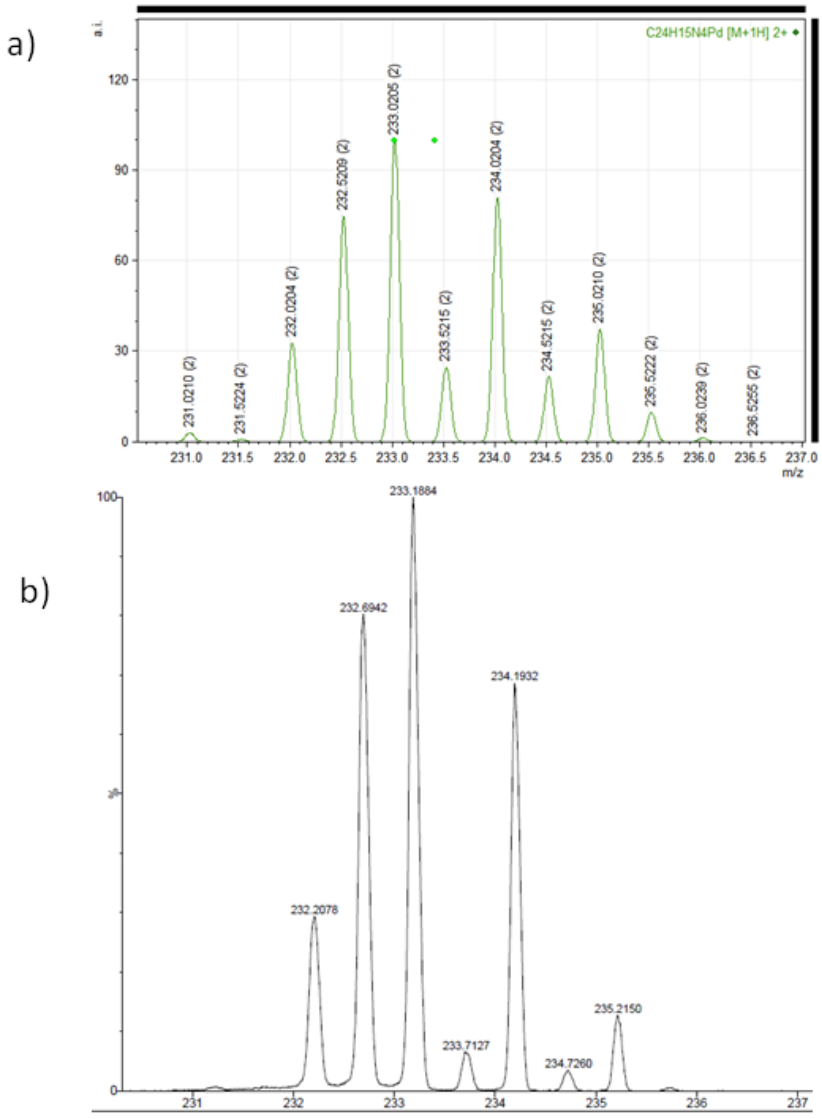

Figure S41. ESI-MS of complex **9** showing the isotopic distribution of the polycatyion [**9** - $2NO_3$]$^{2+}$, a) theoretical and b) experimental.

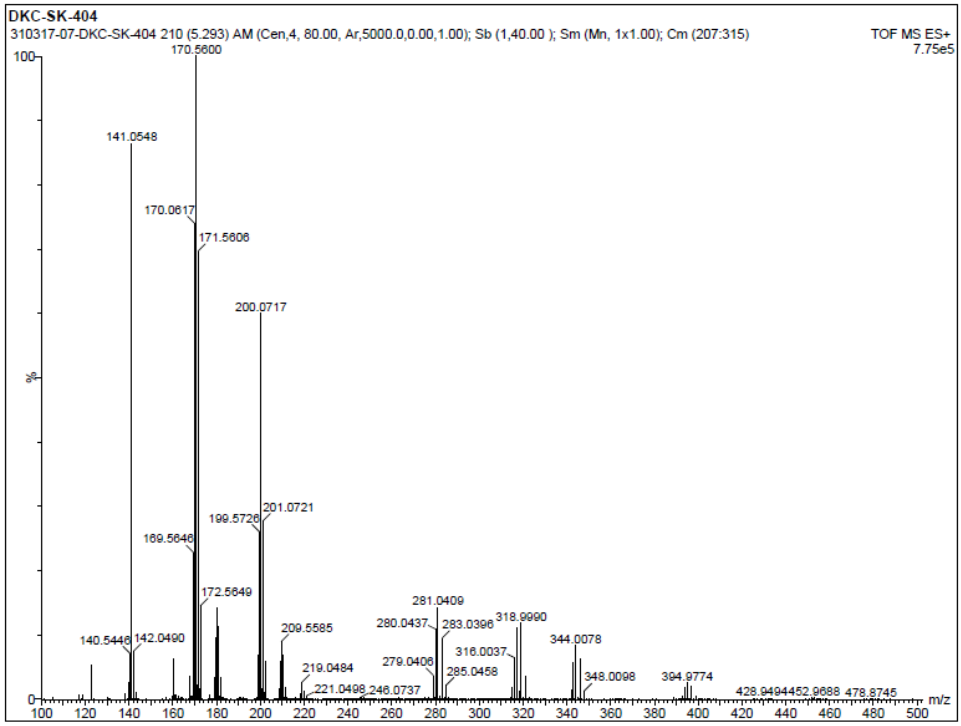

Figure S42. ESI-MS spectrum of **10**.

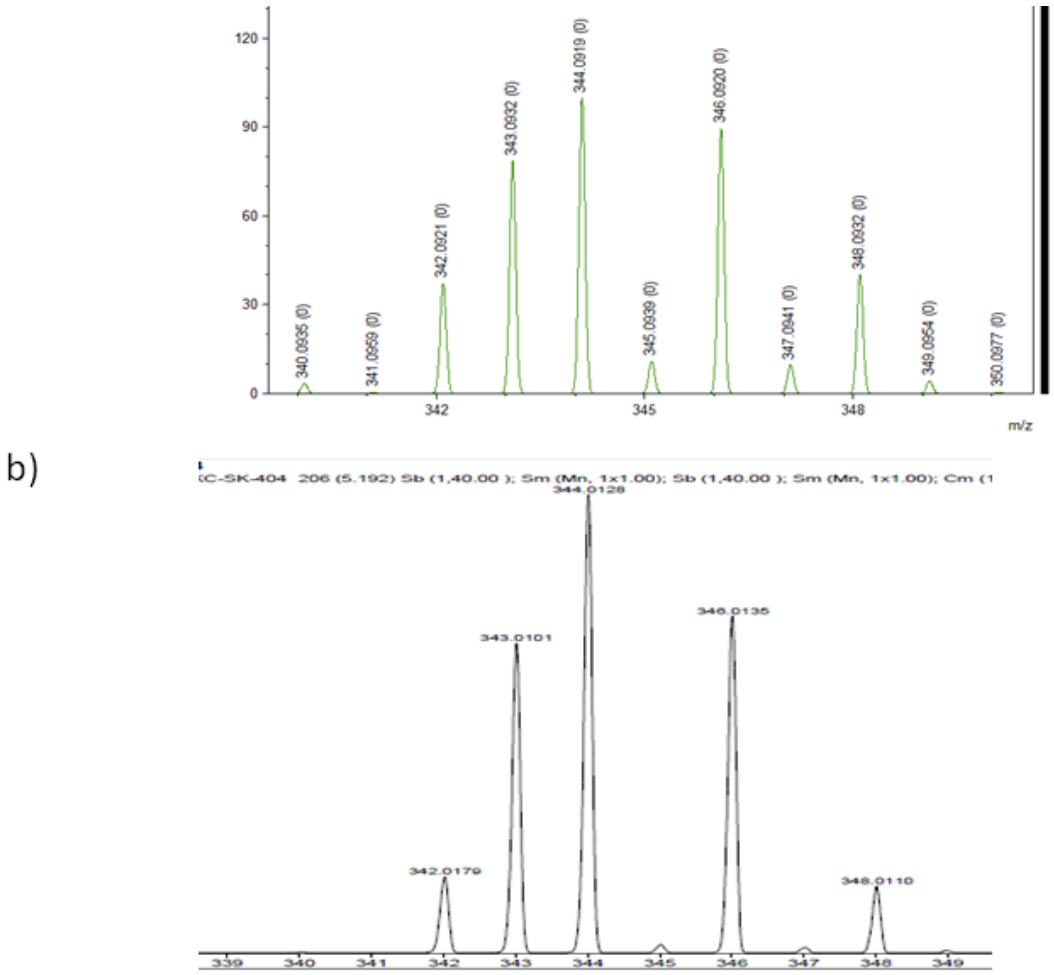

Figure S43. ESI-MS of complex **10** showing the isotopic distribution of the cation [**10**-NO_3]$^+$, a) theoretical and b) experimental.

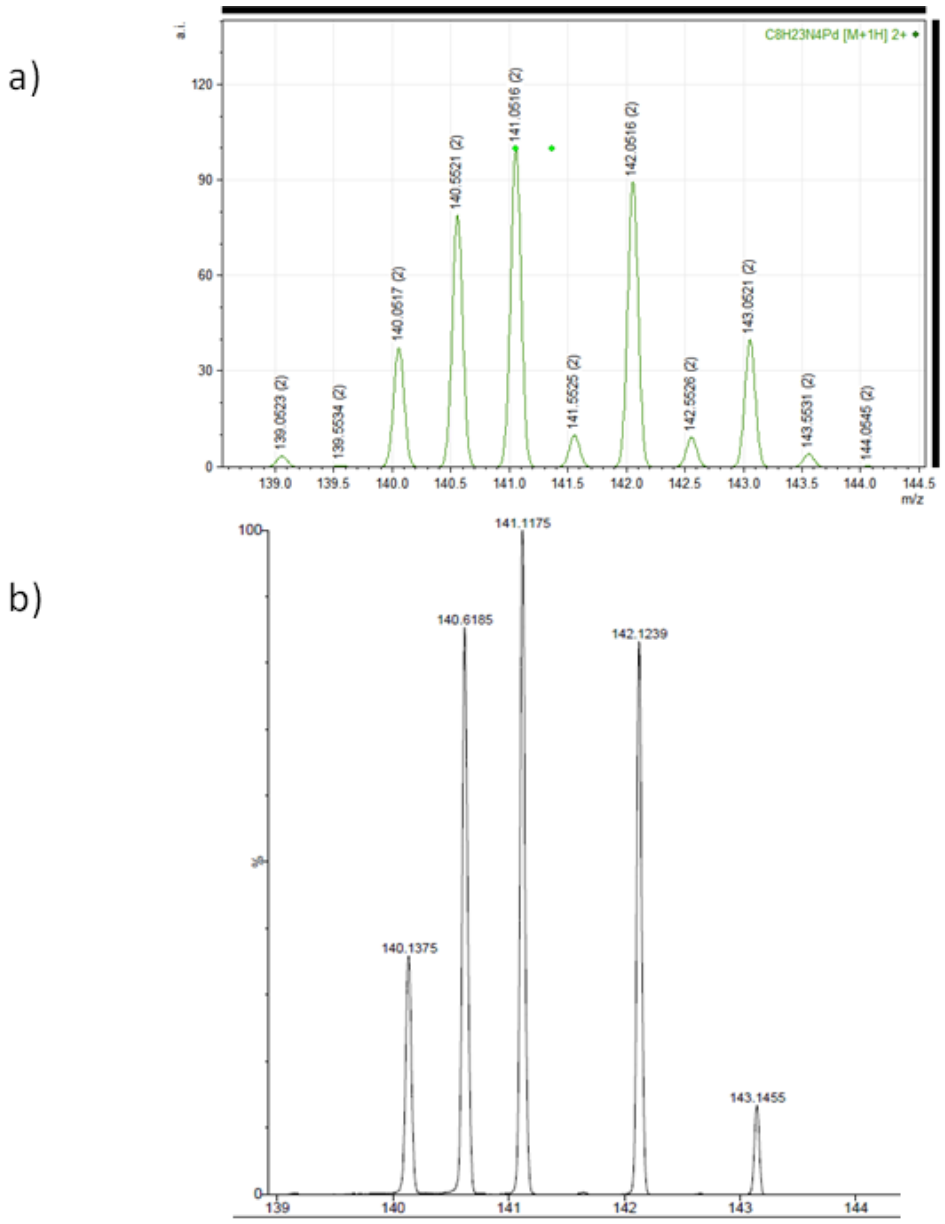

Figure S44. ESI-MS of complex **10** showing the isotopic distribution of the polycation [**10** - $2NO_3$]$^{2+}$, a) theoretical and b) experimental.

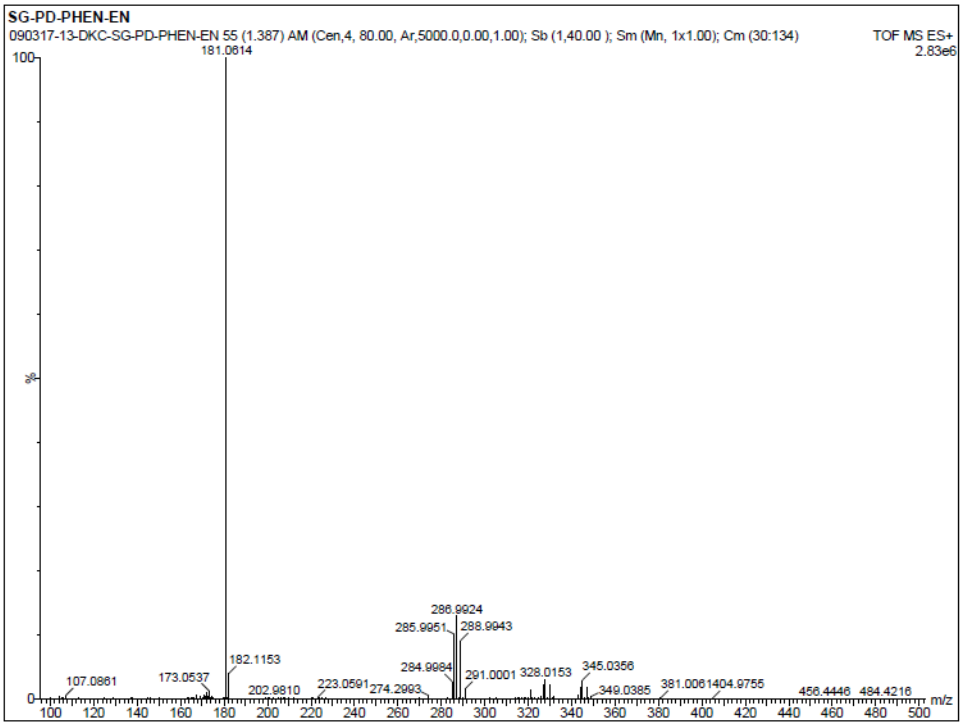

Figure S45. ESI-MS spectrum of **12**.

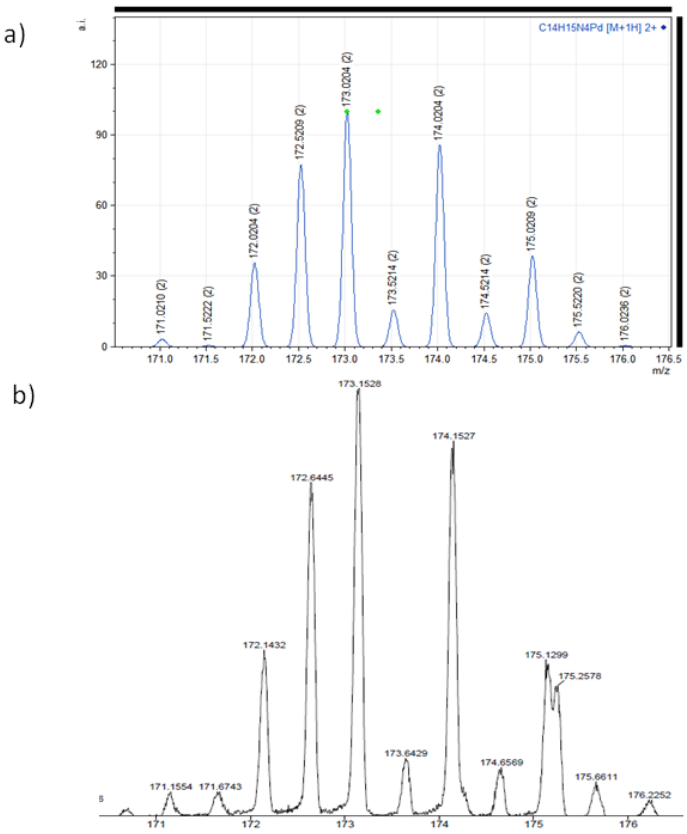

Figure S46. ESI-MS of complex **12** showing the isotopic distribution of the polycation [**12** - $2NO_3$]$^{2+}$, a) theoretical and b) experimental.

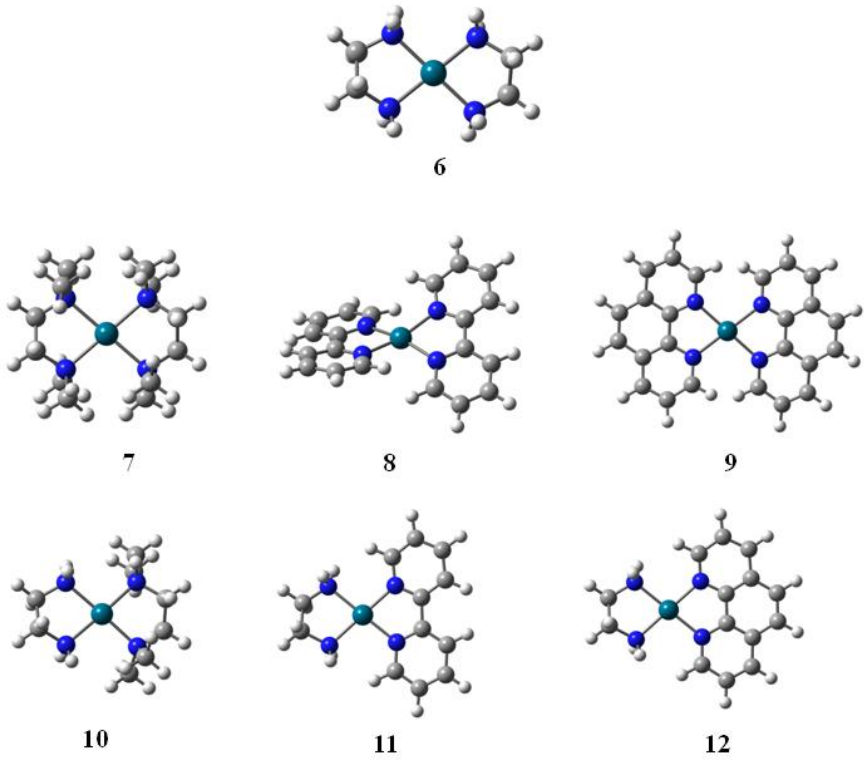

Figure S.47 Energy-minimized structures of the complexes **6-12**.

Table S1: ΔE, ΔH, and ΔG values of (i) $[Pd(en)_2]^{2+}$, **6**, (ii) $[Pd(tmeda)_2]^{2+}$, **7**, (iii) $[Pd(bpy)_2]^{2+}$, **8**, (iv) $[Pd(phen)_2]^{2+}$, **9**, (v) $[Pd(en)(tmeda)]^{2+}$, **10**, (vi) $[Pd(en)(bpy)]^{2+}$, **11**, and (vii) $[Pd(en)(phen)]^{2+}$.

S.NO.	Compound	Total Energy (kcal mol^{-1})	Enthalpy (kcal mol^{-1})	Gibbs Free energy (kcal mol^{-1})
i	**6**	-318196.0903	-318195.4979	-318225.5029
ii	**7**	-515373.4435	-515372.8512	-515416.2058
iii	**8**	-700758.4261	-700757.8338	-700800.9907
iv	**9**	-796414.3306	-796413.7382	-796458.4332
v	**10**	-416791.3259	-416790.7336	-416828.0509
vi	**11**	-509481.3562	-509480.7638	-509517.7109
vii	**12**	-557311.3403	-557310.7479	-557348.1255

Table S2: ΔE, ΔH, ΔG and ΔS values of the mononuclear supramolecular transformations

S.NO.	Equations	ΔE (kcal mol^{-1})	ΔH (kcal mol^{-1})	ΔG (kcal mol^{-1})	ΔS (kcal $mol^{-1}K^{-1}$)
i	**6+7----->10**	-13.11807564	-13.11807564	-14.39317393	0.003512667
ii	**6+8----->11**	-8.195895049	-8.195895049	-8.928198052	0.002017364
iii	**6+9----->12**	-12.25964333	-12.25964333	-12.31486413	0.000152123

(1) **With reference to the equation 1:** The overall free energy and the enthalpy for the formation of $[Pd(en)(tmeda)]^{2+}$ from 1 equiv. of $[Pd(en)_2]^{2+}$ and 1 equiv. of $[Pd(tmeda)_2]^{2+}$ (equation 1) is -14.3932 kcal mol^{-1} and -13.1181 kcal mol^{-1}, respectively, which indicates that the reaction is feasible and exothermic, probably due to steric crowding of methyl groups of tmeda in self-assembled complex $[Pd(tmeda)_2]^{2+}$. The global entropy (ΔS) value is 0.0035 kcal mol^{-1} K^{-1}($\Delta S = (\Delta H-\Delta G)/T$; T = 362 K) indicates that the reaction is non-spontaneous.

(2) **With reference to the equation 2:** The overall free energy and the enthalpy for the formation of $[Pd(en)(bpy)]^{2+}$ from 1 equiv. of $[Pd(en)_2]^{2+}$ and 1 equiv. of $[Pd(bpy)_2]^{2+}$ (equation 2) is -8.9282 kcal mol^{-1} and -8.1959 kcal mol^{-1}, respectively, which indicates that the reaction is feasible and exothermic, probably due to steric crowding in self-assembled complex $[Pd(bpy)_2]^{2+}$. The global entropy (ΔS) value is 0.0020 kcal mol^{-1} K^{-1}($\Delta S = (\Delta H-\Delta G)/T$; T = 362 K) indicates that the reaction is non-spontaneous.

(3) **With reference to the equation 3:** The overall free energy and the enthalpy for the formation of $[Pd(en)(phen)]^{2+}$ from 1 equiv. of $[Pd(en)_2]^{2+}$ and 1 equiv. of $[Pd(phen)_2]^{2+}$ (equation 3) is -12.3149kcal mol^{-1} and -12.2596 kcal mol^{-1}, respectively, which indicates that the reaction is feasible and exothermic, probably due to steric crowding in self-assembled complex $[Pd(phen)_2]^{2+}$. The global entropy (ΔS) value is 0.00015 kcal mol^{-1} K^{-1}($\Delta S = (\Delta H-\Delta G)/T$; T = 362 K) indicates that the reaction is non-spontaneous.

Based on the above transformations, we can confirm that sterically crowded $[Pd(tmeda)_2]^{2+}$, $[Pd(bpy)_2]^{2+}$, and $[Pd(phen)_2]^{2+}$ transforming to less sterically crowded $[Pd(en)(tmeda)]^{2+}$, $[Pd(en)(bpy)]^{2+}$ and $[Pd(en)(phen)]^{2+}$ respectively upon treating with $[Pd(en)_2]^{2+}$. This must be the driving force for the supramolecular transformations explained in the manuscript.

Dynamic equilibrium of 1 with a mixture of 5 and 6 (Figures S41-S42)

$[Pd_2(en)_2\mathbf{L}_2](NO_3)_4$, **1** (3 mg, 0.0028 mmol) dissolved in 0.5 mL of DMSO-d_6 was kept at 90 °C for 24 h. The resulted solution was utilised for ^{1}H NMR studies.

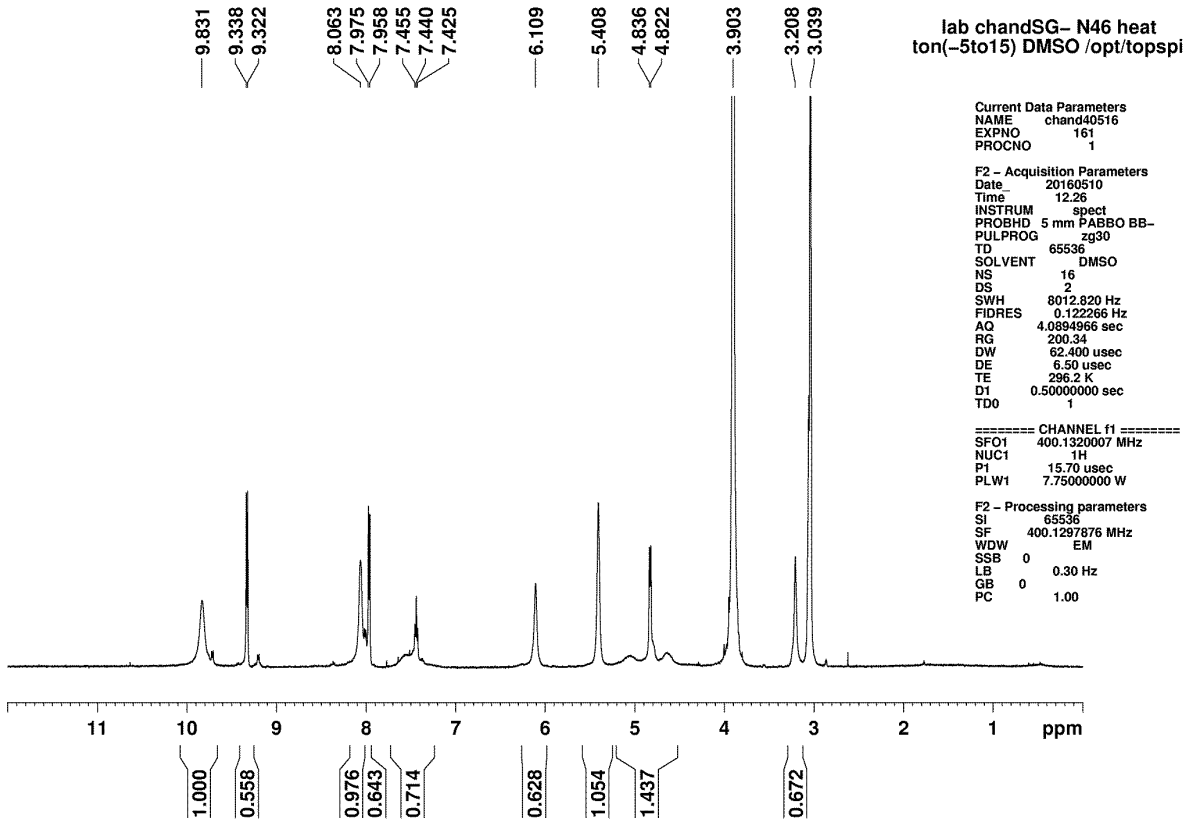

Figure S48. 400 MHz ^{1}H NMR spectrum (in DMSO-d_6 at room temperature) of equilibrium mixture of **1, 5** and **6** obtained by heating a solution of **1** (~11 mM in Pd concentration) at 90 °C for 24 h.

$[Pd_3\mathbf{L}_6](NO_3)_6$, **5** (3 mg, 0.0014 mmol) and $[Pd(en)_2](NO_3)_2$, **6** (1.5 mg, 0.0043 mmol) were dissolved in 0.5 mL of DMSO-d_6 and kept at 90 °C for 24 h. The resulted solution was utilised for ^{1}H NMR studies.

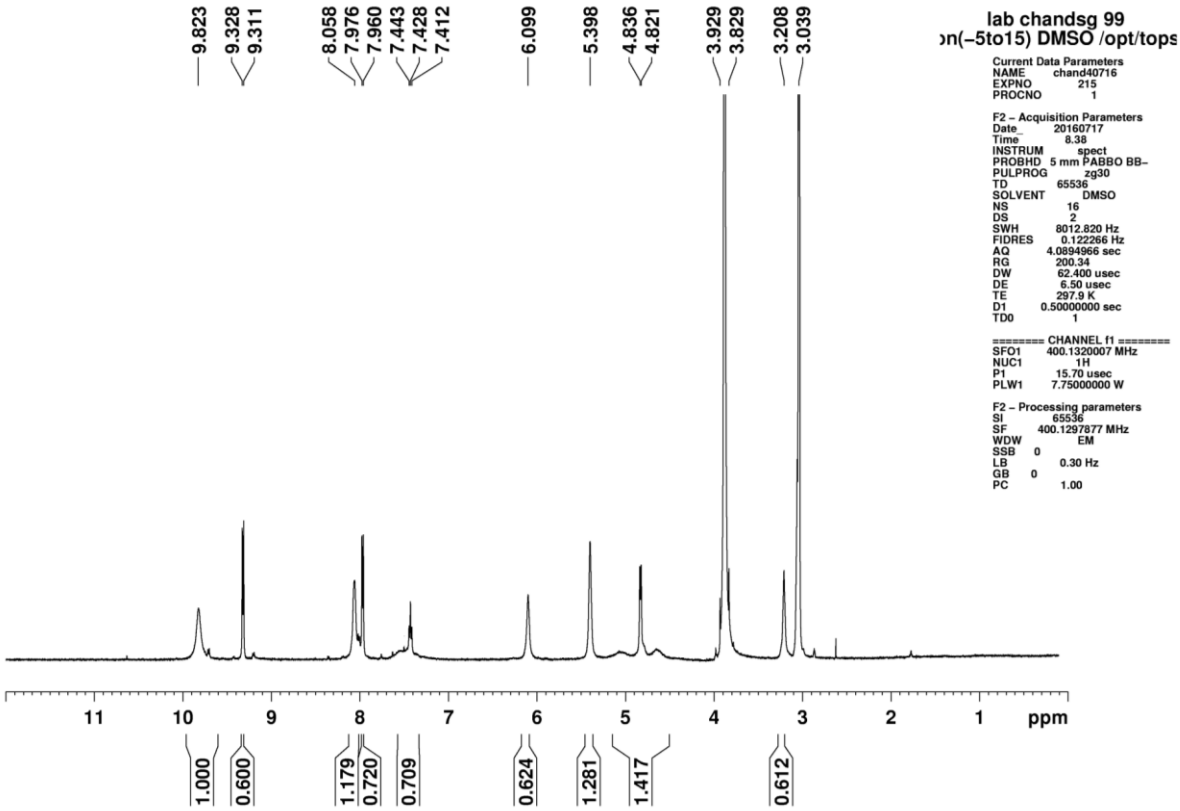

Figure S49. 400 MHz ^{1}H NMR spectrum (in DMSO-d_6 at room temperature) of equilibrium mixture of **1, 5** and **6** obtained by heating a solution of mixture of **5** and **6** (~17 mM in total Pd concentration) at 90 °C for 24 h .

Site-specific recombination with architectural retention (Figures S50 to S64)

$[Pd_2(en)_2\mathbf{L}_2](NO_3)_4$, **1** (3.0 mg, 0.0028 mmol) and $[Pd(tmeda)_2](NO_3)_2$, **7** (1.31 mg, 0.0028 mmol) were dissolved in 0.5 mL of DMSO-d_6 and kept at 90 °C for 24 h. The resulted solution was utilised for ^{1}H NMR studies.

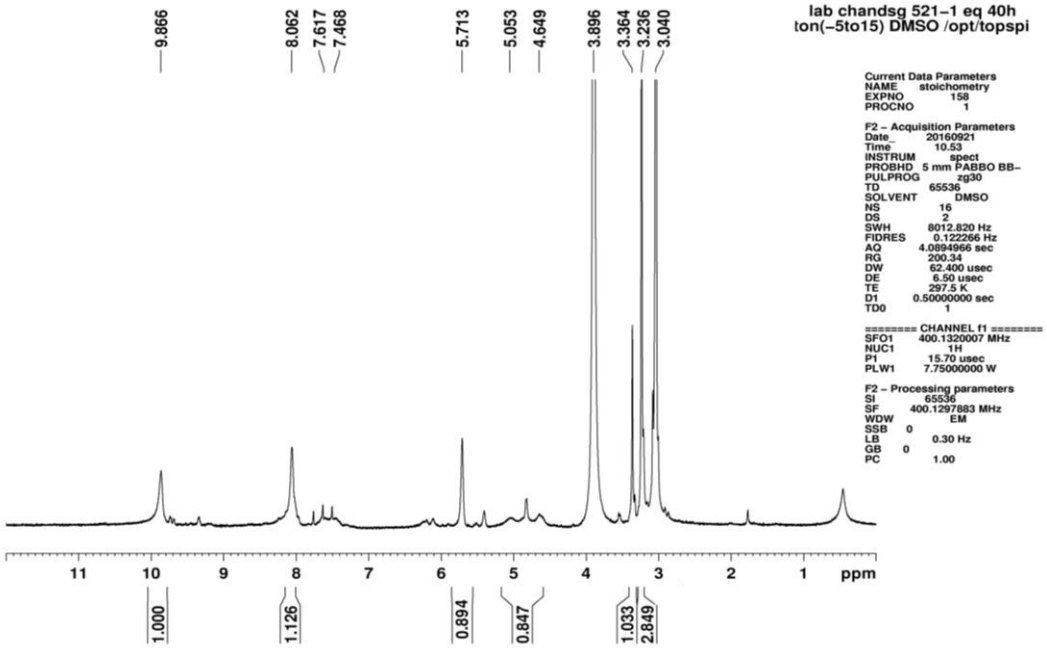

Figure S50. 400 MHz ^{1}H NMR spectrum in DMSO-d_6 showing the evolution of $[Pd_3\mathbf{L}_6](NO_3)_6$, **5** along with **10** by heating a solution of **1** and **7** (1:1) at 90 °C for 24 h.

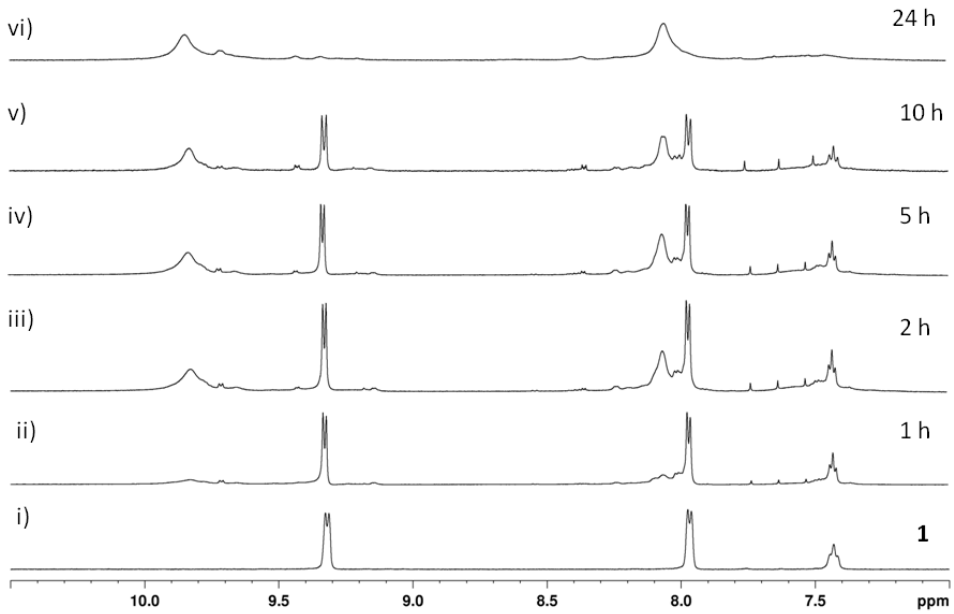

Figure S51. 500 MHz ^{1}H NMR spectra in DMSO-d_6 showing evolution of **5** along with **10** by heating a solution of **1** and **7** (1:1) at 90 °C at different time intervals.

$[Pd_2(en)_2\mathbf{L}_2](NO_3)_4$, **1** (3 mg, 0.0028 mmol) and $[Pd(bpy)_2](NO_3)_2$, **8** (1.55 mg, 0.0028mmol) were dissolved in 0.5 mL of DMSO-d_6 and kept at 90 °C for 24 h. The resulted solution was utilised for ^{1}H NMR studies.

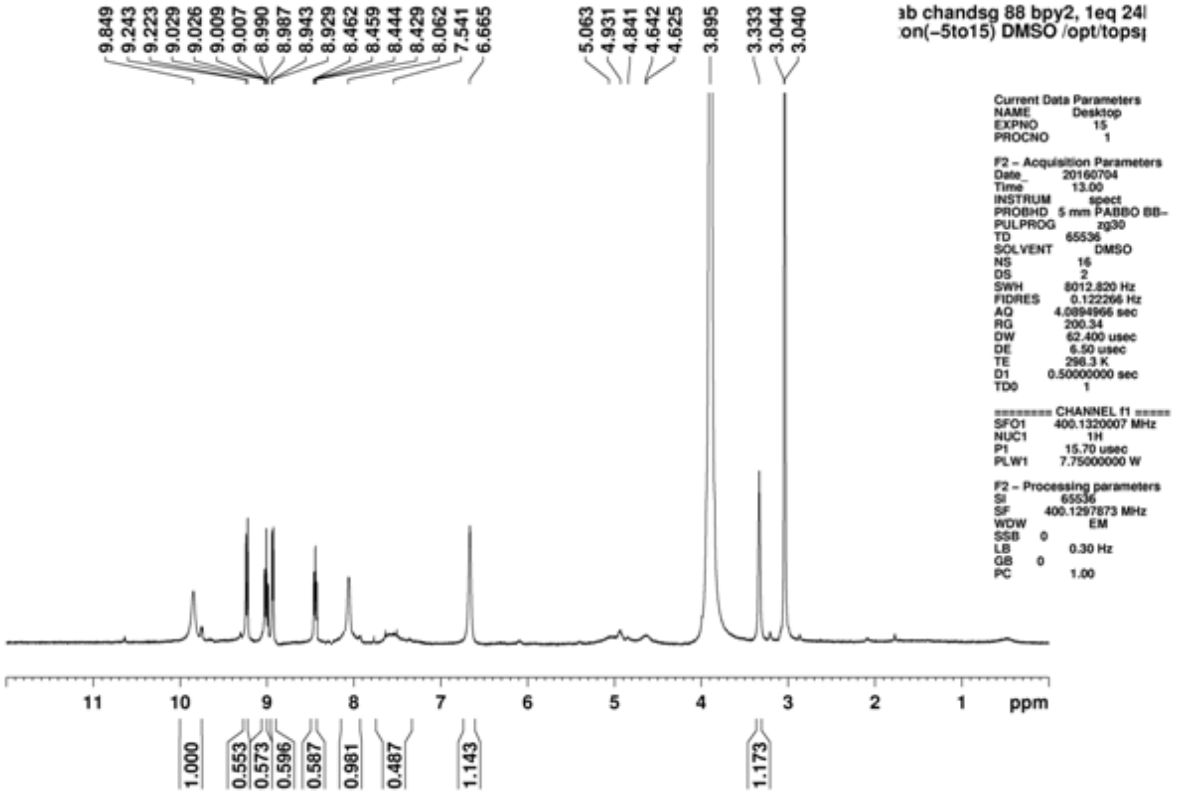

Figure S52. 400 MHz ^{1}H NMR spectrum in DMSO-d_6 showing evolution of **5** along with **11** by heating a solution of **1** and **8** (1:1) at 90 °C for 24 h.

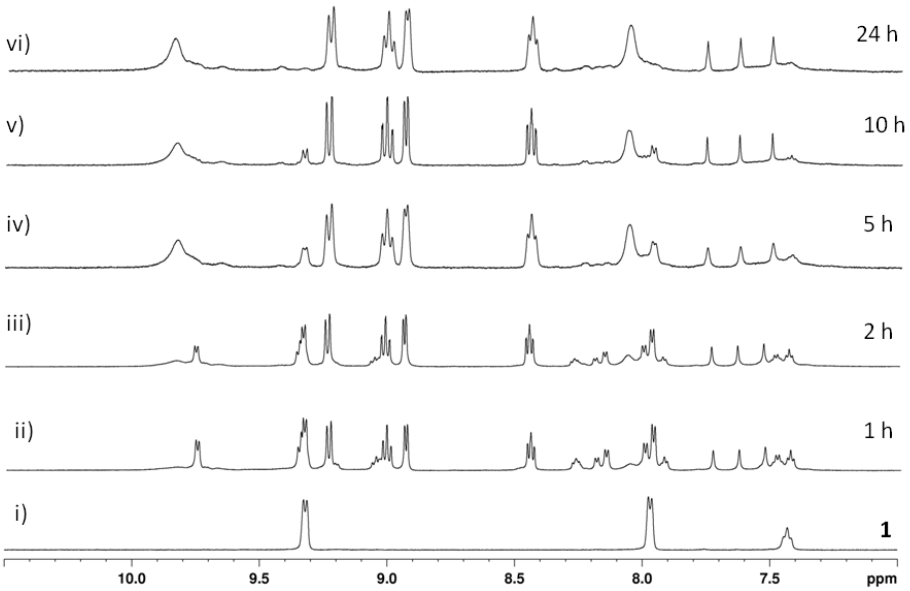

Figure S53. 500 MHz ^{1}H NMR spectra in DMSO-d_6 showing evolution of **5** along with **11** by heating a solution of **1** and **8** (1:1) at 90 °C at different time intervals.

$[Pd_2(en)_2\mathbf{L}_2](NO_3)_4$, **1** (3 mg, 0.0028 mmol) and $[Pd(phen)_2](NO_3)_2$, **9** (1.6 mg, 0.0028 mmol) were dissolved in 0.5 mL of DMSO-d_6 and kept at 90 °C for 24 h. The resulted solution was utilised for ^{1}H NMR studies.

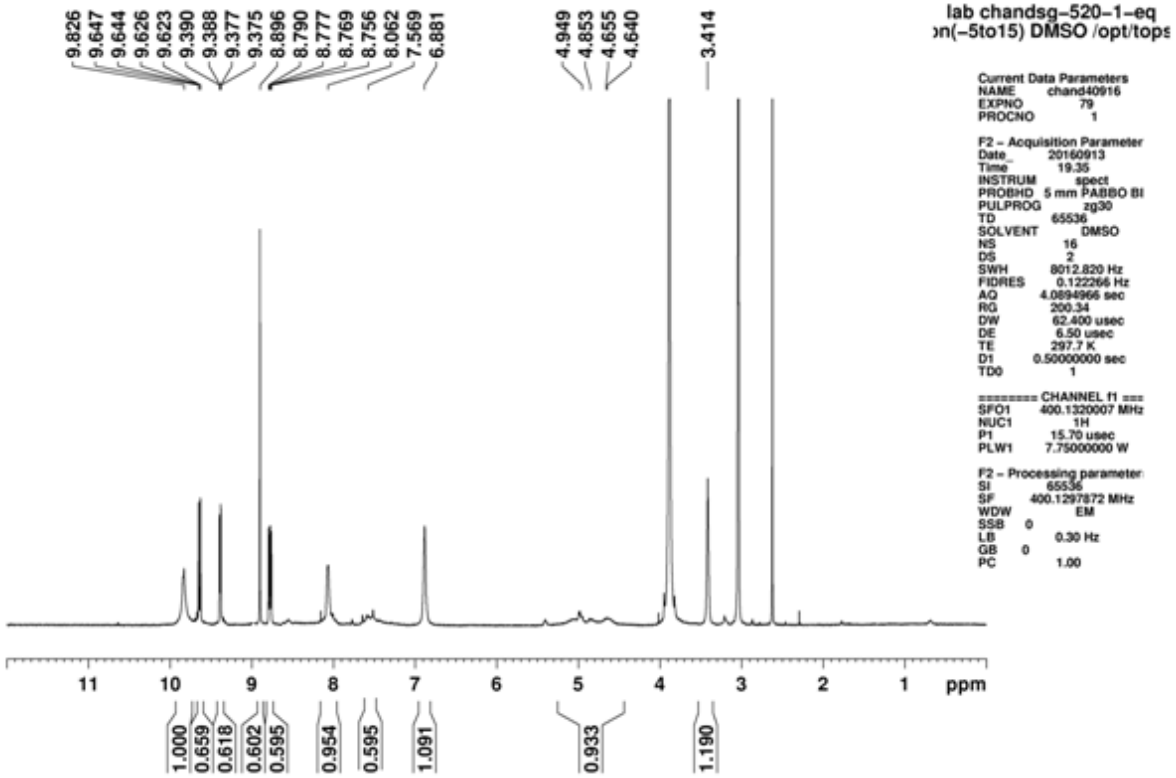

Figure S54. 400 MHz ^{1}H NMR spectrum in DMSO-d_6 showing evolution of **5** along with **12** by heating a solution of **1** and **9** (1:1) at 90 °C for 24 h.

$[Pd_2(en)_2\mathbf{L}_2](NO_3)_4$, **1** (3 mg, 0.0028 mmol) and $[Pd(tmeda)_2](NO_3)_2$, **7** (2.62 mg, 0.0056 mmol) were dissolved in 0.5 mL of DMSO-d_6 and kept at 90 °C for 24 h. The resulted solution was utilised for ^{1}H NMR studies.

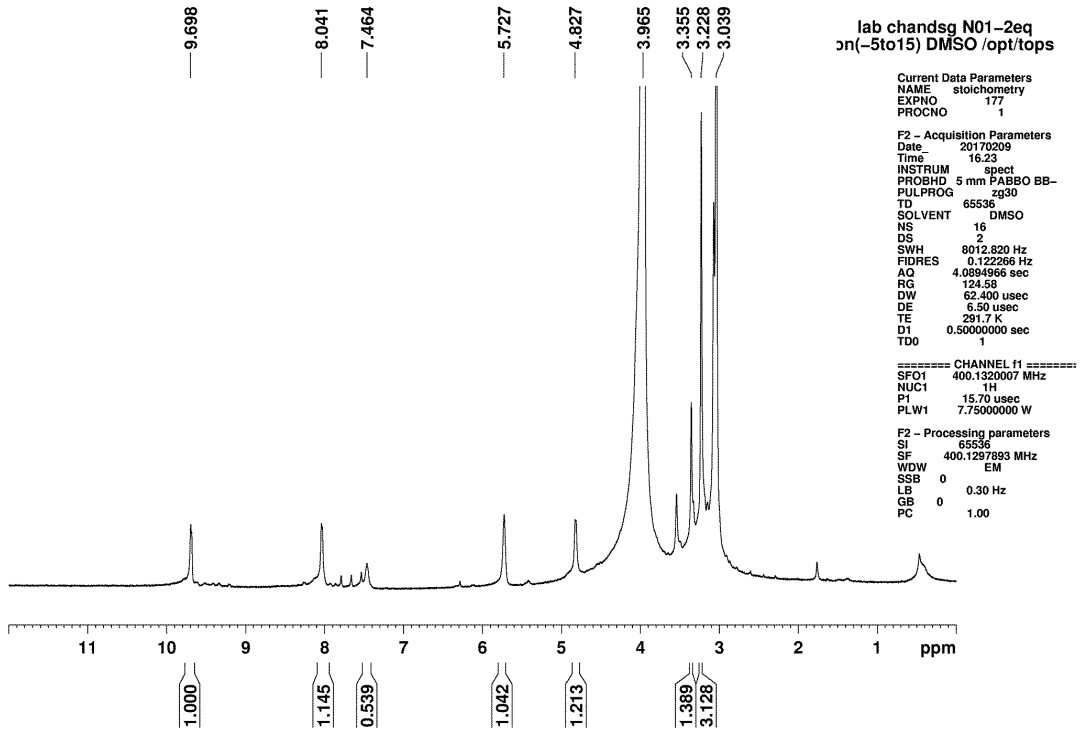

Figure S55. 400 MHz ^{1}H NMR spectrum in DMSO-d_6 showing evolution of $[Pd_2(tmeda)_2\mathbf{L}_2](NO_3)_4$, **2** along with **10** by heating a solution of **1** and **7** (1:2) at 90 °C for 24 h.

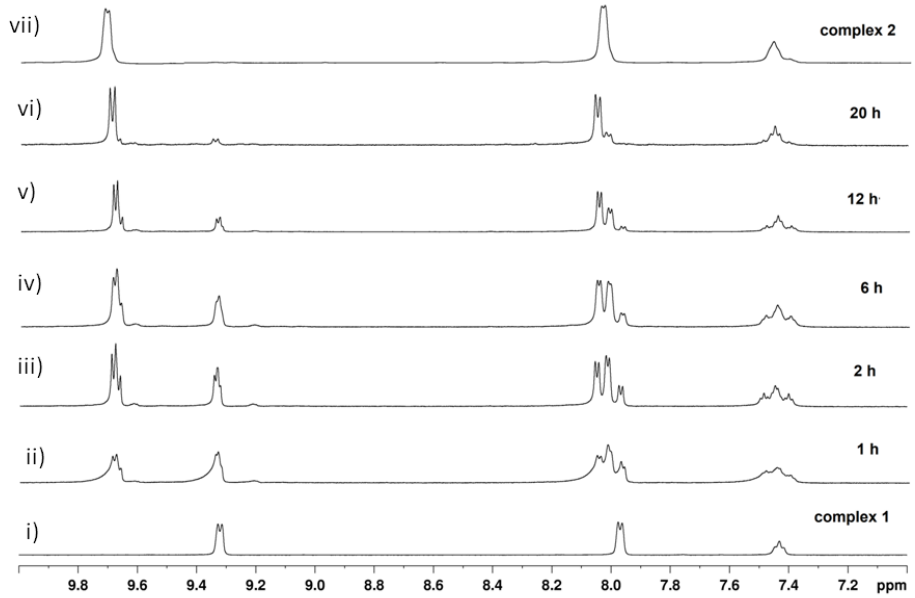

Figure S56a. 400 MHz ^{1}H NMR spectra in DMSO-d_6 showing evolution of $[Pd_2(tmeda)_2\mathbf{L}_2](NO_3)_4$, **2** along with **10** by heating a solution of **1** and **7** (1:2) at 90 °C at different time intervals.

Case 1: $[Pd_2(en)_2\mathbf{L}_2](NO_3)_4$, **1** (2 mg, 0.0019 mmol) and $[Pd(tmeda)_2](NO_3)_2$, **7** (1.75 mg, 0.0038 mmol) were dissolved in 0.5 mL of DMSO-d_6 and kept at room temperature for 24 h. The resulted solution was utilised for ^{1}H NMR studies.

Case 2: $[Pd_2(en)_2\mathbf{L}_2](NO_3)_4$, **1** (6 mg, 0.0056 mmol) and $[Pd(tmeda)_2](NO_3)_2$, **7** (5.25 mg, 0.0115 mmol) were dissolved in 0.5 mL of DMSO-d_6 and kept at room temperature for 24 h. The resulted solution was utilised for ^{1}H NMR studies.

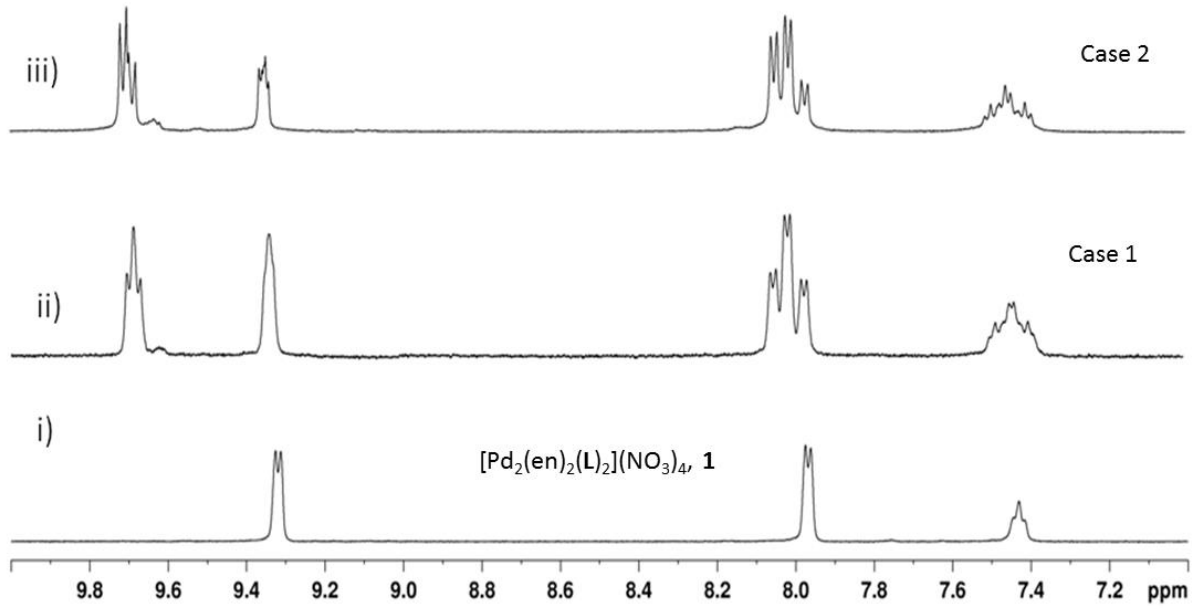

Figure S56b. 500 MHz ^{1}H NMR spectra in DMSO-d_6 at room temperature of i) $[Pd_2(en)_2(\mathbf{L})_2](NO_3)_4$, **1**; ii) case1: further reorganization of a mixture of **1** and **7** that are 7.6 mM in [Pd] each or 15.2 mM in total [Pd] iii) case 2: further reorganization of a mixture of **1** and **7** that are 22.4 mM in [Pd] each or 44.8 mM in total [Pd] at room temperature for 24 h.

$[Pd_2(en)_2\mathbf{L}_2](NO_3)_4$, **1** (3 mg, 0.0028 mmol) and $[Pd(bpy)_2](NO_3)_2$, **8** (3.0 mg, 0.0056 mmol) were dissolved in 0.5 mL of DMSO-d_6 and kept at 90 °C for 24 h. The resulted solution was utilised for ^{1}H NMR studies.

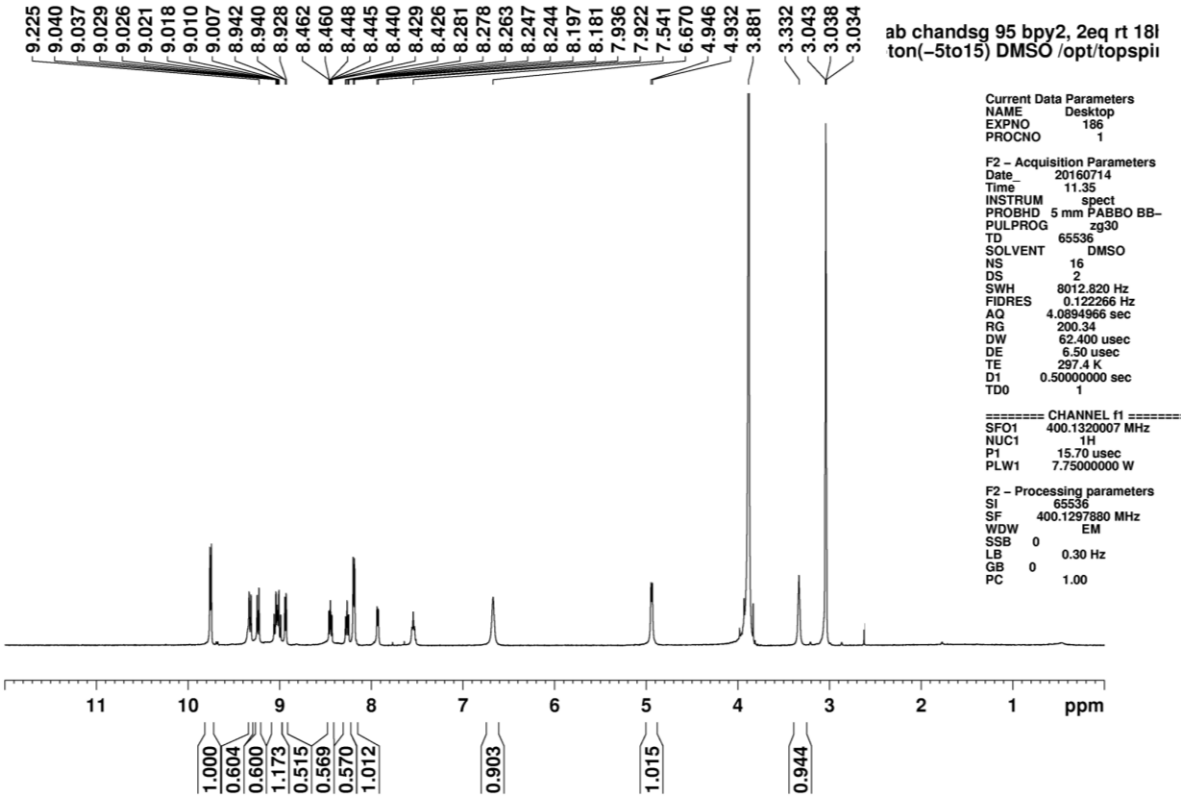

Figure S57. 400 MHz ^{1}H NMR spectrum in DMSO-d_6 showing evolution of $[Pd_2(bpy)_2\mathbf{L}_2](NO_3)_4$, **3** along with **11** by heating a solution of **1** and **8** (1:2) at 90 °C for 24 h.

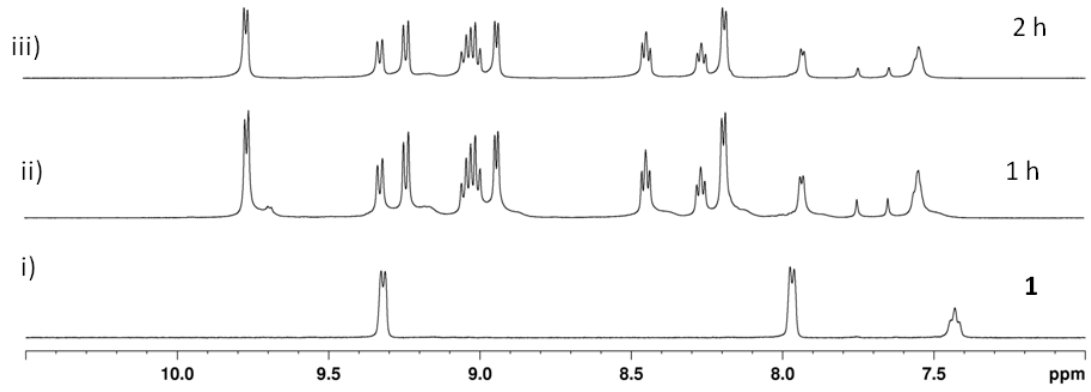

Figure S58. 500 MHz ^{1}H NMR spectra in DMSO-d_6 showing evolution of $[Pd_2(bpy)_2\mathbf{L}_2](NO_3)_4$, **3** along with **11** by heating a solution of **1** and **8** (1:2) at 90 °C at different time intervals.

$[Pd_2(en)_2\mathbf{L}_2](NO_3)_4$, **1** (3 mg, 0.0028 mmol) and $[Pd(phen)_2](NO_3)_2$, **9** (3.3 mg, 0.0056 mmol) were dissolved in 0.5 mL of DMSO-d_6 and kept at 90 °C for 24 h. The resulted solution was utilised for ^{1}H NMR studies.

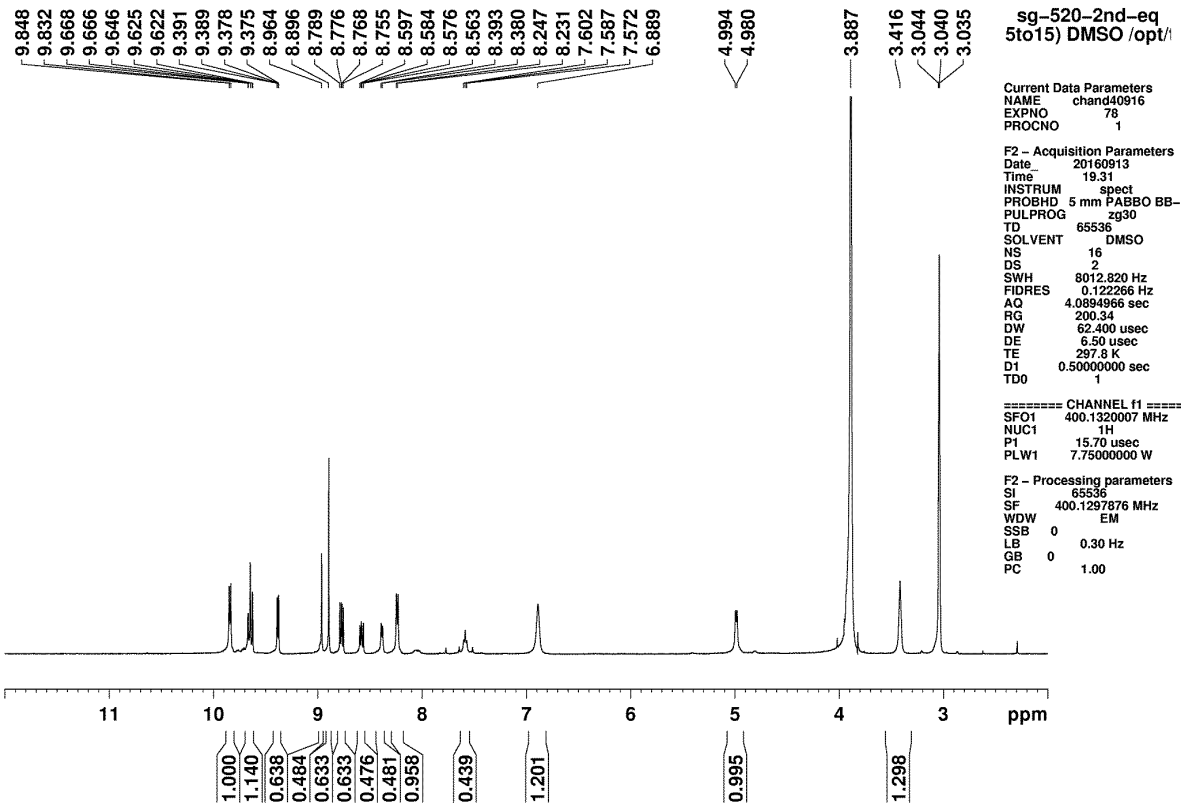

Figure S59. 400 MHz ^{1}H NMR spectrum in DMSO-d_6 showing evolution of $[Pd_2(phen)_2\mathbf{L}_2](NO_3)_4$, **4** along with **12** by heating a solution of **1** and **9** (1:2) at 90 °C for 24 h.

$[Pd_3\mathbf{L}_6](NO_3)_6$, **5** (3 mg, 0.0014 mmol) and $[Pd(tmeda)_2](NO_3)_2$, **7** (1.9 mg, 0.0042 mmol) were dissolved in 0.5 mL of DMSO-d_6 and kept at 90 °C for 24 h. The resulted solution was utilised for ^{1}H NMR studies.

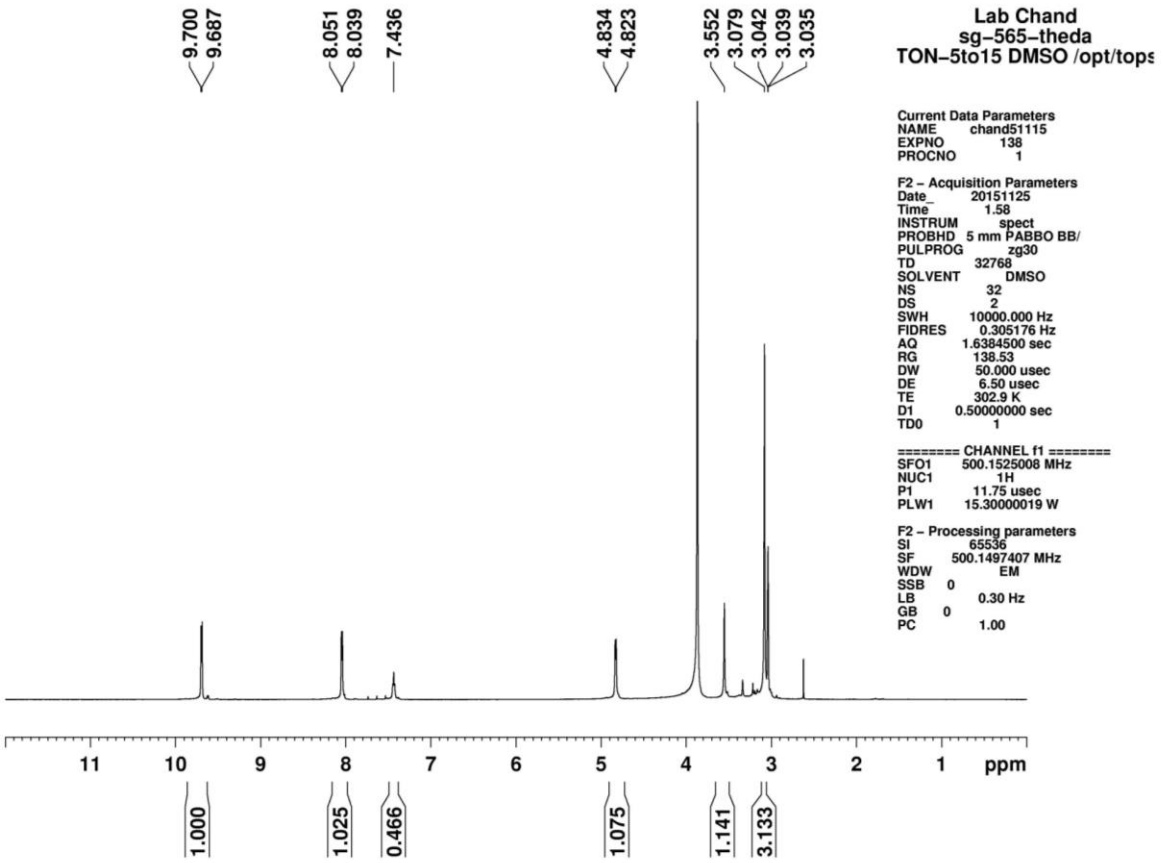

Figure S60. 400 MHz ^{1}H NMR spectrum of complexes in DMSO-d_6 showing evolution of $[Pd_2(tmeda)_2\mathbf{L}_2](NO_3)_4$, **2** by unification of $[Pd_3\mathbf{L}_6](NO_3)_6$, **5** with $[Pd(tmeda)_2](NO_3)_2$, **7** (1:3) at 90 °C for 24 h.

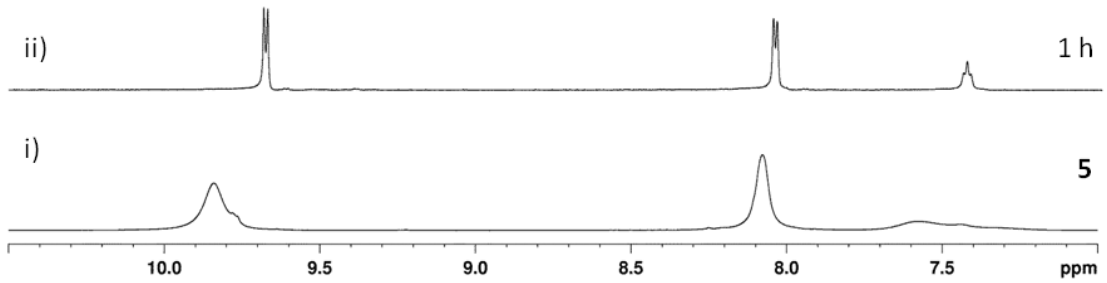

Figure S61. 400 MHz ^{1}H NMR spectra of complexes in DMSO-d_6 showing evolution of $[Pd_2(tmeda)_2\mathbf{L}_2](NO_3)_4$, **2** by unification of $[Pd_3\mathbf{L}_6](NO_3)_6$, **5** with $[Pd(tmeda)_2](NO_3)_2$, **7** (1:3) at 90 °C for 1 h.

$[Pd_3\mathbf{L}_6](NO_3)_6$, **5** (3 mg, 0.0014 mmol) and $[Pd(bpy)_2](NO_3)_2$, **8** (2.3 mg, 0.0042 mmol) were dissolved in 0.5 mL of DMSO-d_6 and kept at 90 °C for 24 h. The resulted solution was utilised for ^{1}H NMR studies.

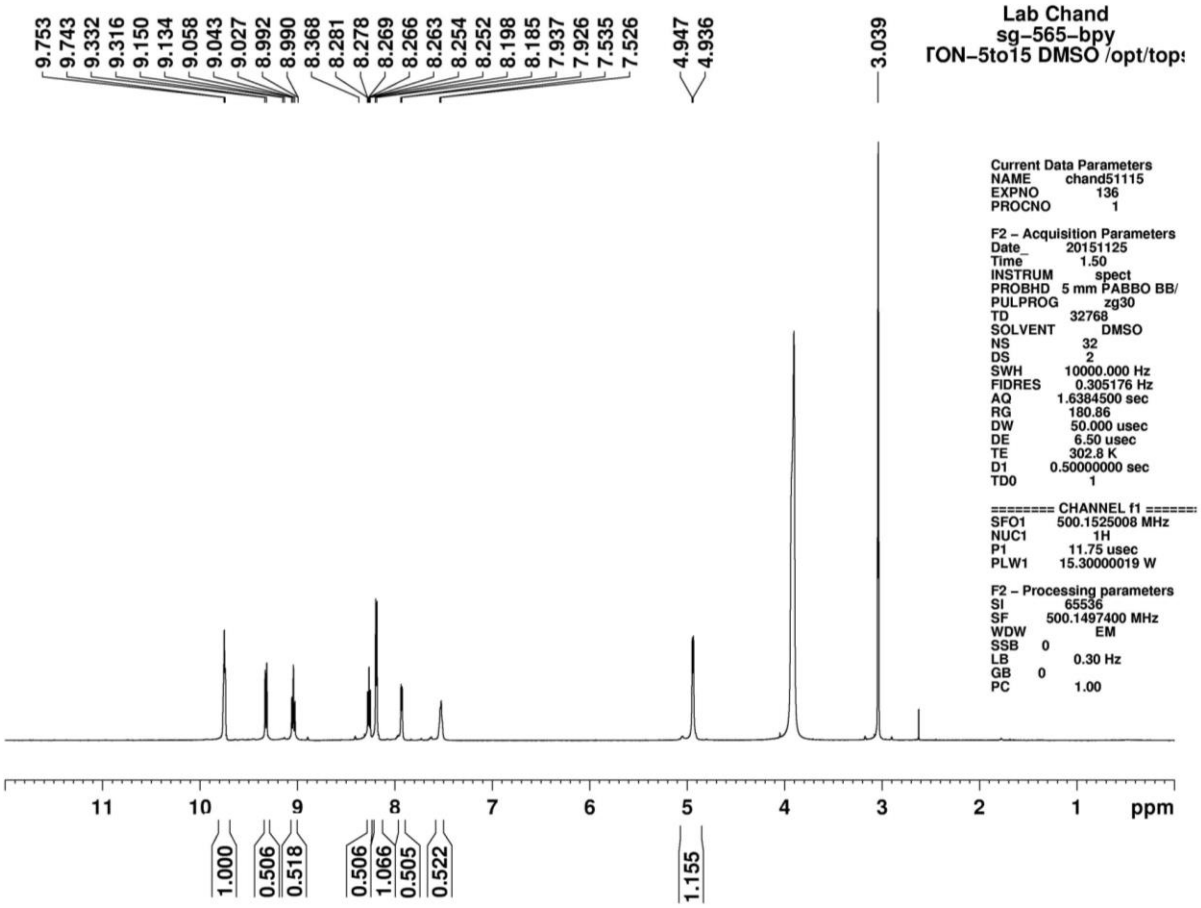

Figure S62. 400 MHz ^{1}H NMR spectrum of complexes in DMSO-d_6 showing evolution of $[Pd_2(bpy)_2\mathbf{L}_2](NO_3)_4$, **3** by unification of $[Pd_3\mathbf{L}_6](NO_3)_6$, **5** with of $[Pd(bpy)_2](NO_3)_2$, **8** (1:3) at 90 °C for 24 h.

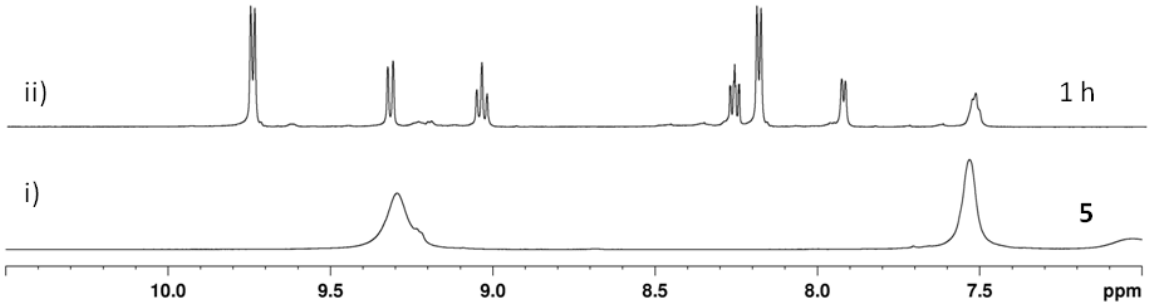

Figure S63. 400 MHz ^{1}H NMR spectra of complexes in DMSO-d_6 showing evolution of $[Pd_2(bpy)_2\mathbf{L}_2](NO_3)_4$, **3** by unification of $[Pd_3\mathbf{L}_6](NO_3)_6$, **5** with of $[Pd(bpy)_2](NO_3)_2$, **8** (1:3) at 90 °C for 1 h.

$[Pd_3\mathbf{L}_6](NO_3)_6$, **5** (3 mg, 0.0014 mmol) and $[Pd(phen)_2](NO_3)_2$, **9** (2.5 mg, 0.0042 mmol) were dissolved in 0.5 mL of DMSO-d_6 and kept at 90 °C for 24 h. The resulted solution was utilised for ^{1}H NMR studies.

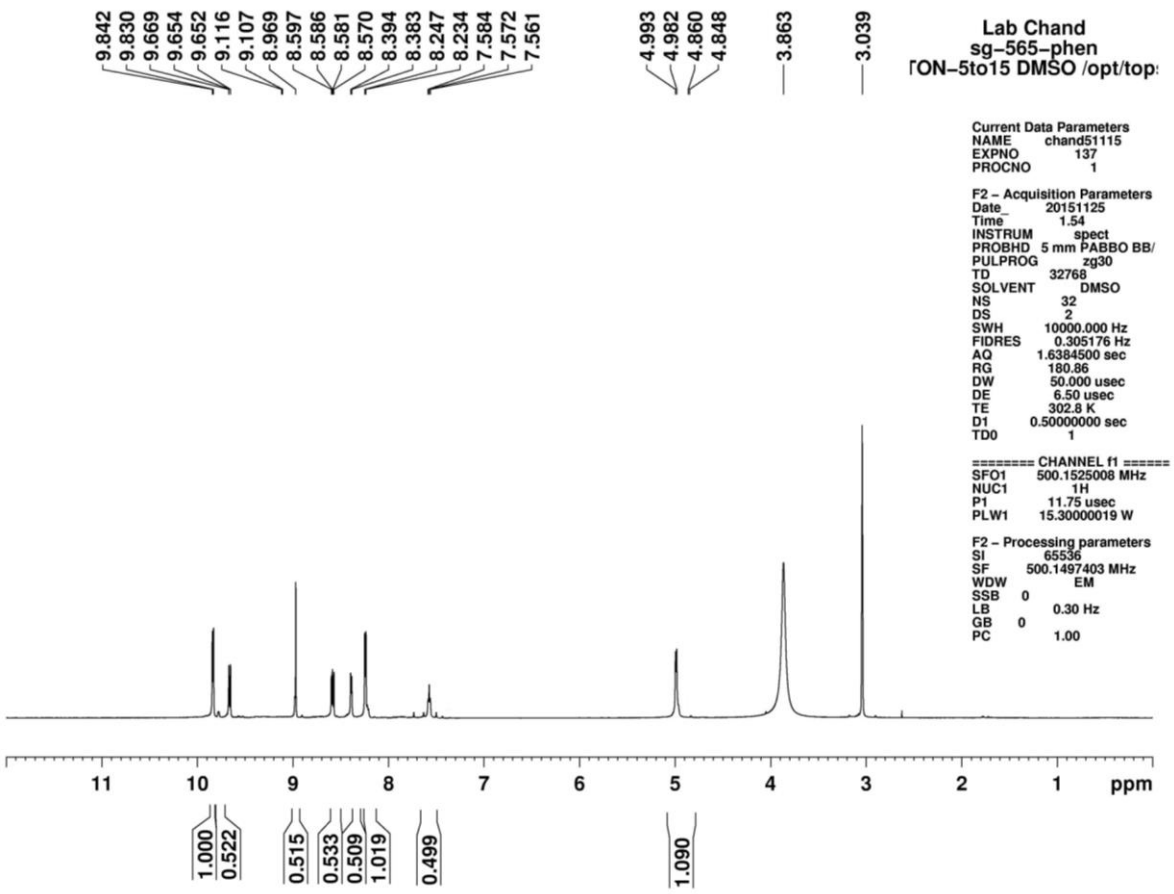

Figure S64. 400 MHz ^{1}H NMR spectrum of complexes in DMSO-d_6 showing evolution of $[Pd_2(phen)_2\mathbf{L}_2](NO_3)_4$, **4** by unification of $[Pd_3\mathbf{L}_6](NO_3)_6$, **5** with $[Pd(phen)_2](NO_3)_2$ **9** (1:3) at 90 °C for 24 h.

Site-specific recombination with architectural annulation (Figures S65 -69)

$[Pd_2(en)_2\mathbf{L}_2](NO_3)_4$, **1** (3 mg, 0.0028 mmol) and $[Pd_2(tmeda)_2\mathbf{L}_2](NO_3)_4$, **2** (3.3 mg, 0.0028 mmol) were dissolved in 0.5 mL of DMSO-d_6 and kept at 90 °C for 24 h. The resulted solution was utilised for ^{1}H NMR studies.

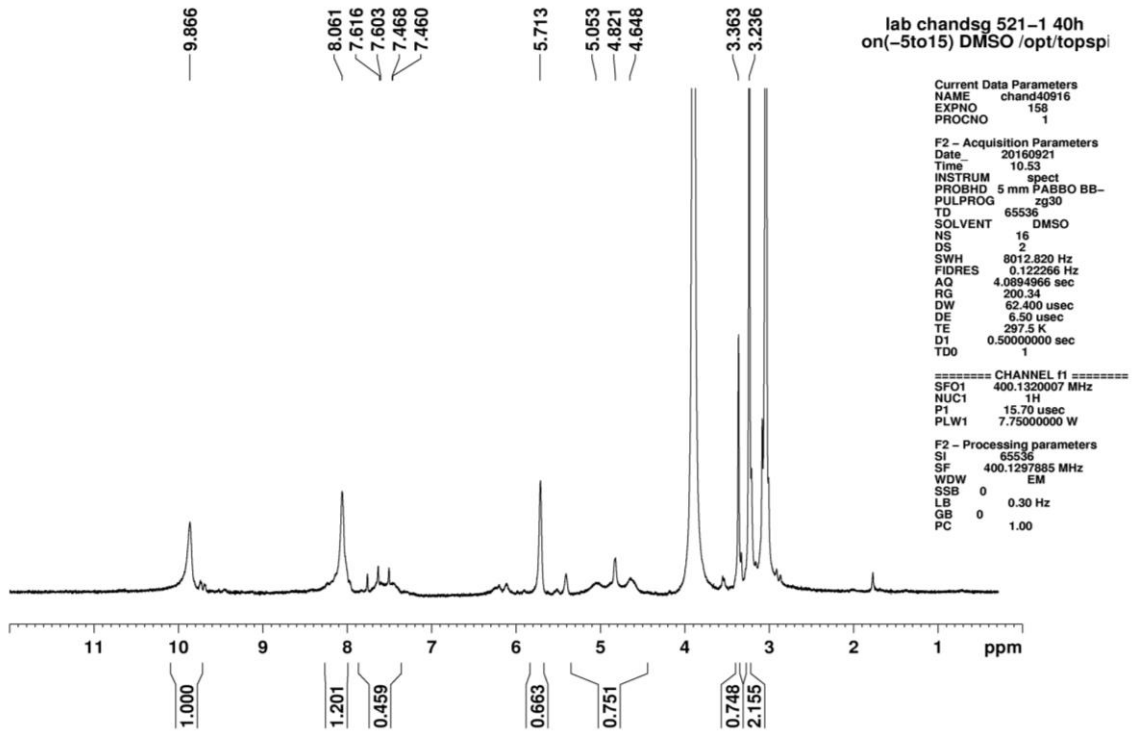

Figure S65. 400 MHz ^{1}H NMR spectrum of complexes in DMSO- d_6 showing evolution of $[Pd_3\mathbf{L}_6](NO_3)_6$, **5** along with $[Pd(tmeda)_2](NO_3)_2$, **10** by heating a solution of $[Pd_2(en)_2\mathbf{L}_2](NO_3)_4$, **1** and $[Pd_2(tmeda)_2\mathbf{L}_2](NO_3)_4$, **2** (1:1) at 90 °C for 24 h.

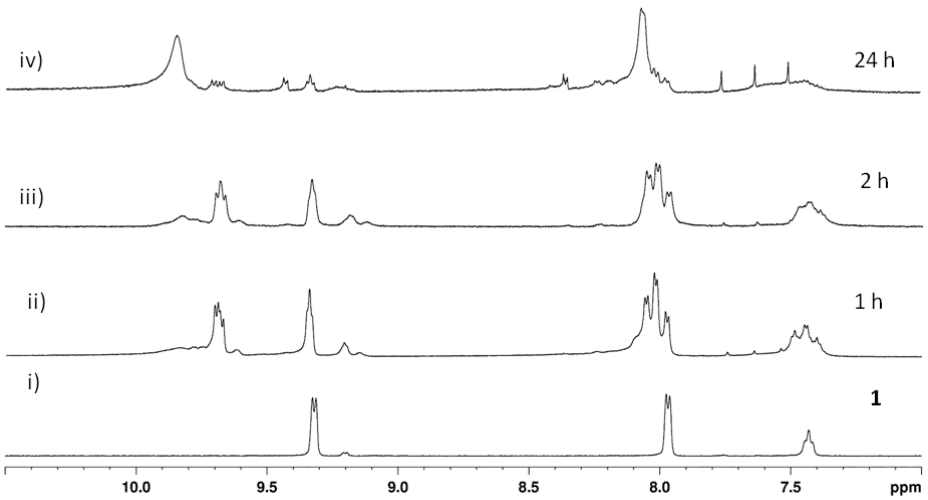

Figure S66. 400 MHz ^{1}H NMR spectra of complexes in DMSO- d_6 showing evolution of $[Pd_3\mathbf{L}_6](NO_3)_6$, **5** along with $[Pd(tmeda)_2](NO_3)_2$, **10** by heating a solution of $[Pd_2(en)_2\mathbf{L}_2](NO_3)_4$, **1** and $[Pd_2(tmeda)_2\mathbf{L}_2](NO_3)_4$, **2** (1:1) at 90 °C at different time intervals.

$[Pd_2(en)_2\mathbf{L}_2](NO_3)_4$, **1** (3 mg, 0.0028 mmol) and $[Pd_2(bpy)_2\mathbf{L}_2](NO_3)_4$, **3** (3.5 mg, 0.0028 mmol) were dissolved in 0.5 mL of DMSO-d_6 and kept at 90 °C for 24 h. The resulted solution was utilised for ^{1}H NMR studies.

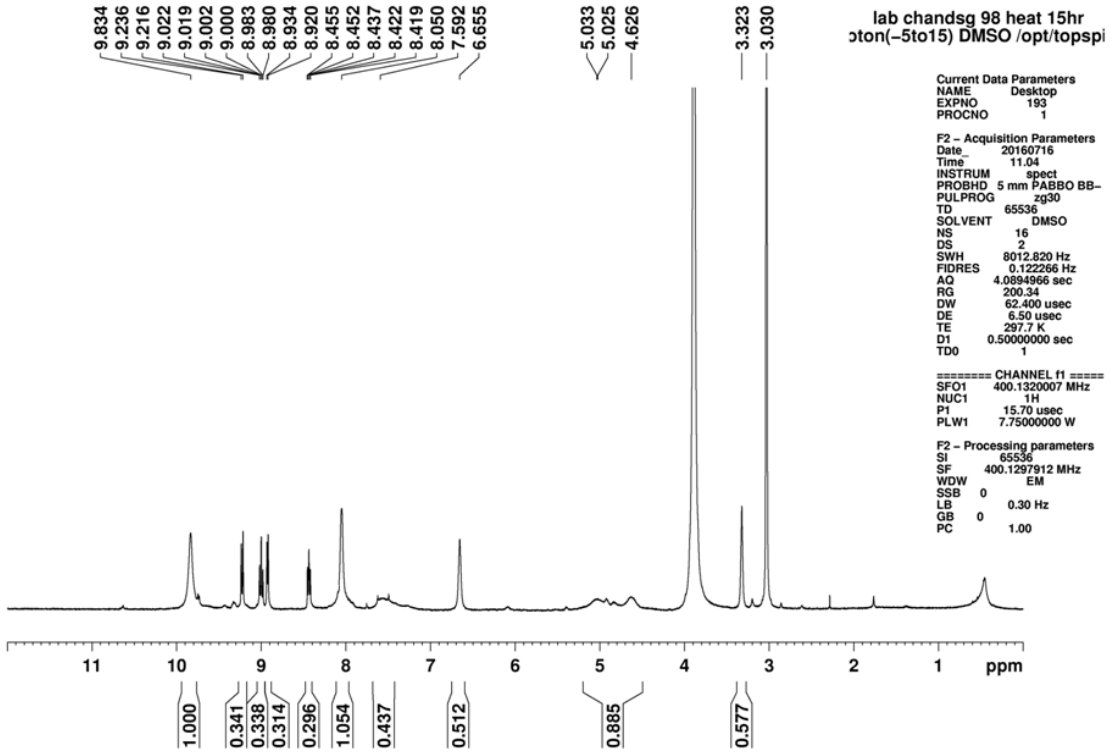

Figure S67. 400 MHz ^{1}H NMR spectrum of complexes in DMSO- d_6 showing evolution of $[Pd_3\mathbf{L}_6](NO_3)_6$, **5** along with $[Pd(bpy)_2](NO_3)_2$, **11** by heating a solution of $[Pd_2(en)_2\mathbf{L}_2](NO_3)_4$, **1** and $[Pd_2(bpy)_2\mathbf{L}_2](NO_3)_4$, **3** (1:1) at 90 °C for 24 h.

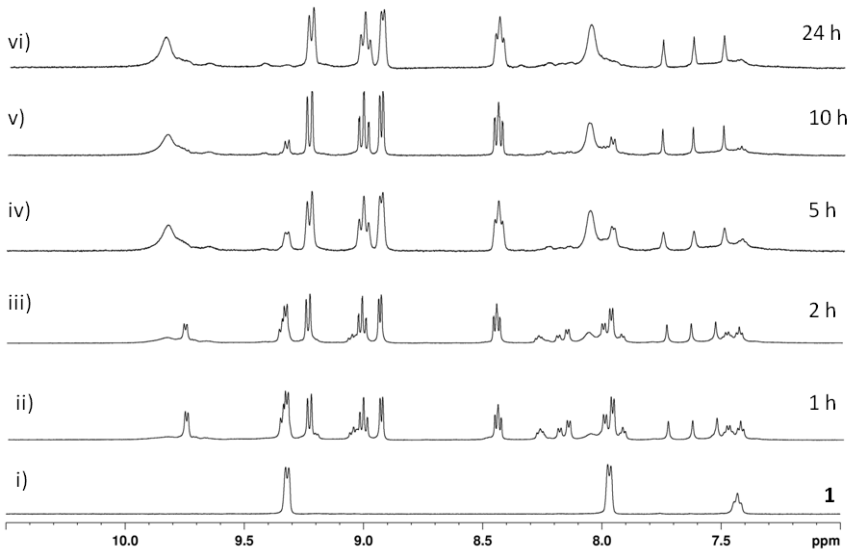

Figure S68. 400 MHz ^{1}H NMR spectra of complexes in DMSO- d_6 showing evolution of $[Pd_3\mathbf{L}_6](NO_3)_6$, **5** along with $[Pd(bpy)_2](NO_3)_2$, **11** by heating a solution of $[Pd_2(en)_2\mathbf{L}_2](NO_3)_4$, **1** and $[Pd_2(bpy)_2\mathbf{L}_2](NO_3)_4$, **3** (1:1) at 90 °C at different time intervals.

$[Pd_2(en)_2\mathbf{L}_2](NO_3)_4$, **1** (3 mg, 0.0028 mmol) and $[Pd_2(phen)_2\mathbf{L}_2](NO_3)_4$, **4** (3.7 mg, 0.0028 mmol) were dissolved in 0.5 mL of DMSO-d_6 and kept at 90 °C for 24 h. The resulted solution was utilised for ^{1}H NMR studies.

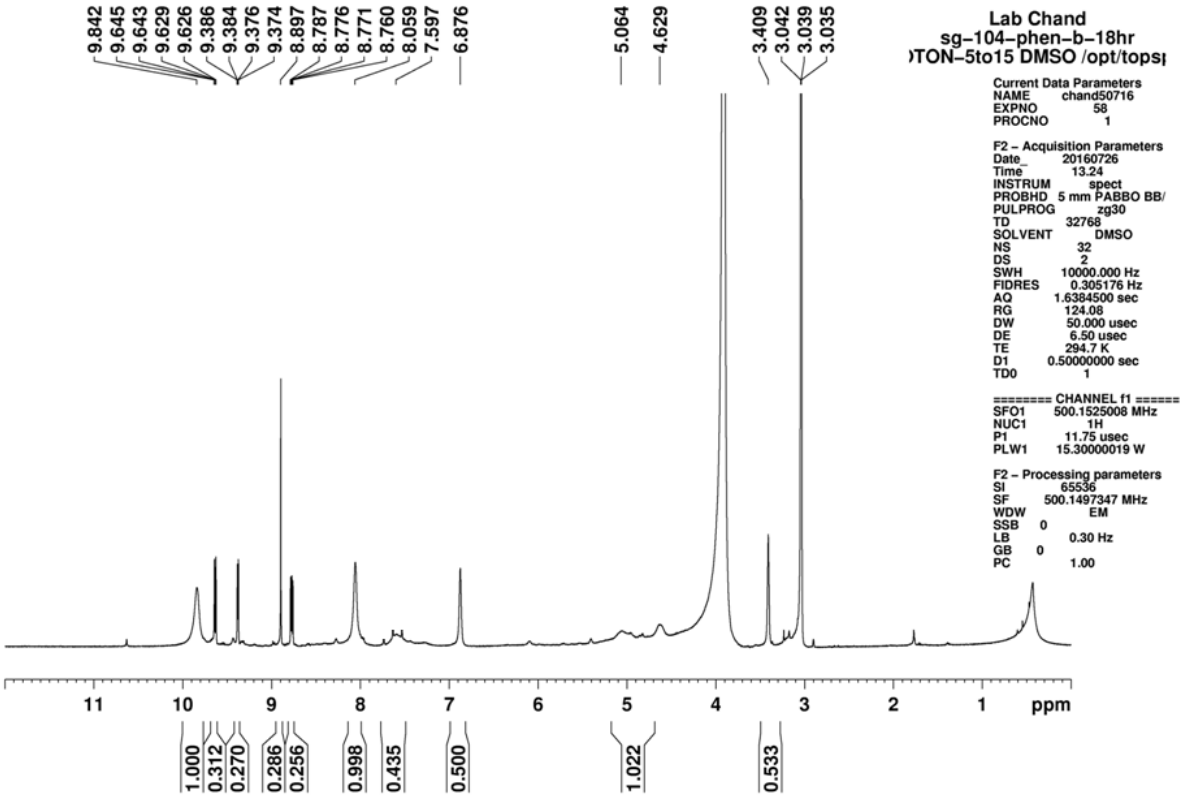

Figure S69. 400 MHz ^{1}H NMR spectrum of complexes in DMSO- d_6 showing evolution of $[Pd_3\mathbf{L}_6](NO_3)_6$, **5** along with $[Pd(phen)_2](NO_3)_2$, **12** by heating a solution of $[Pd_2(en)_2\mathbf{L}_2](NO_3)_4$, **1** and $[Pd_2(phen)_2\mathbf{L}_2](NO_3)_4$, **4** (1:1) at 90 °C for 24 h.

Table S3 Crystallographic Data and Structure Refinement Parameters

Parameters	**2**	**3**	**4**	**5**
CCDC number	1817578	1817580	1817581	1817579
Empirical formula	$C_{38}H_{60}N_{14}O_{13.24}Pd_2$	$C_{46}H_{40}N_{15}O_{13}Pd_2$	$C_{50}H_{44}N_{16}O_{24}Pd_2$	$C_{82}H_{110}N_{34}O_{20}Pd_3$
Formula weight	1137.64	1223.73	1243.80	2211.48
Crystal system	Triclinic	Tetragonal	Monoclinic	Hexagonal
Space group	$P\bar{1}$	$P4_2/nmc$	$C2/c$	$P6_3/m$
***a* (Å)**	13.3576(5)	23.1761(16)	27.5262(8)	19.5406(8)
***b* (Å)**	13.9054(5)	23.1761(16)	17.4706(5)	19.5406(8)
***c* (Å)**	17.6592(6)	12.2799(11)	28.8770(12)	20.1186(8)
***α* (deg)**	101.454(2)	90	90	90
***β* (deg)**	95.122(2)	90	111.060 (10)	90
***γ* (deg)**	104.6700(10)	90	90	120
Volume (Å)^3	3076.07(19)	6595.9(11)	12959.3(8)	6652.8(6)
Z	2	4	8	2
Wavelength (Å)	0.71073	0.71073	0.71073	0.71073
Temperature (K)	296(2)	296(2)	296(2)	296(2)
Calcd. density (g/cm^3)	1.228	1.232	1.275	1.104
Absorption coefficient (mm^{-1})	0.644	0.606	0.642	0.463
F(000)	1168	2468	5903	2276
Crystal dimensions (mm)^3	0.35 × 0.25 × 0.1	0.28 × 0.25 × 0.20	0.35 × 0.25 × 0.25	0.28 x 0.21 x 0.19
θ min/max (deg)	3.12/53.7	1.757 / 21.260	1.410 / 24.769	3.14 / 42.94
Reflections collected/unique	50263 / 13119 [R(int) = 0.0262]	14614 / 1954 [R(int) = 0.0795]	45045 / 11112 [R(int) = 0.0463]	18915 / 2630 [R(int) = 0.0378]
Data/restraints/parameters	13119 / 1 / 528	1954 / 3 / 151	11112 / 36 / 703	2630 / 1 / 215
Goodness-of-fit on F^2	1.465	2.346	1.036	2.019
Final R indices [I > 2σ(I)]	R_1 = 0.0955, wR_2 = 0.3135	R1 = 0.1800, wR2 = 0.5322	R1 = 0.0736, wR2 = 0.2253	R1 = 0.1777, wR2 = 0.4352
R indices (all data)	R_1 = 0.1141, wR_2 = 0.3449	R1 = 0.2125, wR2 = 0.5520	R1 = 0.1008, wR2 = 0.2566	R1 = 0.2102, wR2 = 0.4766
Largest diff. peak and hole/Å^3	2.643 and -2.465	1.435 and -1.169	3.839 and -0.609	2.26 and -0.74

Calculation for the radial displacement angle (θ)

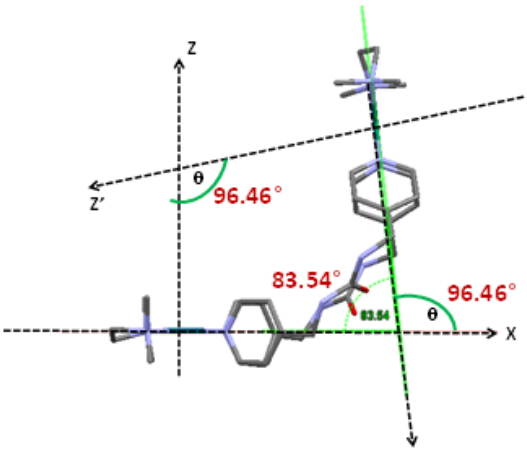

Figure S70. The radial displacement angle (θ = 97°) in $[Pd_2(tmeda)_2\mathbf{L}_2](NO_3)_4$, **2**.

Crystal Packing of $[Pd_2(tmeda)_2L_2](NO_3)_4$, 2

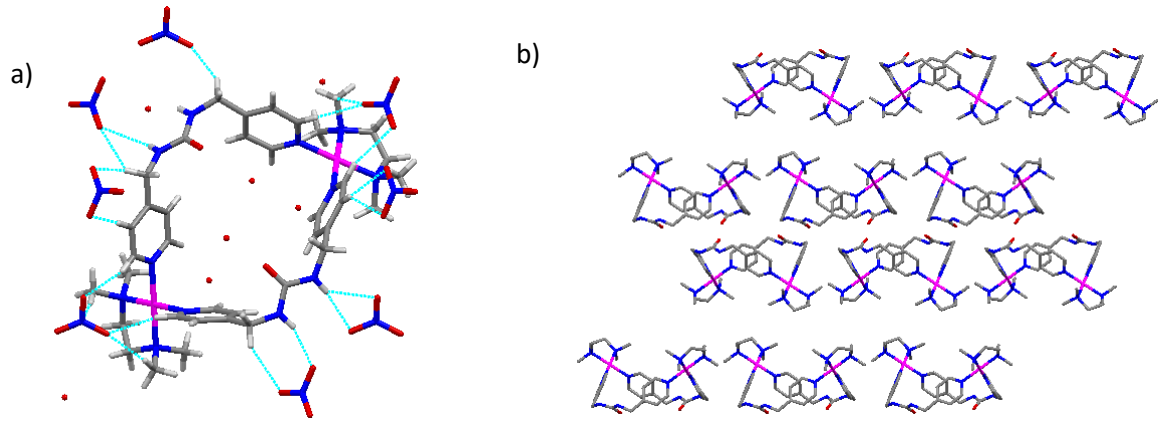

Figure S71. a) Crystal structure of **2** showing interaction of cationic part of **2** with five water molecules and eight nitrate anions and b) packing diagrams showing $[Pd_2(tmeda)_2(\mathbf{L})_2]^{4+}$ units along *a* axis.

Crystal structure of $[Pd_2(bpy)_2L_2](NO_3)_4$, 3

Due to the poor quality of the crystal, the collected data was insufficient to locate the anions and solvent molecules. But the cationic framework was obtained and described below.

Single crystals of **3** were obtained by slow diffusion of *t*-butanol into a MeCN-H_2O (1:1) solution of **3**. The compound crystallized in a tetragonal system with $P4_2/nmc$ space group. The asymmetric unit contains half of the molecule of **3**. Counter anions i.e. nitrate anions could not be located in the structure due to poor quality of the data. The structure represents "opened jaw" type shape (Figure S72) and contains two $[Pd(bpy)]^{2+}$ units which are jointed

together by two ligand moieties. The distance between two palladium(II) units is 11.2 Å. Each palladium(II) centre occupies approximately square planar (PdN_4) geometry. Each metal center in a PdN_4 square plane composed of two nitrogen atoms from two pyridyl units of different strings of the ligand and other two are occupied by bpy unit in a *cis* manner. Both the PdN_4 planes are not located in the same plane but radially displaced toward the other with the $\theta = 67°$ (Figure S73) (θ is the angle between two PdN_4 planes which are radially displaced one above the other).

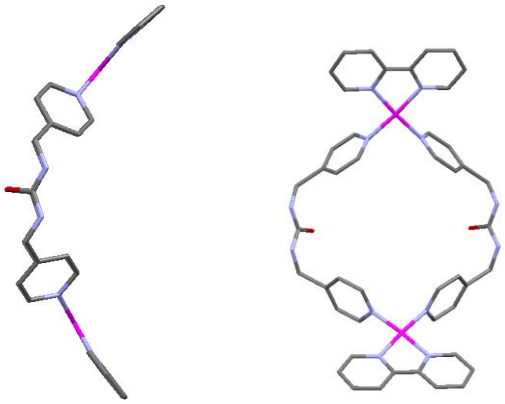

Figure S72 Capped sticks representation of the crystal structure of complexes **3** in two different styles (hydrogens, and co-crystallized solvent molecules are excluded for clarity).

Calculation for the radial displacement angle (θ)

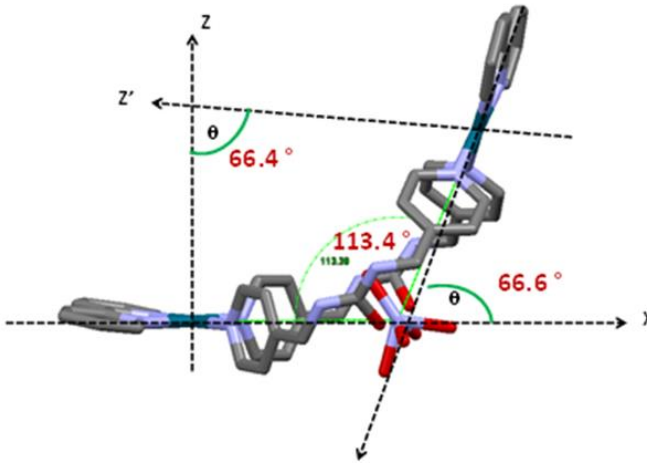

Figure S73. The radial displacement angle (θ) in $[Pd_2(bpy)_2\mathbf{L}_2](NO_3)_4$**, 3**

The complex **3** possesses bpy as *cis*-protected group, it was expected that π-π interactions play a key role in the crystal packing. But the close look into the molecular arrangement in the crystal structure revealed the molecules did not have any kind of π-π interactions. However, Cationic part of the molecule **3**, is connected to the adjacent molecule with the help of C–H···O bonding (Figure S74). Along *a* axis, one molecule located above other, they are not parallel to each other but one is turned approximately 90° to other molecule.

In this arrangement, oxygen atoms from urea moieties of molecule and α hydrogen of the pyridine from the other molecule locate close to each other and have C–H···O bonding (Figure S74 b). The distance between the α hydrogen atom and oxygen atom of the urea moiety is 2.67 Å with the angle (*i.e.* ∠C–H···O) 141.6°. This arrangement continuous along *a* axis and yields 1-D supramolecular network (Figure S74 c) by utilizing C–H···O bonding. This 1-D supramolecular network does not have substantial intermolecular interaction with any of the neighbouring complex.

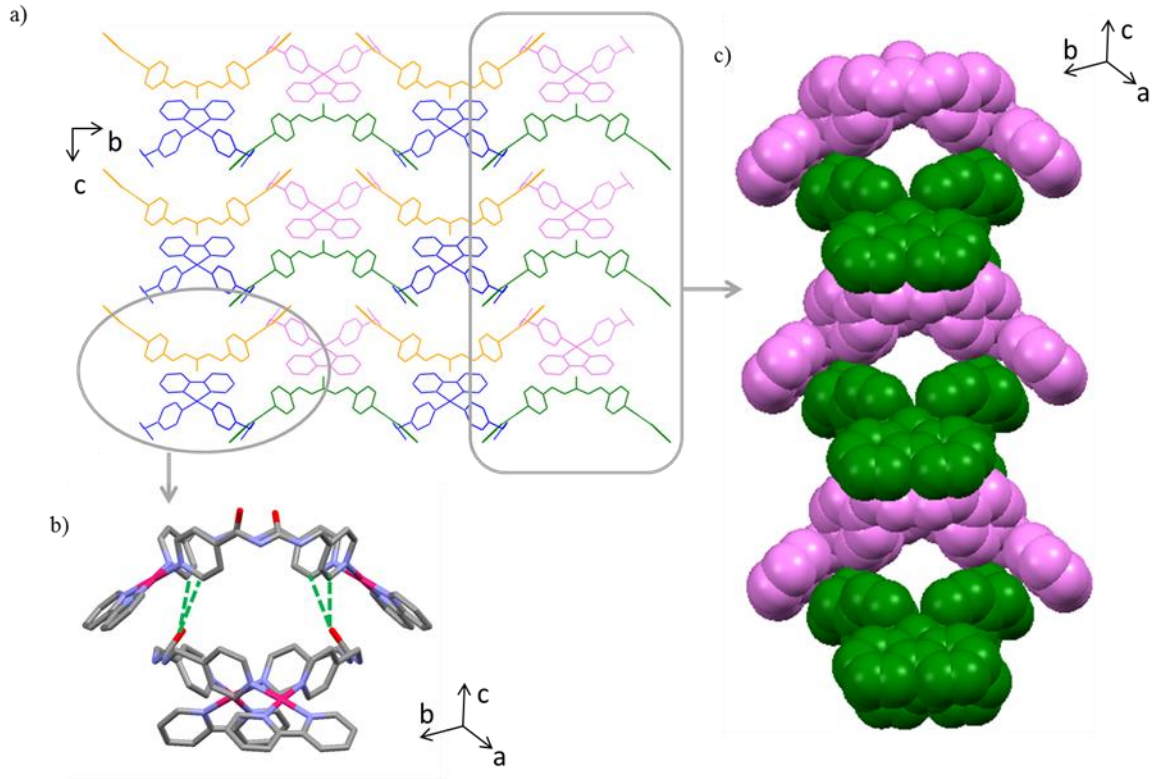

Figure S74 a) Packing diagrams showing $[Pd_2(bpy)_2(\mathbf{L})_2]^{4+}$ units along *a* axis, b) showing C–H···O bonding between two molecules of complex **3**, and c) showing 1-D supramolecular network formed by C–H···O interactions along *a* axis.

Calculation for the radial displacement angle (θ)

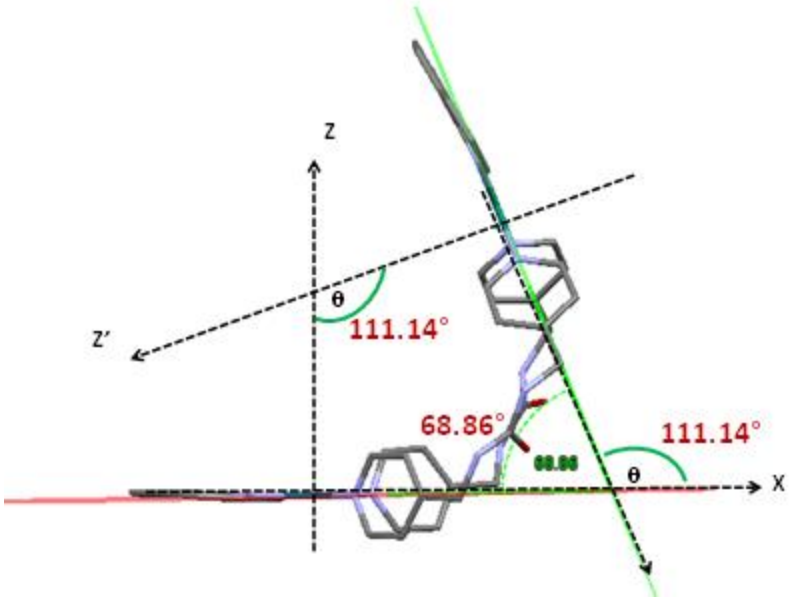

Figure S75. The radial displacement angle (θ) in $[Pd_2(phen)_2\mathbf{L}_2](NO_3)_4$**, 4**

Crystal Packing of $[Pd_3L_6](NO_3)_6$, 5

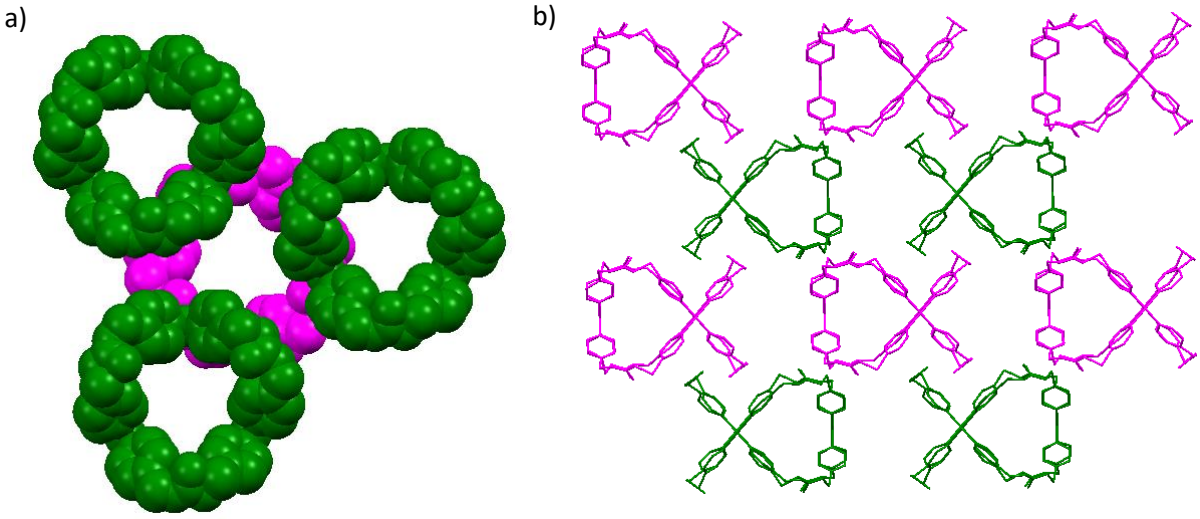

Figure S76. Packing diagrams showing a) channel like arrangement of the $[Pd_3(\mathbf{L})_6]^{6+}$ units along *a* axis (space fling model) and b) ABABAB fashion arrangement along *a* axis (capped sticks model) (hydrogen atoms are excluded for clarity).

Reference 3 is also considered for understanding of the following.
i) **sample-1**: only DMSO-d_6
ii) **sample-2**: DMSO-d_6 with external standard i.e. $CDCl_3$ (with 0.03% TMS). The external standard was taken in a small capillary and dipped in NMR tube containing DMSO-d_6.
iii) **sample-3**: DMSO-d_6 that contains ~2% of $CDCl_3$ (with 0.03% TMS).
iv) **sample-4**: only $CDCl_3$ (with 0.03% TMS).
v) **sample-5**: $CDCl_3$ (with 0.03% TMS) that contains ~2% of DMSO.
vi) **sample-6**: $[Pd(bpy)_2](NO_3)_2$ as a representative complex in DMSO-d_6
vii) **sample-7**: The representative $[Pd(bpy)_2](NO_3)_2$ complex in DMSO-d_6 with external standard i.e. $CDCl_3$ (with 0.03% TMS). The external standard was taken in a small capillary and dipped in NMR tube containing a solution of $[Pd(bpy)_2](NO_3)_2$ DMSO-d_6.

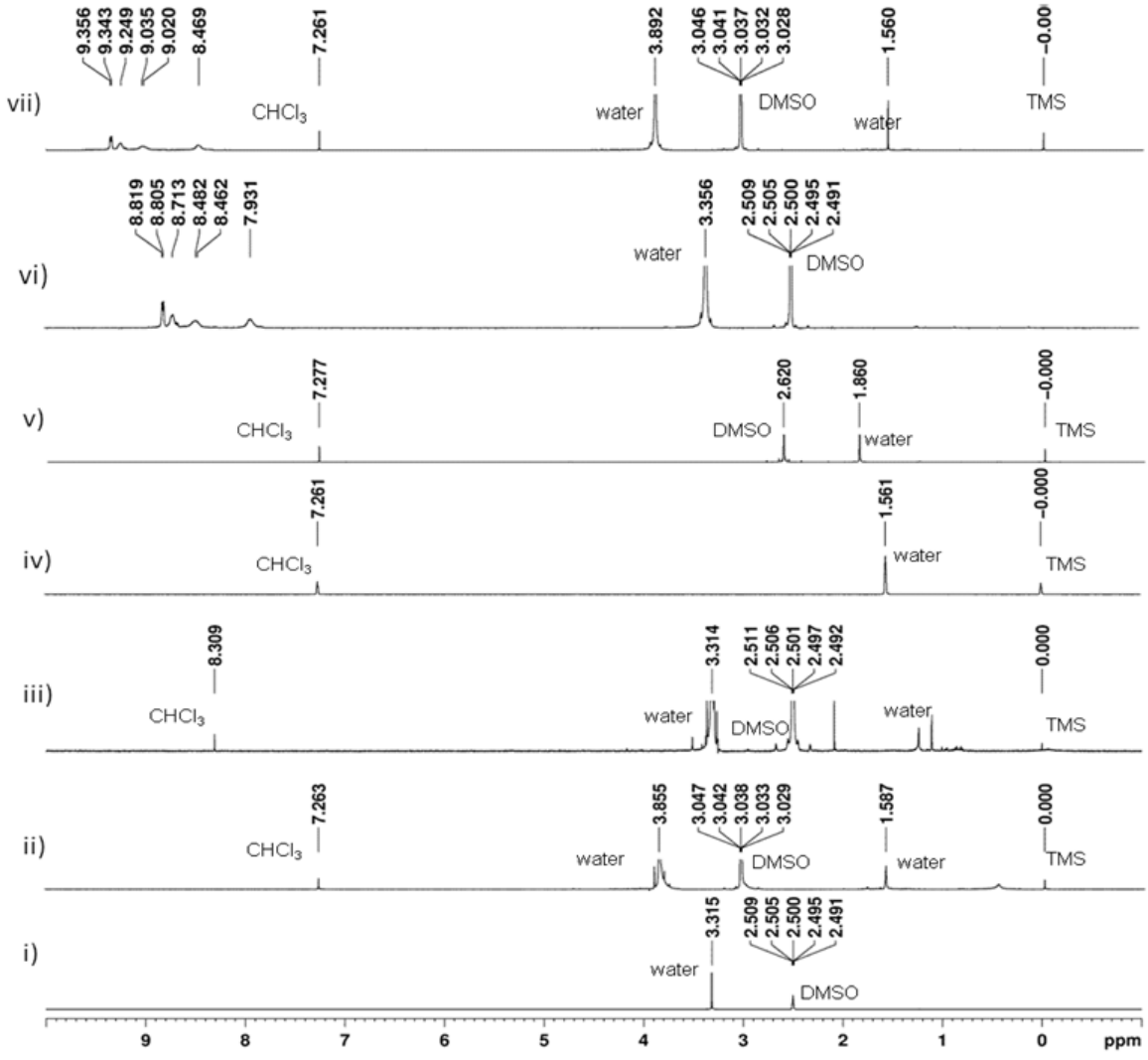

Figure S77: 400 MHz ^{1}H NMR spectra at room temperature for i) **sample 1**, ii) **sample 2**, iii) **sample 3**, iv) **sample 4**, v) **sample 5**, vi) **sample 6** vii) **sample 7**. [wherever TMS was used, it was calibrated at 0.00 ppm as standard reference; otherwise, residual peak calibrated (in case of DMSO-d_6 it is 2.500 ppm in figure (i) and (vi))]

References:

1. Frisch, M. J., Trucks, G. W.; Schlegel, H. B.; Scuseria, G. E.; Robb, M. A.; Cheeseman, J. R.; Scalmani, G.; Barone, V.; Men-nucci, B.; Petersson, G. A.; Nakatsuji, H.; Caricato, M.; Li, X.; Hratchian, H. P.; Izmaylov, A. F.; Bloino, J.; Zheng, G.; Sonnenberg, J. L.; Hada, M.; Ehara, M.; Toyota, K.; Fukuda, R.; Hasegawa, J.; Ishida, M.; Nakajima, T.; Honda, Y.; Kitao, O.; Nakai, H.; Vreven, T.; Montgomer y, J. A.; Peralta, Jr. J. E., Ogliaro, F.; Bearpark, M.; Heyd, J. J.; Brothers, E.; Kudin, K. N.; Staroverov, V. N.; Ko-bayashi, R.; Normand, J.; Raghavachari, K.; Rendell, A.; Burant, J. C.; Iyen-gar, S. S.; Tomasi, J.; Cossi, M.; Rega, N.; Millam, J. M.; Klene, M.; Knox, J. E.; Cross, J. B.; Bakken, V.; Adamo, C.; Jaramillo, J.; Gomperts, R.; Stratmann, R. E.; Yazyev, O.; Austin, A. J.; Cammi, R.; Pomelli, C.; Ochterski, J. W.; Martin, R. L.; Morokuma, K.; Zakrzewski, V. G.; Voth, G. A.; Salvador, P.; Dannenberg, J. J.; Dapprich, S.; Daniels, A. D.; Farkas, O.; Foresman, J. B.; Ortiz, J. V.; Cio-slowski J.; Fox, D. J. Gaussian, Inc., Wallingford CT. *Gaussian 09*, **2009**, Revision A.02.
2. Sahoo, H. S.; Chand, D. K.; Debata, N. B. Influence of *cis*-protecting groups toward ligand exchange reactions in polynuclear Pd(II)-based coordination cages. *Inorg. Chim. Acta* , **2007**, *360*, 31-38.
3. Gottlieb, H. E.; Kotlyar, V.; Nudelman, A. *J. Org. Chem.* **1997**, 62, 7512-7515